Photosensitized reactions contributing to the growth and aging of atmospheric aerosols

Kifle Zeleke Aregahegn

N° d'ordre: **266 - 2014**

Année **2014**

THESES DE L'UNIVERSITE DE LYON

Présentée devant

L'UNIVERSITÉ CLAUDE BERNARD - LYON 1

ECOLE DOCTORAL DE CHIMIE

Pour l'obtention du

DIPLOME DE DOCTORAT

(arrêté du 7 août 2006)

Soutenue et présentée publiquement le 4 Décembre 2014

Par

Monsieur Kifle Zeleke AREGAHEGN

REACTIONS PHOTOSENSIBILISEES CONTRIBUANT A LA CROISSANCE ET AU VIEILLISSEMENT DES AEROSOLS ATMOSPHERIQUES ORGANIQUES

PHOTOSENSITIZED REACTIONS CONTRIBUTING TO THE GROWTH AND AGING OF ATMOSPHERIC AEROSOLS

Directrice de thèse : Barbara NOZIERE

JURY:

Dr. Gilles MAILHOT	Rapporteur	Université Blaise Pascal/ Aubiere
Dr. Sasho GLIGOROVSKI	Rapporteur	Université de Provence/Aix-Marseille
Pr. Patrick RAIROUX	Examinateur	ILM / UCBL-CNRS
Pr. D. James DONALDSON	Examinateur	University of Toronto
Dr. Christian GEORGE	Co-directeur de thèse	IRCELYON / UCBL-CNRS
Dr. Barbara NOZIERE	Directrice de thèse	IRCELYON / UCBL-CNRS

IRCELYON – UMR 5256 CNRS – Université Lyon 1

2, avenue Albert Einstein 69626 VILLEURBANNE Cedex

UNIVERSITE CLAUDE BERNARD - LYON 1

Président de l'Université	**M. François-Noël GILLY**
Vice-président du Conseil d'Administration	M. le Professeur Hamda BEN HADID
Vice-président du Conseil des Etudes et de la Vie Universitaire	M. le Professeur Philippe LALLE
Vice-président du Conseil Scientifique	M. le Professeur Germain GILLET
Directeur Général des Services	M. Alain HELLEU

COMPOSANTES SANTE

Faculté de Médecine Lyon Est – Claude Bernard	Directeur : M. le Professeur J. ETIENNE
Faculté de Médecine et de Maïeutique Lyon Sud – Charles Mérieux	Directeur : Mme la Professeure C. BURILLON
Faculté d'Odontologie	Directeur : M. le Professeur D. BOURGEOIS
Institut des Sciences Pharmaceutiques et Biologiques	Directeur : Mme la Professeure C. VINCIGUERRA
Institut des Sciences et Techniques de la Réadaptation	Directeur : M. le Professeur Y. MATILLON
Département de formation et Centre de Recherche en Biologie Humaine	Directeur : Mme. la Professeure A-M. SCHOTT

COMPOSANTES ET DEPARTEMENTS DE SCIENCES ET TECHNOLOGIE

Faculté des Sciences et Technologies	Directeur : M. F. DE MARCHI
Département Biologie	Directeur : M. le Professeur F. FLEURY
Département Chimie Biochimie	Directeur : Mme Caroline FELIX
Département GEP	Directeur : M. Hassan HAMMOURI
Département Informatique	Directeur : M. le Professeur S. AKKOUCHE
Département Mathématiques	Directeur : M. Georges TOMANOV
Département Mécanique	Directeur : M. le Professeur H. BEN HADID
Département Physique	Directeur : M. Jean-Claude PLENET
UFR Sciences et Techniques des Activités Physiques et Sportives	Directeur : M. Y.VANPOULLE
Observatoire des Sciences de l'Univers de Lyon	Directeur : M. B. GUIDERDONI
Polytech Lyon	Directeur : M. P. FOURNIER
Ecole Supérieure de Chimie Physique Electronique	Directeur : M. G. PIGNAULT
Institut Universitaire de Technologie de Lyon 1	Directeur : M. C. VITON
Ecole Supérieure du Professorat et de l'Education	Directeur : M. A. MOUGNIOTTE
Institut de Science Financière et d'Assurances	Directeur : M. N. LEBOISNE

Acknowledgements

First and foremost, praises and thanks to the God, the Almighty, for His showers of blessings throughout my live and research work to complete my thesis successfully.

I would like to express my deep and sincere gratitude to my supervisors, Barbara NOZIERE and Christian GEORGE for giving me the opportunity to do research and providing invaluable guidance throughout this research. Their dynamism, vision, sincerity and motivation have deeply inspired me. They taught me the methodology to carry out the research and to present the research works as clearly as possible. It was a great privilege and honor to work and study under their guidance. I am extremely grateful for what Barbara Noziere and Christian George have offered me. I would also like to thank them for their friendship, empathy, and great sense of humor.

I would like to say thanks to all permanent and non-permanent members of IRCELYON for their constant support. I express my special thanks to Barbara D'Anna, Ludovic Fine, Nicolas Charbonnel, Yoan Dupart, Badr Rmili, Raluca Ciuraru, Stéphanie Rossignol, Liselotte Tinel, Aurélie Même, Aurelia Maxut, Violaine Gerard, and Christine Delbecque for their genuine support throughout this research work. I particularly grateful for the kind assistance given by Anne-Marie Grezaud during administrative affairs.

I am extremely grateful to my parents for their love, prayers, caring and sacrifices for educating and preparing me for my future. I am very much thankful to my wife, Eyerusalem, and my little son, Henok, for their love, understanding, and continuing support to complete this research work. In addition, I express my thanks to my sisters, and brother for their support. My Special thanks goes to my brother Demisew Z. AREGAHEGN for the keen interest shown and encouragement to complete this thesis successfully.

My special thanks are extended to my friends Solomon Getachew and Getnet Asrat for their continuous friendship support and encouragement in my everyday life.

Finally, my thanks go to all the people who have supported me to complete the research work directly or indirectly.

Kifle Z. Aregahegn

Résumé de thèse de doctorat

L'atmosphère est un milieu hautement hétérogène contenant de la matière condensée : les aérosols. Ceux-ci sont des composants importants de l'atmosphère car ils impactent le bilan radiatif planétaire mais aussi la qualité de l'air. En particulier les aérosols organiques secondaires (AOS), produits par la transformation chimique dans l'air de nombreux composés organiques, plus ou moins volatils, représentent une fraction conséquente dans le budget global des aérosols atmosphériques pour laquelle de nombreuses incertitudes persistent. En particulier, leurs voies de formation et de transformation dans la troposphère restent très mal décrites.

C'est pourquoi, cette thèse décrit principalement l'étude de trois aspects de la croissance et du vieillissement (transformation) des aérosols:

- caractérisation de la croissance des AOS par des processus photosensibilisés ;
- investigations mécanistiques du vieillissement des AOS et de la photochimie des photosensibilisateurs ;
- analyse chimique des composés issus du vieillissement des AOS.

Les photosensibilisateurs sont des composés chimiques capables d'absorber et de transférer leur énergie à un réactif pour initier une réaction chimique. Le transfert d'énergie de l'état excité du photosensibilisateur au réactif peut se produire par différentes voies mais le taux de formation de l'état excité doit être plus rapide que ce transfert au substrat et que la photolyse directe du photosensibilisateur. Par ailleurs, l'état excité du photosensibilisateur doit être capable de transférer son énergie à l'état fondamental du substrat (accepteur), de sorte que le rendement du croisement inter-système doit être élevé.

Les composés aromatiques carbonylés sont connus comme étant d'excellents photosensibilisateurs à l'état triplet. Les deux voies de transitions électroniques possibles, la transition n-π^* et la transition π-π^*, mènent à une conversion inter-système efficace vers l'état triplet, qui de ce fait domine la photochimie de ces composés. Les différents

processus de désactivation de l'état excité du photosensibilisateur sont : les réactions de « quenching », le transfert d'électron, le transfert d'énergie et le transfert d'hydrogène.

La croissance photochimique et les processus de vieillissement chimique des AOS ont été étudiés au moyen d'un tube à écoulement auquel différents analyseurs de gaz et d'aérosols ont été couplés. Par ailleurs, des échantillons d'aérosols ont été collectés sur filtre à la sortie du tube à écoulement, en absence et en présence de lumière et analysés afin de connaître la composition chimique de l'aérosol. Cette analyse chimique et la connaissance de la composition de l'aérosol aide à comprendre les mécanismes à l'origine de la croissance des AOS sous des conditions atmosphériques simulées.

Le tube à écoulement pour aérosols est le système d'instrumentation de base de tous les processus expérimentaux. Il s'agit d'un tube à écoulement horizontal constitué d'un réacteur cylindrique en Pyrex avec un diamètre intérieur de 13 cm et une longueur de 152 cm. Ce réacteur est entouré par sept lampes fluorescentes. Il est équipé avec différents instruments pour l'analyse des aérosols, tels un SMPS et un CPC, et l'analyse des gaz. Ce réacteur nous nous permet d'étudier les premières étapes du grossissement des aérosols et du vieillissement chimique qu'ils subissent suite aux interactions des particules d'ensemencement avec les espèces en phase gazeuse et la lumière. La température et l'humidité relative des aérosols dans le réacteur à écoulement sont contrôlées respectivement par une circulation d'eau dans la double paroi du réacteur et par le barbotage dans une bouteille contenant de l'eau pure.

Les aérosols en eux-mêmes sont générés par un nébulisateur à flux constant et une concentration constante et connue d'un COV donné peut être générée grâce à un système de tube à perméation. En plus du tube à écoulement pour aérosols, l'analyse de la composition des aérosols chimiquement vieillis a été effectuée par échantillonnage sur filtre suivi d'analyses par (±)ESI-HRMS et UPLC/(±)HESI-HRMS.

Différents photosensibilisateurs potentiels ont été testés en phase particulaire, en absence et en présence de lumière, ainsi qu'en présence de composés organiques volatils (COV), afin d'estimer leur capacité à photo-induire une croissance de ces particules.

Toutefois, la chimie du glyoxal en phase condensé a attiré notre attention pour sa contribution à la croissance et le vieillissement d'aérosols préexistants. En effet, le 1H-imidazole-2-carboxaldehyde (IC), qui est un des produits de réaction formé par le glyoxal en phase condensée, s'est avéré être un photosensibilisateur efficace et a été utilisé dans la plupart des expériences de croissance des AOS. Des expériences additionnelles examinant le rôle de différents COV dans la croissance des aérosols ont été menées. La croissance des AOS a ainsi été étudiée dans des systèmes avec comme COV : le limonène, α-pinène, β-pinène, l'isoprène, le toluène, le cyclohexène, l'éthanol, le n-butanol ou l'acétone et en présence de particules préexistantes contenant du sulfate d'ammonium (SA) et le photosensibilisateur IC.

Basés sur la littérature et sur la méthode décrite, différents essais ont été menés sur la chimie du glyoxal. Le glyoxal induit un facteur de grossissement de 24.9% pour des particules d'ensemencement contenant du sulfate d'ammonium en présence de limonène gazeux. Cependant, le grossissement des particules débute uniquement après 30 min de réaction, correspondant à un temps d'induction, et se poursuit jusqu'à près de 2 h de temps de réaction. Par conséquent, le glyoxal semble ne pas lui-même induire la photosensibilisation mais plutôt être le précurseur d'un composé photosensibilisant. Les contributions au grossissement des produits majoritaires de la réaction entre le glyoxal et les ions ammonium, l'IC, le 1H-imidazole (IM) et le 2,2-bi-1H-imidazole (BI), ont été étudiées séparément. L'IC présente les meilleures propriétés de photosensibilisation avec un facteur de grossissement des particules de 27.6% en présence de limonène et après 19 min d'irradiation.

Les AOS présentent une croissance significative en présence de limonène, (croissance observée / concentration COV) (27.6% / 1.8 ppmv), α-pinène (19.3% / 63 ppmv), β-pinène (16.5% / 63 ppmv), isoprène (22.26% / 200 ppmv) et toluène (3.5% / 352 ppmv). Mais aucun des autres COVs testés n'a induit de croissance significative des aérosols lors des 19 minutes d'exposition dans le tube à écoulement, même en utilisant des concentrations plus élevées.

Les propriétés photochimiques et photophysiques de l'IC ont été étudiées en utilisant la technique de la photolyse à laser pulsé (PLP) dans une gamme longueur d'onde de 300 à 500 nm. Ainsi, l'absorbance transitoire triplet-triplet a été mis en évidence, avec une absorption maximale à 330 nm. L'absorbance a été déterminé 1 μs après le pulse du laser. La décroissance de l'absorbance de l'état triplet de l'IC suit une constante de première ordre qui a été déterminée à 7.73×10^5 s^{-1}. Le temps de vie de l'état triplet de l'IC correspondant est donc établi à 1.29 μs dans une solution aqueuse désoxygénée. La constante de vitesse de premier ordre de la désactivation de l'IC est multipliée par quatre en présence de limonène comme réactif. A partir des résultats obtenus à la fois sur le grossissement photosensibilisé des AOS et sur la photochimie de l'IC, un mécanisme réactionnel est proposé dans lequel le glyoxal mène à un grossissement autophotocatalytique des aérosols.

Des produits hautement oxygénés et quelques produits contenant de l'azote ont été observés dans un échantillon d'AOS vieillis chimiquement. Par analyse par infusion directe avec un spectromètre de masse haute résolution avec une ionisation par electrospray ((±)ESI- HRMS) ou par chromatographie liquide ultra haute performance couplée à l'ESI-HRMS (UPLC/(±)HESI-HRMS), des différences fondamentales ont été observées entre les expériences menées avec ou sans irradiation. Ces analyses ont avéré la présence dans les échantillons particulaires de produits hautement oxygénés. Les produits détectés sont similaires à ceux obtenus pour les essais en solution statique irradiée pendant 23 h (lumière UV de 280 à 400 nm) dans un petit réacteur cylindrique en quartz. Pour les deux expériences, sont retrouvés des composés hautement oxygénés, des composés azotés et des produits de recombinaison du photosensibilisateur avec lui-même ainsi que du photosensibilisateur avec le limonène. Ces produits témoignent de la formation de l'état triplet dans le système irradié du tube à écoulement (300 - 420 nm) qui réagit avec le carbone tertiaire insaturé du COV par un transfert d'hydrogène.

Basé sur les résultats de ces trois systèmes, un mécanisme réactionnel expliquant la croissance photosensibilisée des AOS a été proposé. Dans celui-ci, la croissance est initiée par la formation de l'état triplet du photosensibilisateur après absorption de lumière, suivi

par l'arrachement de l'atome d'hydrogène du carbone tertiaire insaturé du COV. Celui-ci, comme dans le cas du limonène, forme alors un radical qui peut réagir avec l'oxygène moléculaire pour donner un radical peroxyle. La chimie de ce dernier mène, par isomérisation notamment, à l'oxygénation de la chaîne carbonée. Le radical formé après addition de l'hydrogène sur le photosensibilisateur excité, peut subir soit des réactions de recombinaison soit un retour à son état fondamental par interaction avec l'oxygène moléculaire du système. Cette dernière réaction favorise la formation de radicaux hydroperoxyle (HO_2) dans le système, formation qui a pu être mise en évidence indirectement en utilisant le monoxyde d'azote (NO). En effet, l'ajout de NO dans ce système de réactions photosensibilisés en présence de COV a en effet montré une consommation du NO et une production de NO_2, preuve indirecte de la formation des radicaux HO_2. La concentration des radicaux HO_2 produits pendant la croissance photosensibilisée des AOS en présence de 500 ppbv de limonène a ainsi pu être calculée : $2.78 \times 10^{+12}$ molécule cm^{-2} s^{-1}.

Pour conclure, nous avons fourni des preuves que la croissance et le vieillissement chimique des AOS sont hautement affectés par des réactions photosensibilisées dans l'atmosphère. Des traces d'IC dans l'atmosphère peuvent influencer significativement la nature et la physico-chimie des AOS. Etant donnée l'omniprésence du glyoxal et d'autres gaz précurseurs dans l'atmosphère, ils devraient se former d'efficaces photosensibilisateurs au sein des aérosols, pouvant entrainer un grossissement et un vieillissement autophotocatalytiques des AOS.

Abstract

Aerosols are important constituents of the atmosphere and secondary organic aerosols (SOA) represent a main fraction of the organic aerosols in the total budget.

This thesis mainly reports the investigation of three aspects of the growth and aging of SOA:

- the photosensitized SOA growth
- the mechanistic investigation of SOA aging and of the photochemistry of photosensitizers
- the analysis of the chemical composition of aged SOA

The photosensitized growth and aging processes of SOA were investigated using an aerosol flow tube coupled with various aerosol and gas sensing instruments. For further analysis of the aerosol composition and a better understanding of the formation and growth of SOA in these experiments the aerosols produced in the dark and in the light were sampled on filters at the exit of the flow tube.

Different potential photosensitizers (1H-imidazole-2carboxaldehyde and 4-benzoylbenzoic acid) were tested for the SOA growth and aging in the presence of a VOC precursor in the light and in the dark. Recent studies had shown that the condensed phase chemistry of glyoxal contributed to the growth and aging of pre-existing atmospheric aerosols. 1H-imidazole-2-carboxaldehyde (IC), one of the products of the condensed-phase reactions of glyoxal, was evidenced in this work to be an efficient photosensitizer, and used as photosensitizer for SOA growth in the remaining part of this work. In addition, the SOA growth resulting from different VOC precursors, such as α-pinene, β-pinene, isoprene, toluene, cyclohexene, ethanol, n-butanol and acetone, was investigated using ammonium sulfate (AS) containing IC as seed particles. The best SOA growth was obtained with limonene (27.6%, 1.8 ppmv), α-pinene (19.35%, 63 ppmv), β-pinene (16.5%, 63 ppmv), isoprene (22.26%, 200 ppmv) and toluene (3.5%, 352 ppmv), while none of the other VOCs induced SOA growth over the 19 min of exposure time, even at high concentrations.

The photochemical and photophysical properties of IC were studied using a Laser Flash Photolysis (LFP) technique operating between 300 and 500 nm in wavelength. These studies evidenced the existence of a triplet-triplet transient absorption with a maximum absorption at 330 nm excitation wavelength. The first-order decay rate constant for this triplet-triplet absorption in a degassed solution was found to be 7.73 x105 s^{-1}. The first order decay rate was reduced by a factor of four when adding limonene to the solution as a quencher.

The analysis of the aged SOA samples collected on filters was performed by ESI-(±) HRMS and UPLC/(±) HESI-HRMS systems and showed the presence of highly oxygenated and of nitrogen-containing products . Striking differences were observed between the composition of the aerosol produced in the dark and in the light in the experiments, the irradiated experiments resulting in the formation of highly oxygenated VOC and of some VOC-VOC and VOC-IC radical recombination products. This indicated that an excited triplet state of IC is formed in the flow tube during irradiation (300 – 420 nm), which later interacts with the tertiary unsaturated carbon of the VOC precursor through hydrogen abstraction.

Based on these three different series of results, a reaction mechanism for the photosensitized SOA growth was proposed. This mechanism begins with the formation of a triplet state from the photosensitizer upon absorption of light, followed by hydrogen abstraction from the tertiary unsaturated carbon of VOC. The VOC, for instance limonene, then forms a radical, which reacts with molecular oxygen to form a peroxyl radical. The peroxyl radical can undergo further oxygenation reaction in the oxygen-saturated system. The radical formed due to the addition of hydrogen atom to the excited triplet photosensitizer can undergo either recombination reactions or a regeneration to its fundamental state by interacting with molecular oxygen. The later process would result in the formation of hydroperoxyl (HO_2) in the system.

The formation of HO2 in this mechanism was investigated in a final series of experiments by adding nitric oxide (NO) to the photosensitized reaction system. The consumption of NO and production of NO_2 was observed, which confirmed the formation

of HO_2. This HO_2 radical production during photosensitized SOA growth and in the presence of 500 ppbv of limonene in the flow tube was estimated to 2.78 x 10^{+12} molecule cm^{-2} s^{-1}.

In conclusion, this work showed that the growth and aging of SOA can be highly affected by photosensitized condensed-phase reactions in the atmosphere. Only traces of photosensitizers such as IC in atmospheric particles were shown to lead to significant differences in the growth and composition of atmospheric SOA. Furthermore, this work shows that the ubiquitous gas precursors in the atmosphere such as glyoxal can produce efficient secondary photosensitizers in aerosols, thereby causing autophotocatalytic SOA growth and aging.

This thesis manuscript is organized in the following way:

Chapter 1 is an introduction to the Earth's atmospheric; chemistry, constituents and aerosol composition. The structure and general composition of the Earth's atmosphere are explained and the nature and modes of formation of atmospheric aerosols are also described in this chapter.

Then, the anthropogenic and natural sources of gases and particulate matter that play an important role in the atmospheric composition are discussed. Secondary photochemical compounds, which are formed by the oxidation of variety of gases present in the atmosphere such as nitrogen oxides, and volatile organic compounds (VOCs), are potentially more harmful than their precursors.

The formation and potential effect of some radicals and oxides such as HOx (= OH + HO_2) and NO_x (= NO + NO_2), including their various reactions and rate constants, are also presented in a tabular form.

In **Chapter 2**, photosensitizers type and properties are discussed based on the available literature. Different possible reaction mechanisms initiated by photosensitizers are presented and discussed.

Photosensitizers are chemical compounds that can absorb light and transfer their energy to a reactant (substrate) to initiate a chemical reaction. The transfer of energy from the excited photosensitizer to the reactant occur in different ways. However, important conditions in these processes are the formation rate of the excited photosensitizer must be faster than those of other reactants, and that the excited photosensitizer must be able to transfer its energy to the ground state of the substrate (acceptor) so that the yield of the inter-system crossing is high.

Aromatic carbonyls are excellent triplet photosensitizer. The two possible electronic transition pathways in these compounds, n-π* and π-π*, lead to efficient intersystem crossings, so that the triplet state processes dominate their photochemistry.

IC is one of the aromatic carbonyl compounds that resembles other photosensitizers. In this chapter, the different possible deactivation processes, quenching reaction, electron transfer, energy transfer and hydrogen transfer, of the excited triplet state photosensitizers are discussed.

In **Chapter 3**, the methodologies and techniques used in this PhD work, as well as the chemical compounds used in the various studies, are presented.

First, the aerosol flow tube used to investigate the SOA growth is described, along with all the instruments and equipment connected to it and their principles. The types of flow in the reactor are also discussed.

The horizontal cylindrical aerosol flow tube is equipped with different aerosol instruments like SMPS, CPC and gas analyzers. This reactor allows us to study the early stage of aerosol growth and aging due to the interaction between gaseous species, seed aerosols and light.

The seed particles are generated using a constant output atomizer. Constant and known concentration of VOC is generated using a permeation device. In addition to aerosol flow reactor, the chemical composition analysis of aged aerosol is performed by filter sampling followed by direct (±)ESI-HRMS and UPLC/(±)HESI-HRMS.

Then the laser flash photolysis technique used for the investigation of the photochemical and photophysical properties of the photosensitizer (triplet state) and its interaction with quenchers is described. .

Chapter 4 describes the investigation of the photosensitized SOA growth from seed aerosols exposed to light and VOC, their aging, and the contribution of glyoxal (Gly) reactions to SOA growth. Based on the method described in Chapter 3 and information from the literature, series of experiments are performed and show that reactions of Gly in ammonium sulfate (AS) seeds and in the presence of gas phase limonene result in a growth factor of 24.9% on the particle diameter. However, this growth starts after a 30-min induction time indicating that Gly is not directly responsible for the photosensitization processes but that one of its reaction product is. The roles of two main reaction products of Gly IC, 1H-imidazole (IM) and 2,2-bi-1H-imidazole (BI), on SOA growth are studied separately. IC is found to have the best photosensitizing properties, inducing a particle growth of 27.6% in the presence of limonene and for 19 min of irradiation time.

Based on the results of these studies, a possible reaction mechanism is proposed, suggesting that glyoxal can result in an autophotocatalytic SOA growth.

In **Chapter 5** the investigation of the excited triplet state of IC, using the laser flash photolysis set-up, is presented. The first order reaction rate constant and decay lifetime of excited triplet state of IC are estimated as a function of limonene concentration as a triplet state quencher.

The influence of nitric oxide (NO) on the particle growth and its application for calculating the radical production flux during photosensitized SOA growth is presented in **Chapter 6**.

The work presented in **Chapter 7** is a product analysis of the aged SOA produced in the flow tube experiments. The analysis of the filter samples by ESI-(±) HRMS and UPLC/(±) HESI-HRMS evidence the presence of oxygenated products with high O:C in the aerosols produced. Similar products are found in bulk static experiment where IC and

limonene solution are irradiated (from 280 nm to 400 nm) in a small cylindrical quartz reactor. In both types of experiments, highly oxygenated products with a limonene skeleton, and nitrogen-containing products of integrating the structures of the photosensitizer and of limonene are found, evidencing the formation of radicals from the triplet state of IC and its recombination on the VOC precursor molecule

Chapter 8 presents a general conclusion on this work and proposes some perspectives.

Table of Contents

List of Tables

List of Figures

1 General Introduction

1.1 The Earth's atmosphere: structure and composition

Average composition

Today's atmosphere is primarily composed, in average, of nitrogen (78%), oxygen (21%), argon (1%), and water vapor, which varies between 0 and 4%. However, this average composition has changed tremendously compared to the early atmosphere. The latter is expected to have had a primitive composition similar to that of the Sun. 4 billion years ago, the composition of the early atmosphere had mainly carbon dioxide, water vapor and nitrogen, and hydrogen, hydrogen chloride and sulfur dioxide are, however, belongs to minor gases. The early atmosphere of the Earth was a mildly reducing chemical mixture, whereas the present atmosphere is strongly oxidizing. The modern or present atmosphere is a result of outgassing of the Earth (Seinfeld and Pandis, 2006). The most important fraction of the present atmosphere, oxygen, rapidly produced by photosynthesis processes. It was initially produced by cyanobacteria, the only prokaryotic organism capable of oxygenic photosynthesis; these emerged by 2700 million years ago (Seinfeld and Pandis, 2006). Cyanobacteria

began the process of increasing atmospheric oxygen, which thereby become high enough to support more complex life, which in turn produced more oxygen. A balance process between photosynthetic production and removal through respiration and organic carbon decay maintains the present level of O_2.

The composition and abundance of Earth's atmosphere is controlled on geologic timescales by the biosphere, up take and release from surface material and degassing of the interior (Seinfeld and Pandis, 2006). In addition to the main components cited above, for which the concentrations are so very stable and large that they are considered as background gases, numerous other gases are present at smaller concentrations. These are presented in Table 1-1, which includes certain gaseous constituents of the atmosphere and their volume ratio.

Table 1-1 Atmospheric composition of certain gases, their origin and concentration (IPCC, 1995, Seinfeld and Pandis, 2006) http://lwf.ncdc.noaa.gov/oa/climate/gases.html,

Gas	Concentration	Natural Source	Anthropogenic Source
CO_2	370 ppmv	CO oxidation, forest destruction, respiration	Fuel combustion
Water vapor	Up to 0.01 ppmv	Evaporation, hydrological cycle	
Ne	18.18 ppmv	Inert	Inert
He	5.24 ppmv	Inert	Inert
CH_4	1.77 ppmv	Oceans/wetlands	Leakage from natural gas system, raising livestock
H_2	0.55 ppmv	Combustion	Oxidation process
N_2O	0.3 ppmv	Oceans	Petroleum combustion
NO_2	100 ppbv	Forest firing, lightening	Petroleum combustion
Tropospheric O_3	10 – 500 ppbv	Stratosphere	Photochemistry of CO and hydrocarbons in the presences NO_x
VOCs	5 – 20 ppbv	Oceans, plants, biomass burning	Combustion
NO_x	10 pptv – 1 ppmv		Soil, fuel combustion, traffics

Argon (0.9%) is the next most abundant next to nitrogen and oxygen, which does not undergo any chemical reaction in the atmosphere and does not affect either human health or global climate change. The remaining trace gases (0.01%) are the most chemically interesting which affect pollution, human health, and climate. These gases are responsible in the production of pollutants and greenhouse gases.

Vertical structure

The Earth's atmosphere consists of several layers defined by change in the temperature trends. The troposphere is the closest layer to the surface.

The troposphere extends from the Earth's surface to the tropopause, which approximately 10 - 15 km in altitude, depending on the location and time of the year (Seinfeld and Pandis, 2006). It is characterized by decreasing temperature with height. At the tropopause, the pressure in the atmosphere is 1/100 of the pressure at the Earth's surface. It is a very small part of the total volume of the atmosphere, but it contains nearly 80% of the total atmospheric mass (Seinfeld and Pandis, 2006).

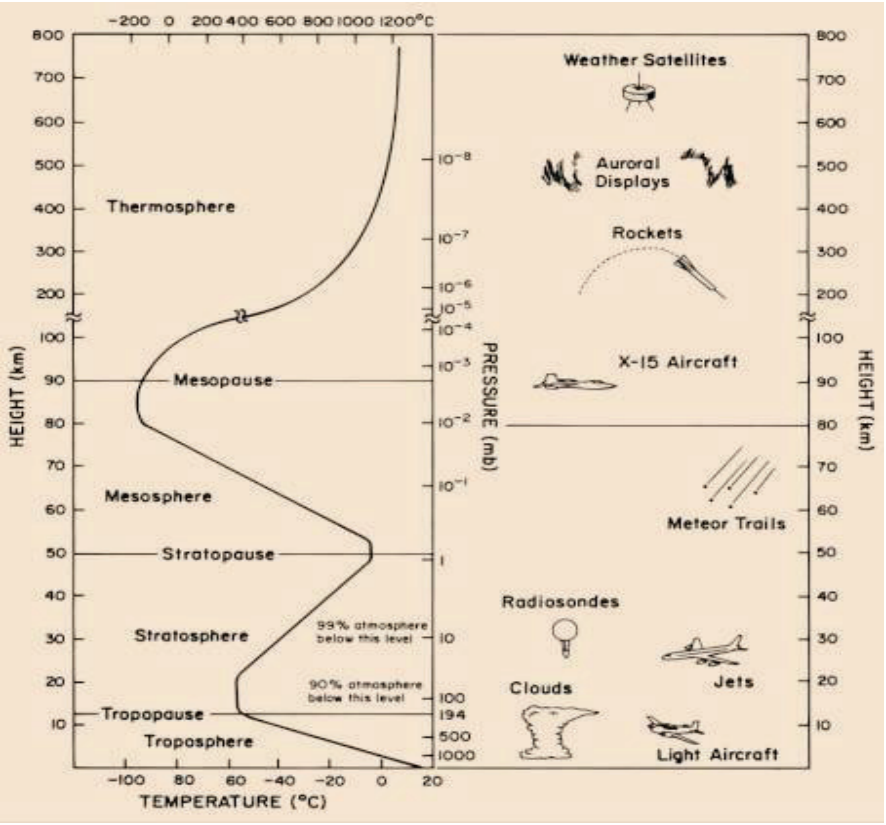

Figure 1-1 Atmospheric layers are determined by the way the temperature changes with increasing height. From J. R. Eagleman, Meteorology: The Atmosphere in Action.

The temperature variation depends on the altitude; it decreases by about 6.5°c per kilometer to reach -56°C.

The tropopause is marked by an inversion of the temperature that is followed by the stratosphere. The stratosphere extends up to 50 km and contains about 90% of atmospheric ozone, which absorbs almost all of the UV-B and UV-C coming from the sun.

The mesosphere extends from the stratopause, up to approximately 80 to 90 km in altitude; its temperature is characterized by decreasing with altitude, and is the coldest point in the atmosphere, reaching as low as -90°C.

The thermosphere is the region above mesopause which is characterized by high temperature due to absorption of short wavelength radiation by N_2 and O_2.

Finally, the outermost region of the atmosphere, extending approximately above 500km in altitude where gas molecules can escape from the Earth's gravitational attraction, is called the exosphere.

Among these layers, the troposphere is one containing the most complex mixture of suspended gases and particles that can interact and react due to light entering from the sun and the heat emitted from the Earth's surface. The tropospheric constituents are influenced by the different emission from the Earth's surface. Biogenic particles and gases are those released into the atmosphere from the natural sources such as plants, microorganisms, oceans and lightening, and anthropogenic species are those emitted as a result of human activities such as from vehicles on industries are also introduced to the troposphere.

In the free troposphere, most meteorological phenomena, such as the formation of clouds, and rain, occur. Therefore, it is important to understand the production and fate of those gases and particulate matter in the atmosphere.

1.2 Atmospheric trace constituents

The change in the composition of atmosphere from its natural component due to the addition of other gases or the change in concentration may affect human and/or other living organism's health. However, the increase in population and human activities have changed the atmospheric composition for last decades.

The emission of gases, volatile and semi-volatile organic compounds and particulate matter, plays an important role in atmospheric chemical equilibrium, despite their presence in very low quantities. Their emission may cause tropospheric ozone depletion, photochemical smog formation which in turns visibility reduction, and direct or indirect health effects, and global warming.

Some of these emissions, like sulfur and nitrogen oxides, are responsible for the alteration of the pH of cloud water which in turn the formation of acid rain (Alfonso and Raga, 2002, Andreae and Rosenfeld, 2008, Finlayson-Pitts and Pitts, 2000).

1.2.1 Tropospheric ozone and Volatile organic compounds (VOC) oxidation

Secondary photochemical pollutants, which are formed by the oxidation of variety of pollutant emitted into the atmosphere such as nitrogen oxides, and volatile organic compounds (VOCs), are potentially more harmful than their precursors. Ozone is one of them. Ozone (O_3) has come to public awareness as a species of high importance to both climate change and its effect on incoming solar radiation. It is predominantly found in the stratosphere in the form of ozone layer which absorbs the incoming ultraviolet rays (UV-C 100 – 280 nm) emitted by the sun. However, tropospheric O_3 is considered as a pollutant, and has adverse effects on human and plant health. O_3 can often be a smog component (Frampton et al., 1999, van Zelm et al., 2008).

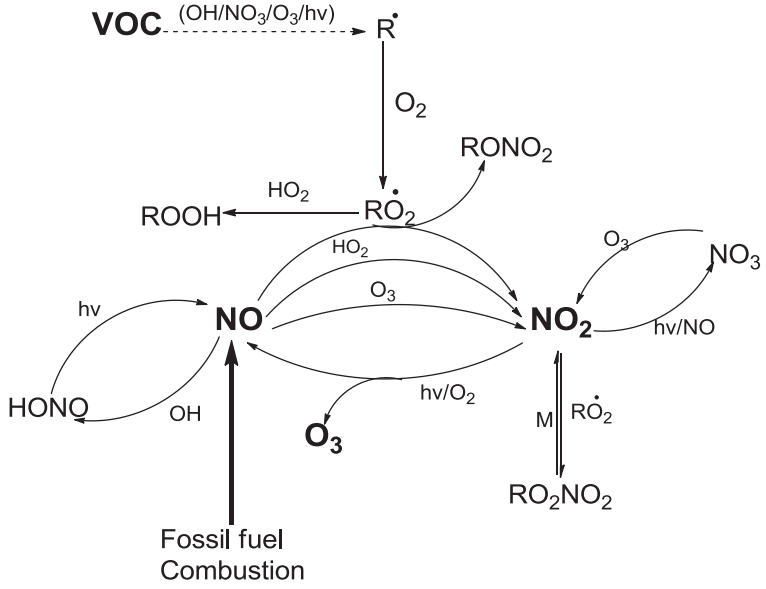

Figure 1-2 Schematic representation secondary photochemical pollutant production in troposphere.

At a typical boundary layer concentration of 30 ppbv of O_3, the reaction with NO leads to NO_2 formation occurs on a timescale of ca. 1 min. During daytime, however, NO_2 photolysis back to NO, which also leads to the regeneration of O_3. These reactions essentially balance each other, which leads no net production or loss of any one of the species. In the absence of competing interconversion reactions, the photo-stationary state concentration of NO and NO_2 are related to the O_3 concentration by the following expression (Eq. 1-1) (Jenkin and Clemitshaw, 2000).

$$[O_3] = \frac{J_3[NO_2]}{k_2[NO]} \qquad \textit{(Eq. 1-1)}$$

where J_3 is the rate constant of NO_2 photolysis, and k_2 is the rate coefficient for the reaction of NO with O_3.

Volatile organic compounds are organic compounds released into the atmosphere by anthropogenic and natural process and / or formed in the atmosphere due to photochemical oxidation

of different compounds. Some may occur naturally in the environment (Zogorski et al., 2006). VOCs include a variety of chemical compounds containing hydrogen (H), carbon (C) and other possible elements that evaporate easily. They can undergoes photochemical reactions in the atmosphere that can contribute to aerosol aging and smog formation. Their oxidation is also coupled to the formation of O_3 in the atmosphere. When these variety of VOCs reacts with gas phase oxidants in the atmosphere, (e.g. RH), they form alkyl peroxy radicals (RO_2) in the presence of O_2. The reactive RO_2 radical then reacts with NO to lose an oxygen atom and form alkoxy radical (RO).

$$RH + OH \xrightarrow{O_2} RO_2 + H_2O \quad \textit{(R. 1-2)}$$

$$RO_2 + NO \rightarrow RO + NO_2 \quad \textit{(R. 1-3)}$$

$$NO_2 + h\nu \rightarrow NO + O\ (\lambda < 420\ nm) \quad \textit{(R. 1-4)}$$

$$RO + O_2 \rightarrow R'CHO + HO_2 \quad \textit{(R. 1-5)}$$

$$HO_2 + NO \rightarrow OH + NO_2 \quad \textit{(R. 1-6)}$$

$$O(^3P) + O_2 \rightarrow O_3 \quad \textit{(R. 1-7)}$$

The formation of NO_2 in the (R. 1-3) perturbs the O_3/NO_x cycle resulting in the formation of tropospheric O_3.

The alkoxy radical can also react with molecular oxygen to form stable carboxyl compounds and HO_2 radical (R. 1-5). The HO_2 radical can further react with another NO in the system to induce extra production of NO_2, which will also perturb the O_3/NO_x cycle and result in even more production of O_3. The resultant reaction is, therefore, leading to extra O_3 formation in the troposphere (Atkinson and Arey, 1998, Atkinson and Arey, 2003a, Atkinson and Arey, 2003b). However, according to the reaction given (R. 1-2 to R. 1-7), the significant formation route of O_3 in the troposphere is photolysis of NO_2, for which the alkyl peroxy radical (RO_2) and hydroperoxyl radical (HO_2) formed in the R. 1-2 and R.1-5 react with NO (R. 1-3 and R. 1-6) to form NO_2 whose photolysis is then leads to net O_3 formation in the troposphere. O_3 concentration is often higher in summertime, because of VOCs

oxidation by the influence of direct sun light (Figure 1-2). Depending on the VOC concentrations, the NO_x may vary which will vary the O_3 formation and thus O_3 concentrations.

Among these VOCs, monoterpenes are the most common, predominantly found over coniferous forests. Monoterpenes are 10-C compounds that volatilize to the atmosphere from storage reservoirs in the needle and bark of conifers. Once they are introduced into the atmosphere, they react readily with oxidative species to form a variety of secondary products that influence atmospheric chemistry and climate (Kokkola et al., 2014, Wuebbles et al., 1989). Limonene is the main component of essential oil extracted from citrus rind. It is one of the major organic compounds emitted directly in to the atmosphere by vegetation, and comprises about 20% of the total monoterpene emissions.

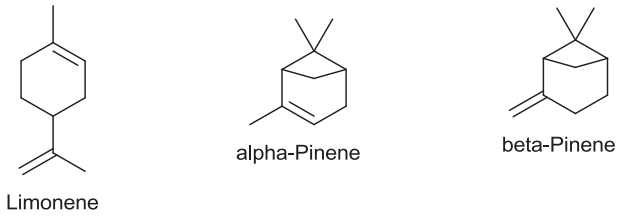

Figure 1-3 Molecular structure of three common monoterpenes.

Limonene demands special attention because it has two very different unsaturations: an endocyclic tri-substituted double bond and an exocyclic terminal double bond. These bonds contribute to limonene's high potential for SOA formation (Kokkola et al., 2014, Maksymiuk et al., 2009, Ehn et al., 2014). It is expected to rapidly under go dark and light gas phase reaction in the atmosphere with photochemically produced hydroxyl radicals, ozone, and nitrate radicals (Atkinson, 1990, Zhang et al., 2006, Atkinson et al., 2003, Atkinson and Aschmann, 1993, Atkinson et al., 2004, Atkinson et al., 1999).

α-Pinene and β-pinene are bicyclic hydrocarbons with a single double bond: endocyclic for α-pinene and exocyclic for β-pinene. Oxidation of these monoterpenes leads to the production of particles and hence significant SOA mass yields (Burkholder et al., 2007). The main reaction pathway for those monoterpenes in troposphere is ozonolysis, which destroys roughly 80% of emitted α-pinene and β-pinene (Griffin et al., 1999). They are very efficient in forming SOA (Hoffmann et al., 1997).

Isoprene or 2 – methyl -1,3 butadiene is another most abundant non methane hydrocarbon emitted into the atmosphere, mainly from biogenic sources (Guenther et al., 2006). It is evidenced that isoprene oxidation contribute for SOA formation by many researchers (Böge et al., 2006, Claeys et al., 2004, Edney et al., 2005, Miyoshi et al., 1994, Pandis et al., 1991, Sato et al., 2011, Zhang et al., 2011). Currently, it is estimated that isoprene is the single largest source of SOA in the atmosphere (Carlton et al., 2009, Hallquist et al., 2009, Henze and Seinfeld, 2006, Henze et al., 2008). Isoprene undergo photo-oxidation in the atmosphere in the presence of OH, NOx and O_3 (Henze and Seinfeld, 2006).

Aromatic compounds are common in urban air (Hurley et al., 2001). Toluene is one of the aromatic VOCs that contribute to organic aerosol in urban air (Hao et al., 2007, Izumi and Fukuyama, 1990, Pandis et al., 1992). The atmospheric oxidation of toluene initiated by OH radicals produces a variety of primary products, including glyoxal (Hoffmann et al., 1997, Smith et al., 1998).

In addition, aerosol formation is the major pathway for a number of cyclic alkenes atmospheric oxidation (Keywood et al., 2004).

1.2.2 Glyoxal in the atmosphere

Glyoxal (Gly) is produced by a wide variety of anthropogenic and biogenic volatile organic compounds (VOCs). Models and experimental or field measurement showed that there is significantly

high amount of global production in the troposphere. Recent studies have shown that, it is the simplest α-dicarbonyl organic compound, and the most prevalent dicarbonyl in the atmosphere.

The sources of glyoxal are manifold. This compound can be directly emitted via biofuel burning (Hays et al., 2002) and vehicle emissions (Grosjean et al., 2000). Such primary sources are highly uncertain due to the large variability of the emission factors. It was reported as 2 to 5 times higher than HCHO (Hays et al., 2002).

Recent studies have also evidenced that glyoxal is produced from VOC atmospheric oxidation process (Volkamer et al., 2005). It is produced via the oxidation of C_n-hydrocarbons, where $n \geq 2$, as a result of anthropogenic activity (Atkinson, 2000, Magneron et al., 2005, Volkamer et al., 2005, Volkamer et al., 2001), biogenic processes (Atkinson, 2000, Spaulding et al., 2003), biomass burning (Volkamer et al., 2007) and in the marine environments (Warneck, 2003). It is a first generation product from the oxidation of a number of unsaturated VOCs by OH and O_3 (Volkamer et al., 2005, Volkamer et al., 2007).

Similarly, glyoxal has been identified as a first generation product of aromatic ring opening pathways during the OH initiated oxidation of aromatic hydrocarbons (Smith et al., 1999, Volkamer et al., 2001).

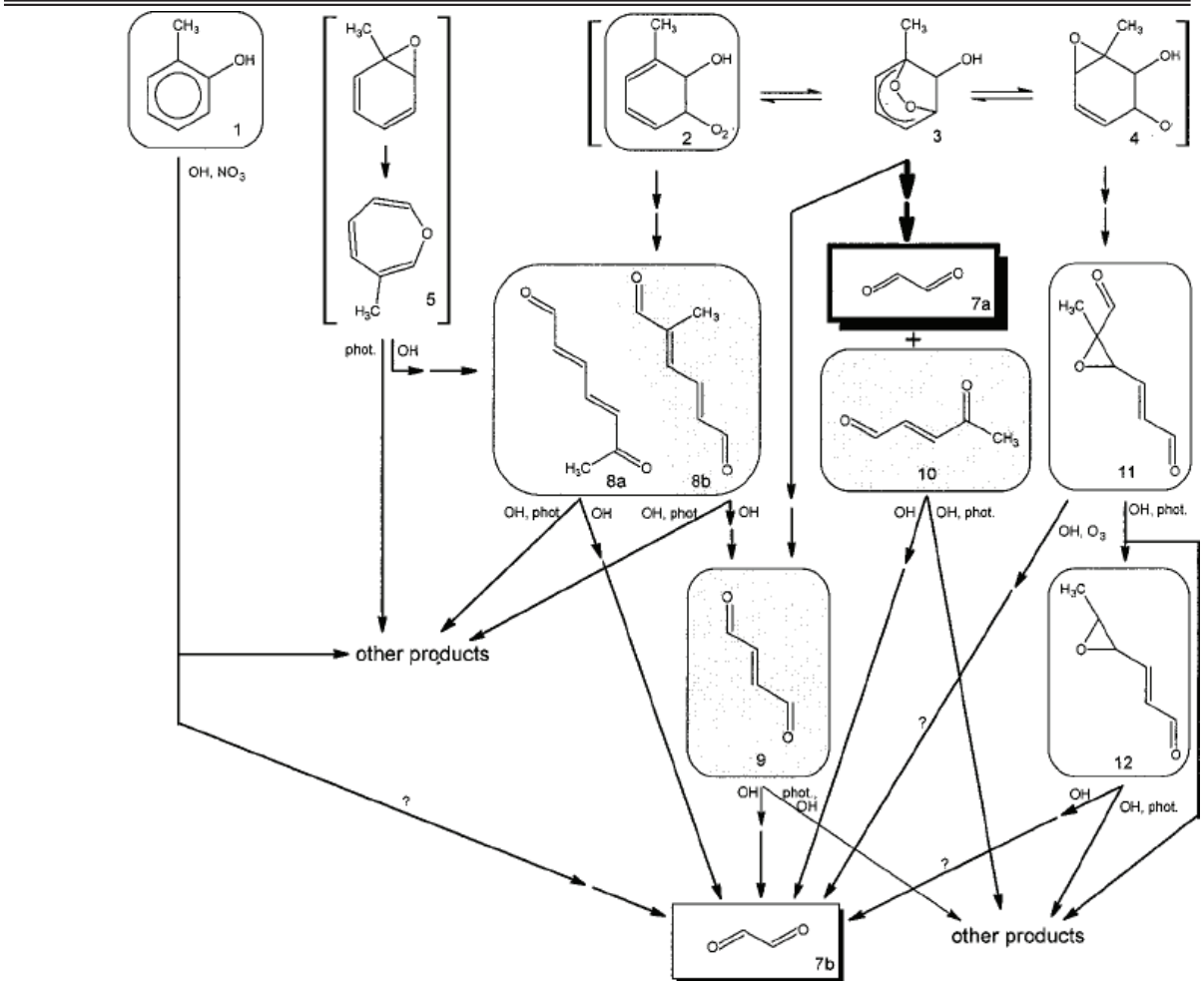

Figure 1-4 Possible pathways for the formation of glyoxal (shaded box) from toluene.(Volkamer et al., 2001)

Rough estimations showed that the isoprene photo-oxidation provides alone ca. 45 Tg/y global burden of glyoxal (Fu et al., 2008), while other simulations indicate a total burden of 56 Tg/y with 70 % being produced from biogenic hydrocarbon oxidation (Myriokefalitakis et al., 2008).

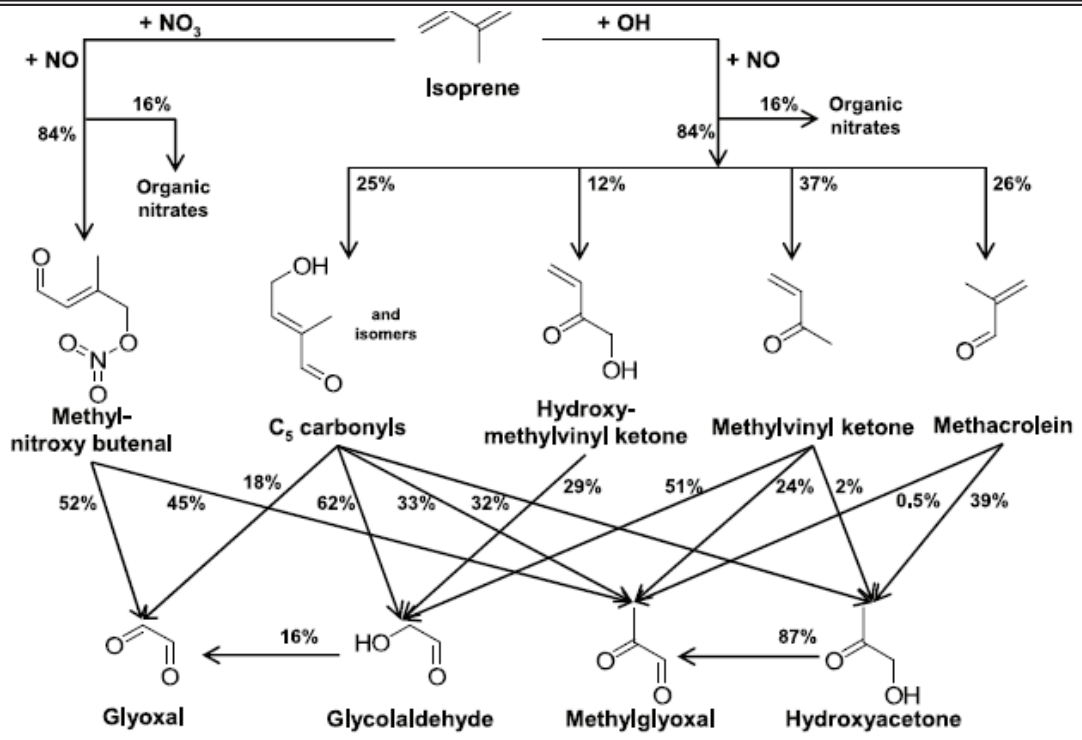

Figure 1-5 Glyoxal and methylglyoxal production from the oxidation of isoprene by OH and NO_3.(Fu et al., 2008)

Glyoxal absorbs in the UV and visible spectral range between 200 and 470 nm (Atkinson et al., 2006). Glyoxal is present at concentration of 5 – 280 µM in cloud water (Munger et al., 1995). The solubility of glyoxal with an effective Henry's Law constant $H_{eff} > 3 \times 10^5$ M atm^{-1} at 25°C; (Betterton and Hoffmann, 1988) is 3 order of magnitude greater than that of SO_2 (Carlton et al., 2007). It is highly reactive in the aqueous phase (Buxton et al., 1997) and is rapidly taken upon acid liquid surfaces (Schweitzer et al., 1998). Glyoxal is more reactive with respect to hydration, polymerization and hemiacetal/acetal formation in the presence of alcohols (Jang and Kamens, 2001).

1.2.3 Glyoxal in atmospheric aerosol

Reversible or irreversible uptake of glyoxal onto aerosol is one the most important sinks for loss of gas phase glyoxal (Volkamer et al., 2007). Many laboratory studies showed SOA formation from glyoxal (Kroll et al., 2005, Liggio et al., 2005a, Liggio et al., 2005b, Volkamer et al., 2009).

Glyoxal is an indicator of VOC oxidation process (Volkamer et al., 2005) and fast photochemistry of anthropogenic VOCs. According to Ervens and Volkamer (Ervens and Volkamer, 2010), there are five parameters that strongly affect the predicted SOA yield from glyoxal namely: 1) timescales to reach equilibrium state, 2) particle pH, 3) chemical composition of the bulk aerosol, 4) particle surface composition and 5) particle liquid water content that is mostly determined by the amount and hygroscopicity of aerosol mass. When these criteria are met, glyoxal uptake onto droplets and water containing particles leads to the formation of low volatile species, thus to SOA formation. For instance, condensation reactions with ammonium cation (NH_4^+) or amines leads to nitrogen containing products (Ervens and Volkamer, 2010, Lim et al., 2010, Nozière et al., 2009). The photochemical oxidation of glyoxal occurs mainly through H-abstraction by OH radical and leads to the formation of small organic acids and large oxygenated products through radical recombination in concentrated solution (Lim et al., 2010).

The condensed phase reactions of glyoxal involve several pathways. The main one is the formation of acetals (C-O-C units) (Jang et al., 2002, Jang and Kamens, 2001), suspected to be responsible for the much larger yields obtained from glyoxal than expected (Kroll et al., 2005). In the presence of ammonium cations in the condensed phase, another pathway of the glyoxal reactions leads to the formation of imidazoles (Debus, 1858, Galloway et al., 2009, Kampf et al., 2012, Yu et al., 2011) in particular imidazole (IM), imidazole-2-carboxaldehyde (IC) and 2,2-bi-imidazole (BI) as seen in (R. 1-8).

The imidazole ring is aromatic, and these compounds tend to absorb in the UV-visible range (Galloway et al., 2009, Kampf et al., 2012, Shapiro et al., 2009, Yu et al., 2011).

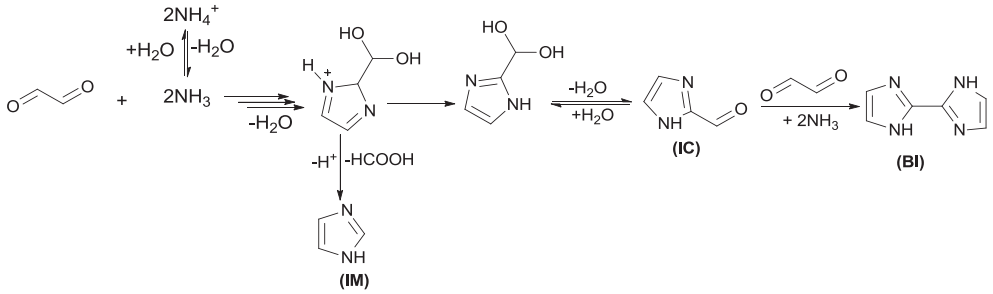

(R. 1-8)

It was also shown that these minor products were nevertheless able to impact the optical and radiative properties of ambient aerosols (Hallquist et al., 2009).

Indeed glyoxal is now expected to be an important source of SOA due to its ubiquity in the atmosphere (Lavvas et al., 2013, Myriokefalitakis et al., 2008, Nozière et al., 2009, Saunders et al., 2003, Volkamer et al., 2009).

1.2.4 Radicals and NO_x cycles

Atmospheric radicals and nitrogen oxides are responsible for the atmospheric degradation and oxidation processes in the troposphere. Among these radicals, (hydroxyl (OH), hydroperoxyl (HO_2)), nitrate (NO_3), halides and also certain oxidants such as ozone (O_3), and nitrogen oxides are well known. In this thesis, the chemistry of nitrogen oxides and hydroperoxyl radical will be more interestingly focused.

The OH radical plays a dominant role in the tropospheric oxidation chemistry that controls the atmospheric lifetime of most anthropogenic or biogenic species present. The main source of OH radical is photo-dissociation of free tropospheric O_3. The presence of relatively low level of O_3 in the troposphere is, therefore, extremely important to reduce the OH radical concentration. Photolysis of

O_3 takes place at wavelength, λ≥290 nm is the cutoff in troposphere and becomes very inefficient at λ>305 nm to form the O(^{1}D) atom. The O(^{1}D) atom is then undergoes either deactivation to ground state oxygen O(^{3}p) atom, or react with water vapor to form OH radicals.

$$O_3 + hv(\lambda \leq 350\ nm) \rightarrow O_2 + O(\ ^1D) \quad \textit{(R. 1-9)}$$

$$O(\ ^1D) + M \rightarrow O(\ ^3p) + M \quad \textit{(R. 1-10)}$$

$$O(\ ^1D) + H_2O \rightarrow 2OH \quad \textit{(R. 1-11)}$$

The formation of OH radical through photolysis of O_3 is during daytime hours, but it has been suggested that OH radical can be formed from the reaction of O_3 with alkenes such as isoprene, and monoterpenes during both daytime and nighttime which could be significant source of OH (Heard and Pilling, 2003, Kroll et al., 2001, Librando and Tringali, 2005).

The annual OH concentration show seasonal variation, having an average global tropospheric concentration of 1.0 x 10^6 molecule cm^{-3} (Atkinson and Arey, 2003b).

HO_2 radical is another secondary photochemical product that is involved in the alteration of O_3 and OH cycle. The annual average concentration of HO_2 is usually 100 times higher than that of OH concentration (Heard and Pilling, 2003).

$$O_3 + OH \rightarrow HO_2 + O_2 \quad \textit{(R. 1-12)}$$

Nitrogen Oxides (NO_x) includes nitric oxide (NO) and nitrogen dioxide (NO_2). They are mainly emitted from combustion of fossil fuels, forest fires, lightening and soil (fertilization). Their oxidation chemistry involving VOCs and (HO_x = OH + HO_2) leads to the formation of O_3 and secondary aerosols. Combustion engines are also main source of NO_x in the cities that leads to increased O_3 concentration. The atmospheric oxidation of some VOCs and radical formation reaction pathways are summarized in Table 1-2.

Table 1-2 Atmospheric fate of some radicals with their rate constant at 298K

Reactions	Rate constant K_{298} (cm^3 $molecule^{-1}$ s^{-1})	Reference
$R^{\bullet} + O_2 \longrightarrow RO_2$	R dependent	
$RO_2 + HO_2 \longrightarrow ROOH$	"	
$RO_2 + RO_2 \longrightarrow$ -CO + -C-OH	"	
$RO_2 + NO_2 \longrightarrow ROONO_2$	"	
$RO_2 + NO \longrightarrow RONO_2$ $\longrightarrow RO + NO_2$	"	
$NO + HO_2 \longrightarrow OH + NO_2$	8.5×10^{-12}	(Bardwell et al., 2003)
$O + HO_2 \longrightarrow OH + O_2$	5.8×10^{-11}	(Ravishankara et al., 1983)
$O + NO_2 \longrightarrow NO + O_2$	9.9×10^{-12}	(Dillon et al., 2006)
$NO_2 + hv \longrightarrow NO + O(^3p)$	Actinic flux dependent	
$O_2 + O \longrightarrow O_3$	1.4×10^{-14}	(Arnold and Comes, 1979)
$O_3 + NO_2 \longrightarrow NO_3 + O_2$	3.5×10^{-17}	(Verhees and Adema, 1985)
$2NO + O_2 \longrightarrow 2NO_2$	2.0×10^{-38}	(Baulch et al., 1973)
$O_3 + O \longrightarrow 2O_2$	2.4×10^{-10}	(Greenblatt and Wiesenfeld, 1983)
$O_3 + NO \longrightarrow NO_2 + O_2$	1.9×10^{-14}	(Moonen et al., 1998)
O_3 + Limonene $\longrightarrow$ Product	2.1×10^{-16}	(Bernard et al., 2012)
NO_3 + Limonene $\longrightarrow$ Product	1.2×10^{-11}	(Martínez et al., 1999)
NO + Limonene $\longrightarrow$ Product	No data available	
OH + Limonene $\longrightarrow$ Product	1.44×10^{-10}	(Peeters et al., 2007)
HO_2 + Limonene $\longrightarrow$ Product	No data available	
$HO_2 + O_3 \longrightarrow OH + 2O_2$	2.0×10^{-15}	(Herndon et al., 2000)
$HO_2 + HO_2 \longrightarrow H_2O_2 + O_2$	1.6×10^{-12}	(Wallington et al., 1992)

Nitric oxide (NO) is emitted into, or produced in the troposphere. Soils and natural fires are main biogenic emitter of NO. It is also formed in situ in the troposphere from lightning (National

Research Council, 1991). NO is emitted from anthropogenic activities by combustion processes such as vehicle emission and fossil fuel power plants (National Research Council, 1991, Guenther et al., 2000). In polluted area sufficient amount of NO is present (more than ~10 parts per thousand (pptv)) and remote area is characterized by small concentration of NO which will affect the photochemical reaction with RO_2 and HO_2 radicals (Finlayson-Pitts and Pitts, 1997).

1.3 Atmospheric aerosol

The atmosphere is not only composed of gases but also of liquids and solids in suspensions. Atmospheric aerosols are suspended particles that can be solid, liquid or combination of both, being one of atmosphere constituent (IPCC, 2013). Aerosols consist of different composition and sizes. Based on the sources of aerosols, they are either primary, which are directly emitted into the atmosphere, or secondary aerosols that are formed by gas phase oxidation occurring in the atmosphere. Secondary organic aerosols (SOA) is formed when gas phase species react with atmospheric oxidants, OH or O_3, or other photochemical process to form volatile species that will condensed on the surface of pre-existing particles(Finlayson-Pitts and Pitts, 1997, Seinfeld and Pandis, 2006).

Particle in the atmosphere arises from natural sources as well as anthropogenic activities (Seinfeld and Pandis, 2006). Dust, volcanic activities, biomass burning and sea spray all belongs to natural sources of particles, whereas particles emitted through the attribution of human activities like fuel combustion, industrial processes, and transportation are called anthropogenic.

Particles in the atmosphere can change their size and composition by condensation of vapor species or by evaporation, coagulation with other particles, chemical reactions or by activation in the presence of water.

1.3.1 Classification of atmospheric aerosols

There are different ways to classify aerosols, the main ones being either from their size or from their origin.

a) Particle size classification

Particle size is the most important parameter for characterizing the behavior of aerosols. The size of aerosol particle related with the formation process and visibility effect, health and climate (Seinfeld and Pandis, 2006). The number concentration and size distribution are the most important aerosol factors that affect the efficiency of scattering of both short and long wave radiation. This classification of aerosol particle includes the distribution function of the number concentration, surface area, or volume of the particles per interval of radius diameter.

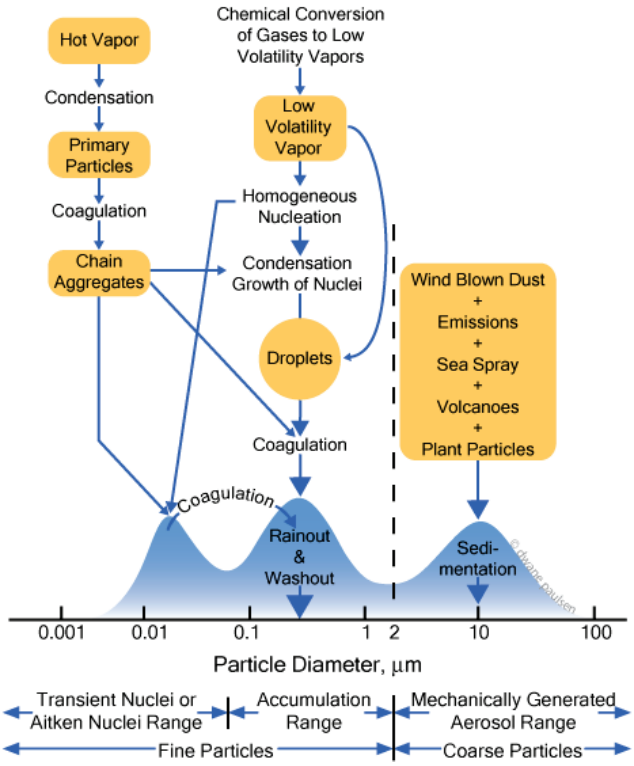

Figure 1-6 Illustration of the range of size distribution of aerosol particles(Whitey, 2007).

PM_{10} – particles with aerodynamic diameter less than or equal to 10 μm.

$PM_{2.5-10}$ - coarse particles with aerodynamic diameter between 2.5 and 10 μm.

$PM_{2.5}$ – fine particles, with aerodynamic diameter less than or equal to 2.5 μm.

$PM_{0.1}$ – ultrafine particles, whose diameter less than or equal to 0.1 μm.

Figure 1-6, the accumulation mode represents particle diameter between 0.1 to 1.0 μm. This mode represents a region of particle growth due to coagulation of particles diameter less than 0.1 μm. The Aitken mode of particles include from 0.01 to 0.1 μm diameter range. It is the mode of condensation and/or nucleation.

b) Primary and secondary aerosols

The mode of formation of aerosols in the atmosphere is one way of categorizing aerosols. There are two ways of formation of aerosol regardless of their sources.

Primary aerosols - are particles, which are directly emitted to the atmosphere through different processes in different forms (liquid or solid).

Secondary aerosols – are particles formed in the atmosphere due to atmospheric transformation of gases, liquids or solids.

Chemical components of atmospheric particles are highly diverse. They vary from nearly neutral to highly soluble substances. As the origin of atmospheric aerosols varied, the chemical composition and their atmospheric lifetime are different. Nevertheless, it is important to understand the formation, composition and behavior of aerosol particle in order to better quantify their effect on human health and global climate. The chemical composition of ambient aerosol particles are poorly

characterized, in particular its organic fractions. Generally, the composition varies according to their origin.

1.3.2 Effect of atmospheric aerosol on air quality and human health

Atmospheric aerosols have different effect on terrestrial and aquatic ecosystem. They affect the air quality, visibility, public health and climate (Seinfeld and Pandis, 2006, Perraud et al., 2012). Air pollution has a long history (Bowler and Brimblecombe, 1992). Up to the mid-20th century, documented air pollution were primarily related with high concentration of sulfur dioxide and soot particle (Noble and Prather, 1998). It was referred to as" London smog" because of a severe pollution episode in that city in 1952. Furthermore, the discovery of photochemical air pollution in Los Angeles area in 1940s have shown high concentration of O_3 and photochemical products that can affect human health.

The increase in particulate air pollution has been associated with decline in the function of lung and hence effect the respiratory system (Pope et al., 2002). There effect depends on their size, for instance, fine particulate matter can cause lung cancer and cardiopulmonary mortality (Pope et al., 2002), whereas bigger particles can trapped in the nasal cavity.

The particulate matter composition of the atmosphere also affect visibility and radiative balance of the Earth's surface by their absorptive capacity of IR radiation, and reflection and absorption of visible light (Pöschl, 2005, Program, 2009). The direct effect shown by particle is absorption or scattering of solar radiation. Certain aerosol contributes in warming the Earth's surface by absorbing IR radiation, whereas the others contribute in cooling the Earth by reflecting back the solar radiation.

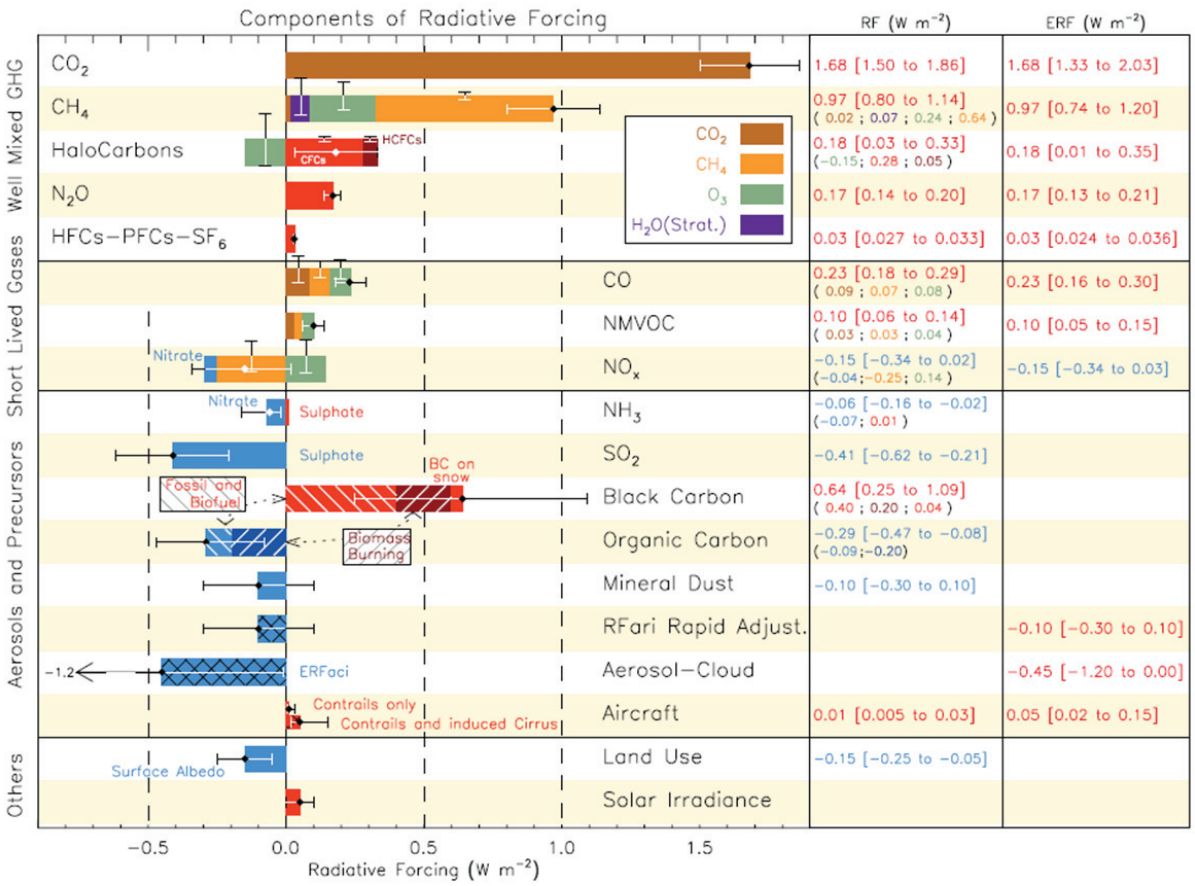

Figure 1-7 The effect of radiative forcing and external factors of aerosol and gases on the global climate system(IPCC, 2013)

The indirect effect of aerosol is through their interaction with clouds. Aerosol can affect the microphysical properties of clouds: soluble submicron particles serve as cloud condensation nuclei thereby increasing the water droplets. However, the increase in the number of droplet may leads to the decrease in the average size of droplets that cause delay or elimination of precipitation of clouds. Indeed, if there were no aerosol in the atmosphere, cloud would be much less common (Rosenfeld and Woodley, 2000, Twomey, 1977).

1.3.3 Primary and secondary organic aerosols

Organic compounds are ubiquitous in ambient aerosols, accounting for up to 50% of the fine particulate mass (Jacobson et al., 2000, Kanakidou et al., 2005, Seinfeld and Pankow, 2003, Zhang et al., 2004). The organic fraction plays an important role in determining their formation, growth, and removal of ambient aerosols (Prather et al., 2001). Organic particulate matter emitted directly from their sources into the atmosphere such as fossil fuel combustion or biomass burning are referred to as Primary Organic Aerosol (POA) whereas organic particles formed in the atmosphere are referred to as Secondary Organic Aerosol (SOA). However, the distinction between them is ambiguous that one aerosol particle may contain both forms simultaneously. Moreover, some individual particles may also contain both organic carbon materials (Kanakidou et al., 2005, Seinfeld and Pankow, 2003).

Among organic aerosols, secondary organic aerosols are the most important fractions, formed by the transformation of different VOCs by atmospheric oxidants (OH, O_3 and NO_3) and/or photochemical activities (Figure 1-8).

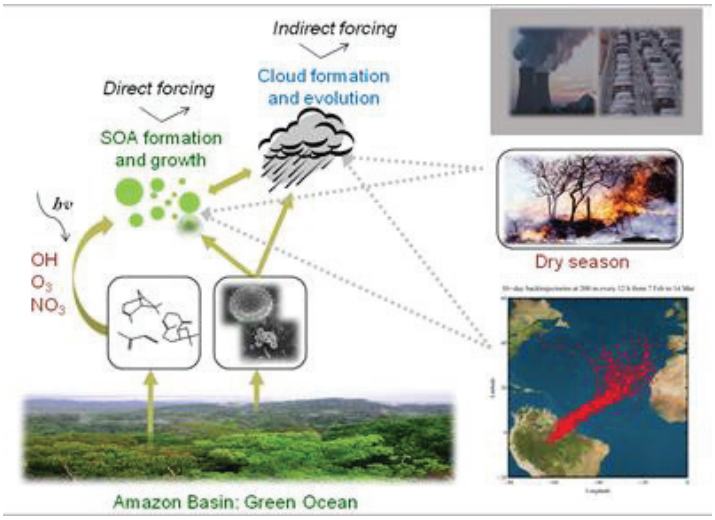

Figure 1-8 Mode of formation, source and effect of atmospheric aerosol (http://www.seas.harvard.edu/environmental-chemistry).

The carbonaceous component of atmospheric aerosol may varies from elemental carbon such as soot that mainly emitted from combustion process, and organic carbon such as organic compounds that are directly emitted to the atmosphere from primary sources such as biomass burning and combustion process or introduced by photochemical transformation called secondary organic aerosol (SOA). The latter are formed within the atmosphere when volatile organic compounds undergo oxidation reaction to form low volatile product which later condensed or partitioned on the pre-existing seed particles (Hoffmann et al., 1997, Odum et al., 1996, Ortega et al., 2013, Pandis et al., 1992). Volatile organic compounds are emitted in to the atmosphere from anthropogenic and biogenic sources (Odum et al., 1996, Seinfeld and Pandis, 2006). Anthropogenic VOCs consists of alkanes, alkenes, aromatics and carbonyls while biogenic are isoprene, monoterpenes and sesquiterpenes. However, aromatics and monoterpenes are important constituents of atmospheric chemistry and are being identified as SOA precursors (Griffin et al., 1999, Odum et al., 1996, Seinfeld and Pankow, 2003).

The seed aerosol can act as the absorption or adsorption center for SOA formation. The number size distribution of the seed aerosols play a crucial role for the condensation and coagulation process of the reaction products. The surface area of the particle can also have a great influence in the absorption and catalytic reactions (Oh and Andino, 2000).

The ubiquitous trace atmospheric gas, NH_3, reacts with inorganic acids (e.g. H_2SO_4 & HNO_3) in the atmosphere to produce secondary particulate species such as $(NH_4)_2\ SO_4$ and NH_4NO_3. They are common components of atmospheric aerosols (Mensah et al., 2012, Rood et al., 1989). A report showed in Hao (Hao et al., 2007), that the presence of seed aerosol shorten the time to reach the gas-particle partitioning equilibrium.

Organic acids such as succinic acid and adipic acid are identified as major constituents of the organic aerosols (Grosjean et al., 1978, Limbeck and Puxbaum, 1999). Anthropogenic and/or biogenic processes emit them (Chebbi and Carlier, 1996, Kerminen et al., 2000, Röhrl and Lammel, 2002). According to Monge et al., ((Monge et al., 2012), organic acids can potentially contribute to aerosol growth and photochemical processes may occur within aerosol and/or at the gas particle interface through energy transfer from the compounds such as humic acid triplet state. The triplet state of the compound can either interact directly with VOCs or induce a radical on the surface of aerosol particles. The particle growth was observed when the seed, ammonium salts and organic acids, containing photosensitizer (i.e. humic acid or 4-benzoylbenzoic acid) were exposed to gaseous VOC and light.

Predicting atmospheric process and effect of particulate matter starts from understanding the composition and formation mechanism of atmospheric aerosol particles. Nevertheless, it is difficult to quantify and identify the chemical components of atmospheric aerosol because of complex transformation and atmospheric system with a wide range of chemical and thermodynamic properties (Rudich et al., 2007, Saxena and Hildemann, 1996). There are no easily way to characterize aerosol composition and separation of primary and secondary sources.

Several researchers use different indirect methods to characterize chemical composition and formation mechanism of aerosol and their possible sources. Reaction chamber is one method to investigate the formation of SOA from the photo-oxidation of anthropogenic and biogenic precursors coupled with different aerosol instruments. In this work, an aerosol flow tube reactor was used to characterize some reactions that potentially contribute for SOA formation and aging. Indeed, different aerosol instruments are employed for the chemical composition analysis of these reaction products.

Having the potential importance of the new photosensitized pathway for SOA growth and aging defined by Monge et al., (Monge et al., 2012), this work is intended to investigate the contribution of

photosensitized reactions to the growth and aging of atmospheric aerosols. To accomplish this objective, a series of experiments were performed using aerosol flow tube, coated-wall flow tube, mass spectrometer and gas detectors based on the following specific objectives:

- To study the direct contribution of glyoxal to SOA growth and aging;
- To identify the important condensed phase glyoxal reaction products that can act as a photosensitizer;
- To identify the determinant parameters that can possibly affect the SOA growth in the flow tube;
- To formulate the SOA growth mechanism;
- To characterize the excited triplet stat of imidazole-2-carboxaldehyde;
- To calculate the SOA growth rate in the flow tube;
- To investigate the formation of HO_2 and calculate its flux during SOA growth;
- To identify the major components of photosensitized aged aerosol.

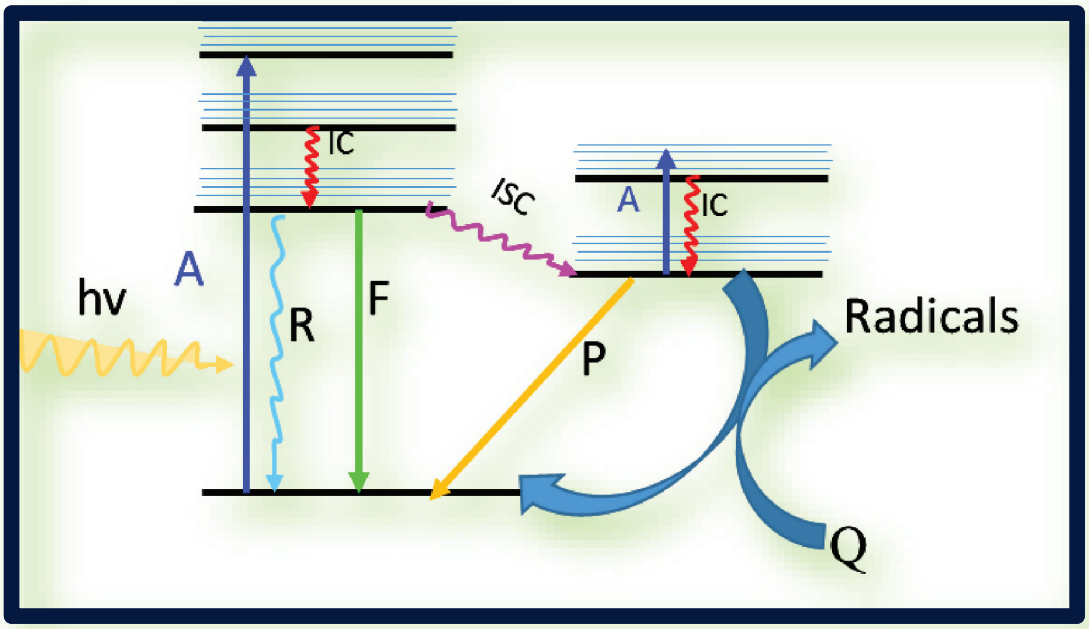

Photosensitizers

2.1 Introduction to Photosensitizers

The absorption of radiation by a molecule in the UV-vis range results in electronic transition from ground state (lower molecular orbital) to an excited state, or orbital of higher energy. The excited molecules can undergo a number of processes, such fast decay back to the ground state (10^{-9}- 10^{-8} s), accompanied by vibrational relaxation or fluorescence. However, the excited state can also potentially result in chemical reactions (Figure 2-1). Compounds for which the photo-induced excited state results in chemical reactions of a different species are called photosensitizers.

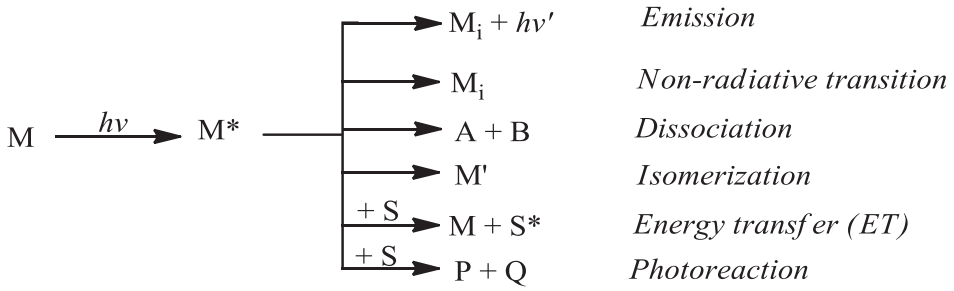

Figure 2-1 Photochemical processes for a molecule (M).

Note, however, that only photochemical reactions involving a molecule capable of absorbing light and transferring the energy to a reactant(s), also called acceptor, is considered as photosensitization process. The photosensitized reaction proceeds by transfer of energy, hydrogen or electron between the excited photosensitizer ("PS (T_1)") and a reactant molecule called acceptor ("Acceptor (So)"), as described below (Vione et al., 2006):

$$PS(S_0) + hv \longrightarrow PS(S_1) \qquad (R.\ 2\text{-}1)$$

$$PS(S_1) \xrightarrow{ISC} PS(T_1) \qquad (R.\ 2\text{-}2)$$

$$PS(T_1) + Acceptor(S_0) \xrightarrow{ET} PS(S_0) + Acceptor(T_1) \qquad (R.\ 2\text{-}3)$$

$$Acceptor(T_1) \longrightarrow Products \qquad (R.\ 2\text{-}4)$$

where the photosensitized reactions usually requires the formation of an excited triplet state, "PS (T_1)", through radiationless transition of electron from lowest excited singlet state to lowest exited triplet state, intersystem crossing (ISC), of longer lifetime than the excited state "PS (S_1)". For the photosensitized reaction to occur, the formation rate of exited triplet state of photosensitizer (PS (T_1)) must be faster than that of acceptor (T_1), otherwise the direct photolysis of the acceptor will be faster. In addition, the excited triplet state of photosensitizer (PS(T_1)) must be able to transfer its energy (i.e. energy transfer, ET) to the ground state of the acceptor (Acceptor (So)) so that the yielding of the inter-system crossing must be high.

2.2 Types of Atmospheric Photosensitizers

Most Carbonyl compounds may undergo triplet photosensitization because of the proximity between the S_1 state and the triplet state T_1, that increases the efficiency of the absorption process and triplet formation (Vione et al., 2006, Zhao et al., 2013). These electronic transition pathways are n-π* and π-π*. Aromatic carbonyls have the lowest S_1 (n-π*) state and the n-π* and π-π* triplet states are close together in energy. Thus, processes involving the triplet state dominate the photochemistry of these compounds.

Many aromatic compounds such as quinones and aromatic carbonyls, have been shown to be efficient photosensitizers (Vione et al., 2006). Humic acid, benzophenone and 4-Benzylbenzoic acid (4-BBA), for example, are the potential photosensitizers for atmospheric aerosol which are able to induce the photo-transformations of organic molecules (Ammar et al., 2010, Monge et al., 2012, Stemmler et al., 2006, George et al., 2005).

2.3 Photosensitized reactions

2.3.1 Quenching reaction

The excited triplet state of a photosensitizer can undergo deactivation through different processes. Quenching reaction is one of the common radiative or non-radiative deactivation processes. The rate of deactivation due to the interaction between excited triplet state of a photosensitizer, PS and another molecule, Q can be simplified as:

$$PS \xrightarrow{h\nu} {}^1PS^* \xrightarrow{ISC} {}^3PS^* + Q \longrightarrow X + Y \qquad \textit{(R. 2-5),}$$

where X – is the PS or ionized PS, Y – is the chemically modified Q and Q – is the quencher.

The rate of decay of PS due to Q, υ, is defined by the following formula (Eq. 2-5):

$$\upsilon = k^{I}[PS] + k^{II}[PS][Q] \qquad \textit{(Eq. 2-6)}$$

where k^{I} is first order deactivation rate constant of triplet state of PS, k^{II} is second order rate constant of PS resulting from the reaction with quencher (Q), and [PS] and [Q] are respective concentration of PS and quencher, respectively.

Quenching reactions are dependent on the nature of solvent and temperature of the system. The reaction can occur either by molecules of the same kind (PS), self-quenching or by the presence of another potential reagent (Q) in the system. The deactivation of triplet state can be proceed via electronic energy transfer, electron transfer and hydrogen transfer.

2.3.2 Energy transfer

In photochemical reaction intermolecular electronic energy transfer may be considered as being the transfer of energy from the excited state of one molecular entity (the donor, D*) to another molecule (the acceptor, A). By transferring energy to the acceptor, the donor is deactivated to the fundamental electronic energy state, which raises the acceptor to a higher electronic energy state.

$$D^{*} + A \rightarrow D + A^{*} \qquad \textit{(R. 2-7)}$$

According to the spin multiplicity of the donor and acceptor, the electronic energy transfer can be singlet-singlet, singlet-triplet or triplet-triplet electronic energy transfer, expressed as follows:

Singlet-singlet energy transfer: $^{1}D^{*} + {}^{1}A \rightarrow {}^{1}D + {}^{1}A^{*}$

Triplet-triplet energy transfer: $^{3}D^{*} + A \rightarrow D + {}^{3}A^{*}$

Singlet-triplet energy transfer: $^{1}D^{*} + A \rightarrow D + {}^{3}A^{*}$

Among these energy transfers, triplet-triplet energy transfer is the most common and most important in organic photochemistry. Since the excited state of donor molecules are preferentially formed by photon absorption and the energy is transferred to the acceptor, the process is referred to as photosensitization of A or quenching of excited state of D. The acceptor molecule is then activated to a lower energy triplet state by collisional exothermic energy, thereby returning the donor to its ground state. The donor is technically representative of a general photosensitizer and the acceptor is a quencher.

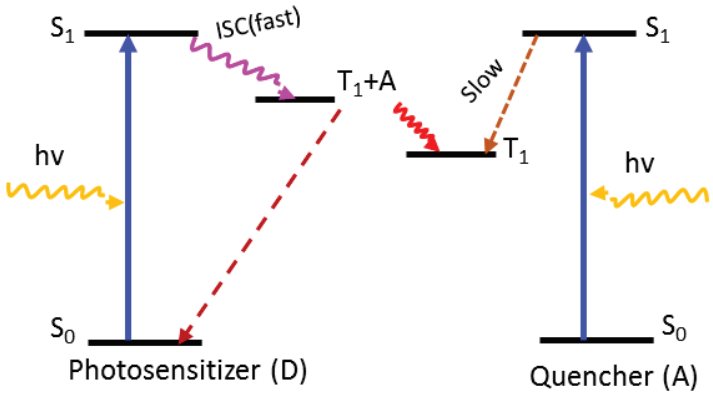

Figure 2-2 Energy transfer from excited triplet state of photosensitizer to quencher.

2.3.3 Electron transfer

The redox properties of molecules are affected by absorption of light because of promoting an electron to a higher energetic level, makes the molecule a better electron donor. In addition, electronic excitation also creates an electron vacancy in the highest occupied molecular orbital; so that the excited molecule can also be better electron acceptor. Based on this, an electron transfer can be defined as the promotion of an electron from a donor species to an acceptor species induced by a photon absorption. Consequently, the electrochemical properties (ionization potential and electron affinity) changed in such a way that the donor molecule becomes more reactive.

In the case of a photo-induced electron transfer, the photosensitizer (e.g. IC) in its excited triplet state can potentially react directly with another molecules (Q) via an electron transfer to produce reactive species as is given reaction (Figure 2-3). This reaction mechanism depends on the concentration of photosensitizer and substrate species.

The first phenomenon in electron transfer reaction is absorption of light by photosensitizer into singlet-excited state followed by intersystem crossing to produce a triplet-excited state, which becomes both more oxidant and more reductant. Consequently, two possible but different probability electron transfer reaction (either donating or accepting) pathway can occur. The third electron transfer step is deactivation or unwanted back electron transfer (BET) with in the contact ion pair ($PS^{+\cdot}$---- $Q^{-\cdot}$ or $PS^{-\cdot}$---- $Q^{+\cdot}$) which leads to fundamental state of reactants. Generally, BET reduces the overall radical generation quantum yield or reaction.

After the excitation of the acceptor A, A* and PS diffuse towards each other and given rise to a complex, wherein each entity maintains their own identity. If the electron transfer takes place, the activated complex relaxes towards the successor complex, that is to say formation of a pair of radical ions. Based on Rehm-Weller model (Rehm and Weller, 1970), Canonica proposed electron transfer mechanism between excited triplet aromatic carboxyl and phenol as electron donor (Canonica et al., 2000). The electron transfer between the triplet state of aromatic carboxyl, (e.g. IC), and the donor occurs in different steps.

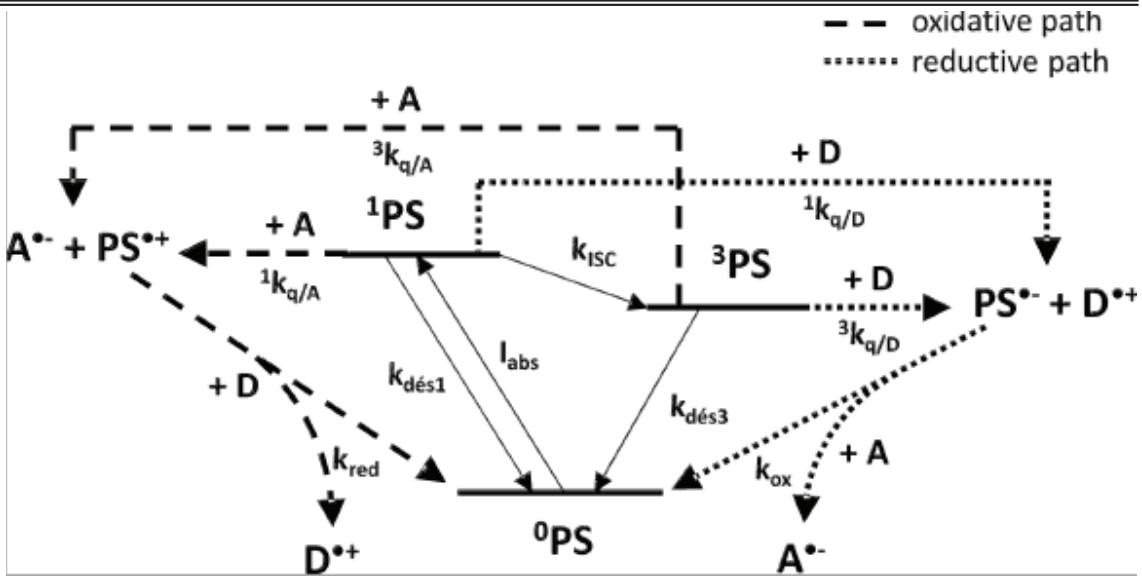

Figure 2-3 Alternative reaction path ways for electron transfer by Rehm-Weller, where Acceptor (A) and donor (D) are triplet state quenchers, and PS is a photosensitizer (Ley et al., 2014).

The quenching rate constant, $k_{q/A}$ or $k_{q/D}$, is determined using the Stern-Volmer relation

Using this mechanism, Canonica et al., (Canonica et al., 2006, Canonica et al., 2000) explained that the electron transfer efficiency can possibly occur for photosensitized oxidation mechanism of all organic compounds having a one-electron oxidation potential in the same range as or lower than those of phenols.

2.3.4 Hydrogen transfer

The process of hydrogen abstraction is the most thoroughly studied in the field of photochemical reactions of aromatic ketones (Das et al., 1981, Formosinho, 1976, Lathioor and Leigh, 2001, Leigh et al., 1996). The hydrogen abstraction mechanism primarily depends on the identity of the hydrogen donor ranging from pure alkoxy-radical abstraction (Griller et al., 1981, Walling and Gibian, 1965) to one initiated by full electron transfer to the excited carbonyl compounds.

This process is mainly depend on the solvent polarity, viscosity and ability to transfer proton, dissociation energy and oxidation potential of hydrogen donor and the reactivity of carbonyl. For a specific type of photosensitizer, i.e. imidazole-2-carboxaldehyde, deactivation of its triplet state may proceed under two mechanism, electron and/or hydrogen transfer based on reduction potential of the triplet state and the solvent polarity.

The competition between the electron and hydrogen transfer was proposed to stem from increased mixing of the lowest (n-π*) triplet with the higher laying (π-π*) state (due to a reduced (n-π*)^3 – (π-π*)^3 energy gap), coupled with increasing basicity of (π-π*) state of donor substituted carbonyl triplet state. The triplet quenching mechanism of benzophenone by the hydrogen transfer from phenol were extensively studied (Canonica et al., 1995, Lathioor et al., 1999, Leigh et al., 1996). However, the hydrogen transfer can also possible for any potential carbonyl photosensitizer and hydrogen donor (Canonica et al., 1995, Formosinho, 1976).

Accordingly, the hydrogen transfer mechanism primarily proceed by forming oxygen-hydrogen bond bridge to facilitate the hydrogen transfer process by lowering both the reduction potential of carbonyl compound and the oxidation potential of hydrogen donor, as is given in the following equation (Eq. 2-8):

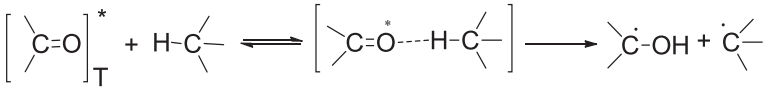

(Eq. 2-8)

As a result, hydrogen transfer is initiated by a simple charge transfer interaction that increases the acidity of hydrogen on the donor and activates its transfer.

2.3.5 Singlet oxygen generation reaction

Singlet oxygen generation is one of the important issue during photosensitized reaction. Ground state molecular oxygen exist exceptionally in a triplet form, which can quench the excited triplet state of photosensitizer to form energetic singlet molecular oxygen.

Singlet molecular oxygen can exist in two different forms, O_2 ($^1\Delta_g$) and O_2 ($^1\sum_g^+$) are spin singlet, O_2 ($^1\Delta_g$) (approximately 22.5 kcal mol^{-1} above the ground triplet state) has a sufficient lifetime to allow it to play a role in chemical reaction in solution (Clennan and Pace, 2005, Foote, 1968, Greer, 2006, Ogilby, 2010, Ragone et al., 2013). Singlet oxygen often exhibits radical-like behavior in a chemical reaction.

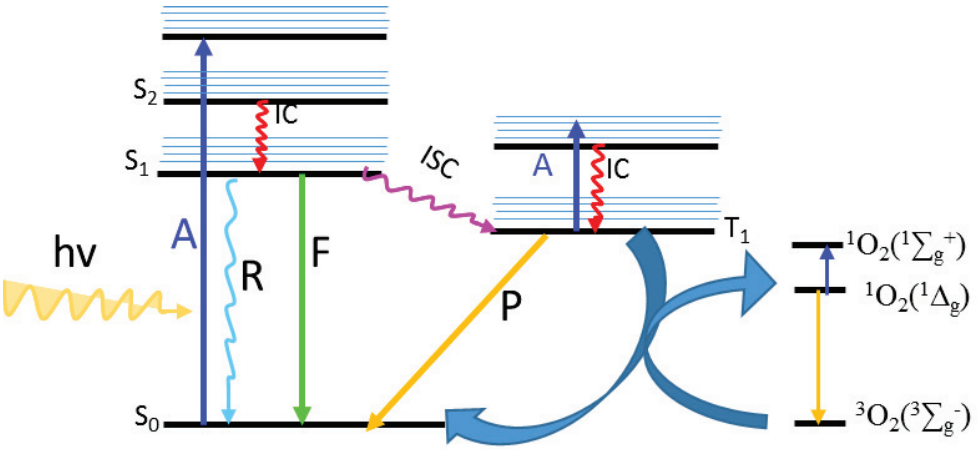

Figure 2-4 Triplet-state photosensitized production of singlet-oxygen, where S donates discrete states of the sensitizer with singlet spins multiplicity, T denotes state with triple multiplicity, and IC and ISC donates internal crossing and intersystem crossing respectively.

Accordingly, photosensitizers like IC can possibly generate molecular singlet oxygen in oxygen rich system that can potentially react with unsaturated VOCs to form peroxyl radicals during photosensitized SOA growth.

The production of singlet oxygen can be detected using different techniques; scavenging and lifetime reduction are most commonly used chemical and/or physical methods. The lifetime of singlet oxygen is 13 times longer in D_2O than in H_2O, and NaN_3 is a selective singlet oxygen quencher that can quench at the rate of $1x\ 10^6\ s^{-1}$ (the second order rate constant for singlet oxygen quenching by oxide is $5 \times 10^8\ M^{-1}s^{-1}$ (Haag and Mill, 1987).

2.4 Photosensitized reactions in the natural environments

Photochemical transformations are an important phenomenon of organic compounds in the natural environment (soil, natural water…). Photosensitizers facilitate the photochemical transformation of organic compounds. Humic substances, which are ubiquitous in nature, strongly absorb sunlight and can cause photochemical transformation of non-absorbent organic material (Burdon, 2001, Vione et al., 2006).

Humic substance (HS) absorb solar energy most often between 300 and 500 nm and generate excited triplet state (^{3}HS*) and thereby produce reactive species such as hydroxyl radical and singlet oxygen (Aguer and Richard, 1993, Aguer and Richard, 1996, Monge et al., 2012).

It has been shown in previous works that photosensitizers could also play important role in the atmosphere (Stemmler et al., 2006, Jammoul et al., 2008, Monge et al., 2012) by either promoting the chemical conversion of atmospheric gases (NO_x, O_3) at the surface of atmospheric particles (Ammar et al., 2010, Stemmler et al., 2006), generating important gases (HONO, (Stemmler et al., 2006)) or by contributing to SOA growth (Monge et al., 2012). Based on the argument that traces of carbonyl compound in the atmosphere may induce photochemical reactions, which in turns initiate formation and aging of organic aerosol, IC is the promising candidate photosensitizer that causes SOA growth and aging. This work aimed at investigating the reactions that contribute for aging and formation of

SOA using different strategies. In these previous studies, however, the exact type of molecules that could act as photosensitizers in the atmosphere were not identified. In laboratory model compounds such as humic substances or 4-BBA have been used. This work focuses on the identification of a new type of photosensitizer, which could be common in atmospheric aerosols, the characterization of its role in SOA growth, and the investigation of its reaction mechanism.

3 Experimental techniques and methodologies

Different techniques and methodology were employed in this work to investigate the photosensitized aerosol growth and aging and will be presented in this chapter according to the technique used. Two types of flow tubes, aerosol flow tubes and an organic-coated flow tube, were used to study the aerosol growth and the interaction between organic film and flowing gases (nitric oxide and VOCs), respectively. The technique used to investigate the chemical composition of aged aerosol was filter sampling followed by direct ESI-(±)HRMS and UPLC/(±)HESI-HRMS. Finally, laser flash photolysis (LFP) was used to study the excited triplet state of the photosensitizer and its interaction with quencher.

3.1 Aerosol growth studies

Aerosol growth was studied using aerosol flow reactors, in which seed particles generated by a continuous aerosol generator (section 3.1.1), dried, mono-dispersed and neutralized were introduced. The growth of the organic phase onto the seed particles inside the flow tube was then studied as a function of different parameters such as VOC concentration and type, light intensity, and photosensitizer concentration and type by using various tools such as Scanning Mobility Particle Sizer (SMPS) and Condensation Particle Counter (CPC) (section 3.1.4). A constant concentration of VOCs was generated (section 3.1.2) and introduced in the flow tube together with the seed particles. The VOC concentration change due to it interaction with seed particle was measured at the exit of the aerosol flow tube using PTR-MS (section 3.1.6). Furthermore, some gas analyzers were coupled with the flow tube to measure the formation and/or change in concentration of nitrogen oxides and/or ozone (section 3.1.5).

Unlike smog chamber experiments, involving very long residence times and many processes simultaneously, the short residences time of the aerosol flow tube allowed to investigate the very beginning of SOA growth and provided a better understanding of the processes involved. In particular, this technique allows to investigate the role of different external parameters on the process studied.

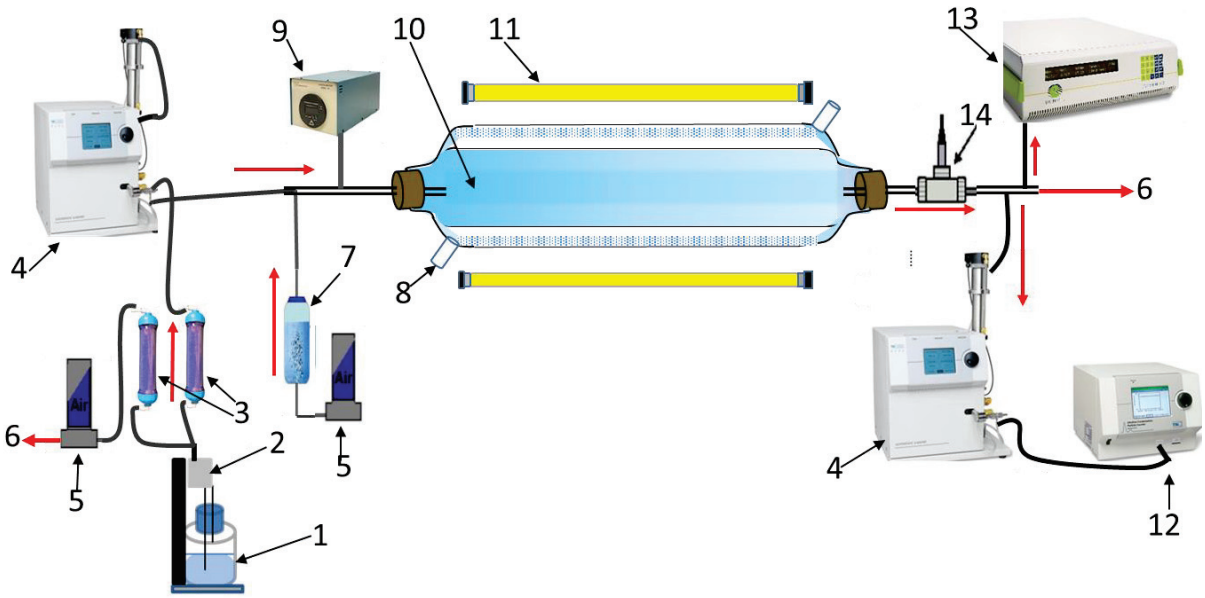

1. **Sample solution**
2. **Atomizer**
3. **Diffusion drier**
4. **SMPS**
5. **Flow controller**
6. **Exhaust pump**
7. **Humidifier**
8. **Water inlet**
9. **VOC generator (oven)**
10. **Aerosol flow tube**
11. **Irradiation lamps**
12. **U-CPC**
13. **Gas analyzer(NO_x or O_3)**
14. **Humidity sensor**

Figure 3-1 Scheme for aerosol flow tube for studying the aerosol-gas-light interaction within different contact time.

The flow reactor setup shown in Figure 3-1, allowed us to study the aerosol aging due to the interactions between gases such as VOCs, ozone or nitrogen dioxides on aerosol surface in different light conditions.

3.1.1 Seed particle generator

A spray of seed particles containing the photosensitizer to be studied was generated by a constant output atomizer (Model 3076). This device created constant number of polydispersed aerosol particles having the number diameter about 0.3 μm with a standard deviation less than 2.0, depending on the composition, concentration of the solution and the nature of solvent used as well.

The sample was prepared by dissolving the inorganic proxy (ammonium sulfate (AS, 0.95 mM) or ammonium nitrate (AN, 1.5 mM) and/or organic proxy (succinic acid (SuA, 10.5 mM) and the photosensitizer (IC, 1.3 mM) in distilled water (18 MΩ). A solution containing the compound(s) of interest was connected to the atomizer with a liquid feed tube where the liquid is drawn into the atomizing section. Compressed air was connected to the orifice of the atomizer to form a high-velocity jet perpendicular to the liquid feed. This jet atomized the liquid. The large droplets were removed by impaction on the opposite wall and the excess liquid was drained at the bottom of the atomizer assembly block to the same bottle. The fine spray left the atomizer through a fitting at the top.

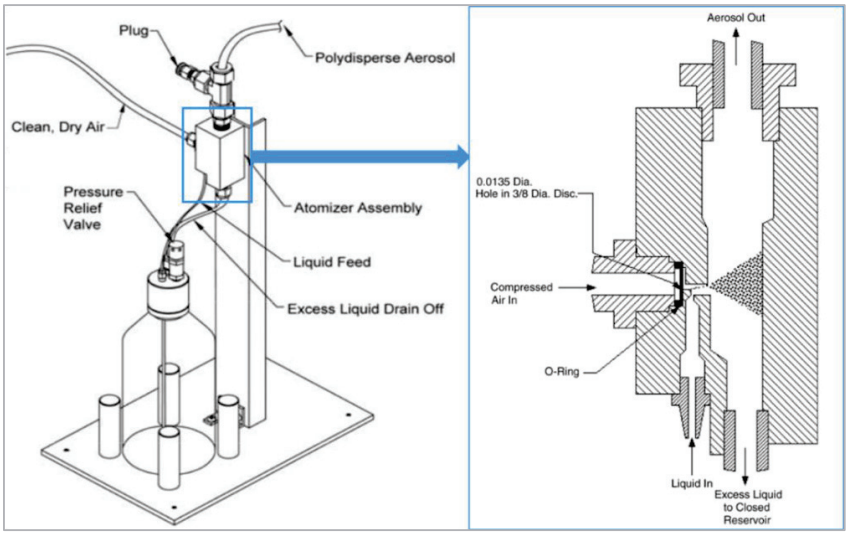

Figure 3-2 Schematic of the aerosol generator and atomizer assembly block (Model 3076).

The fine spray leaving the atomizer was connected to another bottle used to collect the larger droplets. The seed particles were introduced to the SMPS where they are neutralized and size selected through a 60 cm silica gel diffusion drier as shown on Figure 3-1.

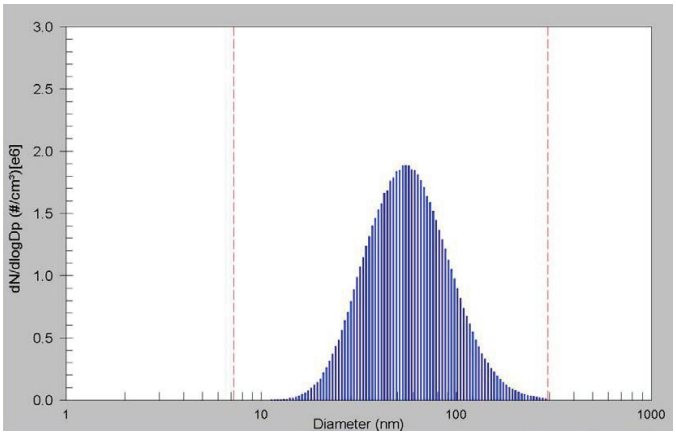

Figure 3-3 Typical number distribution of a sodium chloride aerosol atomized from 0.0001 g/cm^3 solution.

3.1.2 VOC generator

VOCs were generated by permeation tubes. The VOC generator (Metronics Dynacalibrator® Model 150) allowed to generate constant concentrations of various gases from ppbv to high ppmv, (Figure 3-4a).

The permeation device was placed in the passivated glass-coated permeation chamber house of the oven where it was heated and the gas vaporized. The temperature of the chamber was controlled to ±0.01°C. The wide range of temperature setting, 30°C to 110°C, allowed us to generate a wide range of volumetric concentration of VOC. The concentration of VOC in the flow tube can also be controlled by varying the carrier gas flow rate in the oven chamber as well as in the flow reactor.

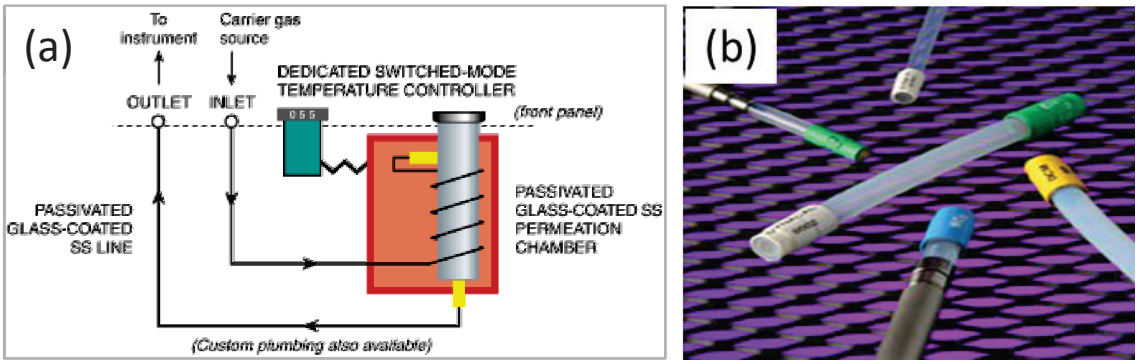

Figure 3-4 VOC generator Model 150 Dynacalibrator® from VICI Metronics: a) The permeation oven, and b) permeation tubes containing the volatile organic compound (VOC).

The permeation tube was calibrated gravimetrically through the mass loss in ng/min measured over time for a given temperature and carrier gas flow.

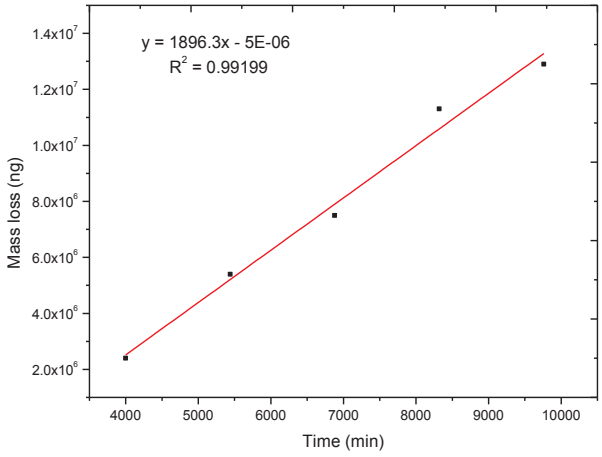

Figure 3-5 Calibration curve for limonene permeation tube at 90°C of the permeation chamber temperature and 100 ml min^{-1} carrier nitrogen flow.

The determination of a calibration curve from a given VOC proceeded, for example, Limonene, as follows; 1.25 ml of liquid d-limonene was sealed in 8 cm length of PolyTetraFluoroEthylene (PTFE) tube having PTFE rod at both end. The mass of sealed limonene was measured and placed

inside the permeation chamber house of the oven. The set point of the temperature was adjusted at 90°C and pure and dry N_2 passed through the chamber at the rate of 100 ml min^{-1} to sweep the vapor from the chamber. The mass loss of limonene was measured for different time interval. The slope of the graph (Figure 3-5) of mass loss (ng) versus time interval (min) corresponded to the permeation rate (ng/min) of the chemical compound at the specified temperature, carrier gas flow and volume of the liquid in the tube and length of the tube. The calibrated limonene permeation tube was used for other experiment in the same condition as used for calibration.

The VOC concentrations in the flow tube were determined based on the permeation rate of the tubes which was calculated as follows:

$$P = \frac{CF}{\left({}^{22.4}/_{M}\right)} \qquad \textit{(Eq. 3-1),}$$

where P is permeation rate (ng/min), C is the output concentration (ppm), F is the flow rate of the carrier gas (ml/min), and M is the molecular mass of the chemical compound placed in the permeation tube (g/mol).

The permeation constant is a function of temperature, characteristics of chemical compound and the tube properties.

$$P_G = P_G^0 e^{{}^{-E_p}/_{RT}} \qquad \textit{(Eq. 3-2),}$$

where: P_G is the gas permeability constant and P^0_G is a constant, E_p is the activation energy of the gas, R is the molar gas constant, and T is the temperature.

The only variable that can change during experimental operation is temperature. From Eq. 3-2 and if the permeation rate (P_0) of the tube is known for some reference temperature (T_0), the rate (P) at a second temperature (T) can be estimated using the following relation:

$$logP = logP_0 + 0.034(T - T_0) \qquad \textit{(Eq. 3-3)}$$

The accuracy of the calculation ±5% for a 10°C change in temperature. In this work, almost all permeation rate of the VOC were used at the reference temperature unless it is specified.

The lifetime of permeation tube (Lt in month) is an important characteristic which determined by the permeation rate, the volume to surface ratio of the tube (P in ng/min/cm) and density (ρ in g/ml) of the compound. The lifetime of permeation tube for a standard tube with ¼" OD can be estimated by using:

$$Lt = \frac{5600\rho}{P} \qquad \textit{(3-4)}$$

The permeation lifetime of limonene that we used in most experiment for this study, for instance, for the permeation rate given in Figure 3-5 with density equal to 0.8411 g/ml has service life not more than 19 months.

3.1.3 Aerosol flow tube

The aerosol flow tube is the main component in which the aerosol growth and aging was studied. The generated seed particles and VOC were introduced into a horizontal cylindrical flow tube made of Pyrex (13 cm internal diameter, 152 cm of length); surrounded by seven fluorescent lamps (Philips CLEO) with a continuous emission spectrum that allowed a homogeneous irradiation of the gas/aerosol mixture (Figure 3-6). It is equipped with Teflon stoppers and different flow controller that adjust the contact time of gas/aerosol/UV-light between 15 and 50 minutes. The total flow rate in the

flow tube(s) was between 400 and 1000 ml min^{-1}, ensuring laminar flow conditions. This implied that the contact between the particles and gases present in the reactor was efficient and not limited by diffusion.

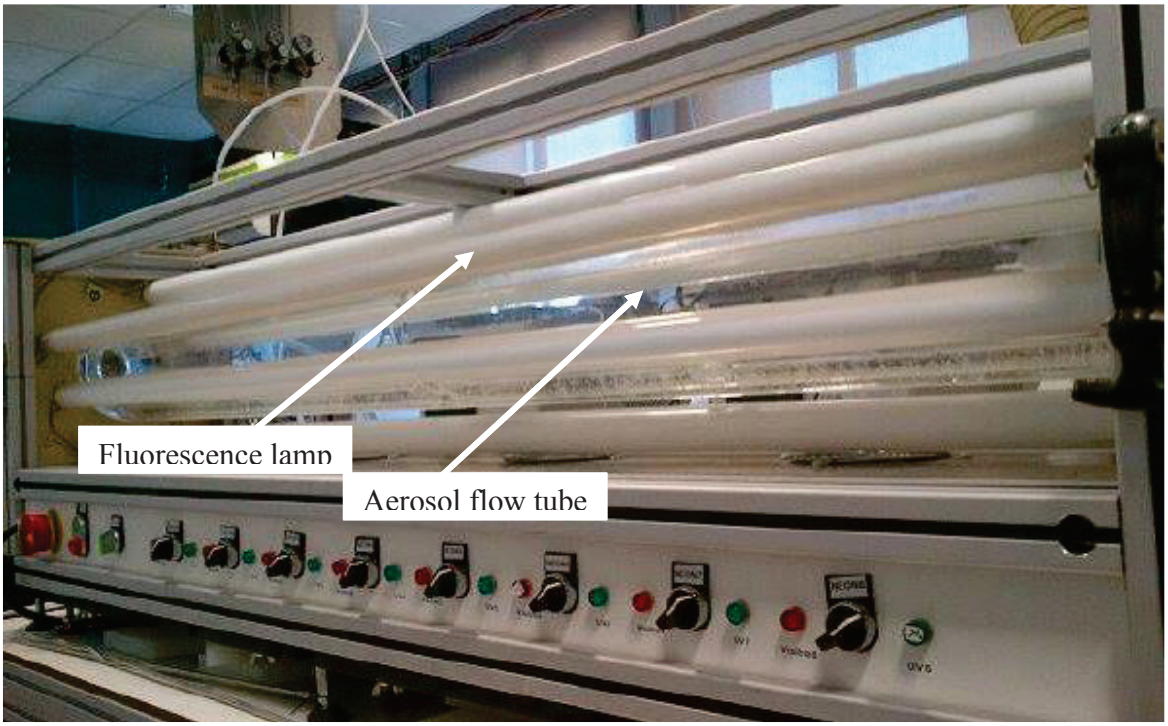

Figure 3-6 Picture of aerosol flow tube used for SOA experimental investigation.

Gas/Particle flow regime

The flow in the flow tube can be considered as laminar when the Reynolds number (Re) is less than 2000, turbulent when it is otherwise. However, for Re between 2000 and 4000, the flow may be in a transition between turbulence and laminar.

Reynolds number (Re) is a dimensionless number, which is used for characterizing the nature of flows. It can be defined as the ratio of inertial force (ρuL) and viscous force (μ) and interpreted as the ratio of twice the dynamic pressure (ρu2), and the shearing stress (μu/L) can be expressed as:

$$Re = \frac{\rho u^2}{\mu u/L} = \frac{\rho uL}{\mu} = \frac{uL}{\upsilon} \qquad \textit{(Eq. 3-5)}$$

where ρ is density (kg cm^{-3}), u – is the flow velocity (m s^{-1}), μ is the dynamic viscosity (N s m^{-2}, kg $m^{-1}s^{-1}$), L is the characteristic length of the flow reactor (m) and ν is the kinematic viscosity (m^2 s^{-1}).

For a cylindrical tube, the characteristic length is the hydraulic diameter (d_h), which will be equal to the internal diameter of the cylindrical flow tube. The Reynolds number of a cylindrical pipe, is therefore, be given as:

$$Re = \frac{\rho u d_h}{\mu} \qquad \textit{(Eq. 3-6)}$$

The density of dry air can be calculated using the ideal gas law, expressed as a function of temperature and pressure; for temperature of 298 K and 1 atm pressure, the value of density is 1.18 kg m^{-3}.

The dynamic viscosity, μ, of a circular pipe is calculated using the formula:

$$\mu = \mu_0 \frac{a}{b} \left(\frac{T}{T_0}\right)^{3/2} \qquad \textit{(Eq. 3-7)}$$

where μ is the viscosity at specific temperature T, μ_0 – is the viscosity at reference temperature T_0, a = $0.555T_0$ + C, b = 0.555T + C, and C – Sutherland constant.

For a given temperature, T = 300 K, the dynamic viscosity, μ, of dry air is 1.87 x 10^{-5} kg m^{-1} s^{-1}.

By taking the maximum total flow rate in the flow tube as 1 L min^{-1} and internal diameter of the flow tube 13 cm, the maximum speed of particle in the flow tube is equal to 1.26 x 10^{-3} m s^{-1}. The summative effect of these parameters gives the Reynolds number, Re < 50 (Re ≈ 10) which confirms

that the entire flow in the aerosol flow tube is laminar. The residence time (Rt) and the corresponding Re for consecutive experiments are given Table 3-1 as follow:

Table 3-1: Nature of flow in the aerosol flow tube for different flow rate

Rt (s)	Total flow rate ($ml.min^{-1}$)	u ($m.s^{-1}$)	Re	Flow nature
1200	1000	1.27E-03	10.0	Laminar
1800	670	8.44E-04	6.7	Laminar
2400	500	6.33E-04	5.0	Laminar
3000	400	5.07E-04	4.0	Laminar

A complementary method for the characterization of the nature of the flow of a fluid can be found in the criterion of the Péclet number (Pe), a dimensionless number in the study of transport phenomena in fluid flows, defined by the expression:

$$Pe = \frac{uL}{D_{ax}} = Re.Sc \qquad \textit{(Eq. 3-8)}$$

where D_{ax} is an axial diffusion coefficient, and Sc is the Schmidt number, is a dimensionless number defined as the ratio of viscous diffusion rate and mass diffusion rate of the fluid.

The Péclet number compares the phenomena of advection and diffusion of an analyte in a flow. This number is less than 50 for all our experimental conditions used in this study and hence axial diffusion cannot be important (Bennadji et al., 2011).

Average flow velocity

For this study, a cylindrical aerosol flow tube was used and laminar flow was observed (Table 3-1). The velocity profile of the flow in the aerosol flow tube was estimated based on the theory that the fluid velocity in a cylindrical tube is uniform in all directions. In a fully developed laminar flow, where

the velocity profile does not change downstream, the fluid particles move at a constant axial velocity along a streamline with a parabolic velocity distribution. There is no fluid particle motion in the radial direction, and thus the velocity component in the direction normal to the flow is everywhere zero. The fluid particle velocity is then zero at the surface (r = r0) and maximum at the center (r = 0) of the flow tube.

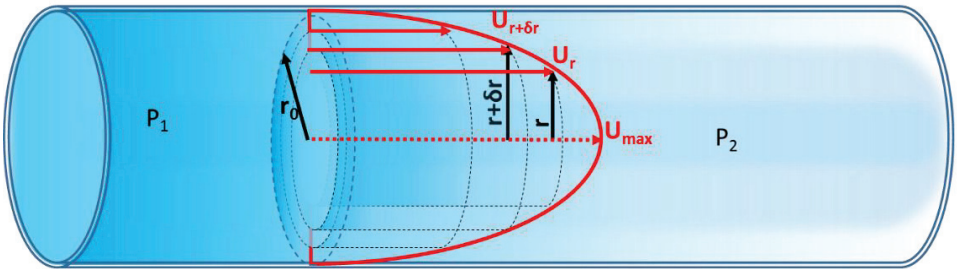

Figure 3-7 Velocity profiles as a function of reactor radius under laminar flow condition.

In a laminar flow tubular reactor, the Navier–Stokes equations, combined with the continuity equation for incompressible flow and the well-known Hagen-Poiseuille equation are used to determine the analytical solution of the parabolic velocity profile.

$$u_r = \frac{1}{2\mu}\frac{dP}{dL}(r_o^2 - r^2) = U_{max}\left(1 - \frac{r^2}{r_o^2}\right) \qquad \textit{(Eq. 3-9)}$$

where U_{max} is the maximum velocity at the center of the reactor (r = 0). By definition, the average velocity is one-half of the maximum velocity: $U_{max}=2U_{av}$), U_{av} is the average velocity, and dP is the pressure drop with the reactor length (dL).

The pressure variation (ΔP/L) along the tube can be calculated from Poiseuille's law as follows:

$$q = \frac{\pi\, r_o^4}{8\mu}\frac{\Delta P}{L} \qquad \textit{(Eq. 3-10)}$$

where q is the volume flow rate, μ is the viscosity and L is the length.

For a range of gas flow rate of 400 and 1000 ml min^{-1}, we find that the axial pressure drop is negligible: 1.8 $x10^{-5} < \frac{\Delta P}{L} < 4.5 \times 10^{-5}$ Pa m^{-1}. This pressure gradient was, therefore, not considered in this work.

Gas/ Particle contact time

The contact time, also called residence time (Rt), is the reaction time whereby the particles are directly interact with light and the gaseous species. The length (L) and the average velocity (u) of the flow in the flow reactor determine it.

$$Rt = \frac{L}{u} \qquad \textit{(Eq. 3-11)}$$

where L is the distance of the interaction between gaseous species and aerosol particles (cm); $0 \leq L \leq 152$. In this work, the average flow velocity ranges from 5.1×10^{-4} and 1.3×10^{-3} m s^{-1} that corresponds to the contact time from 20 to 50 min.

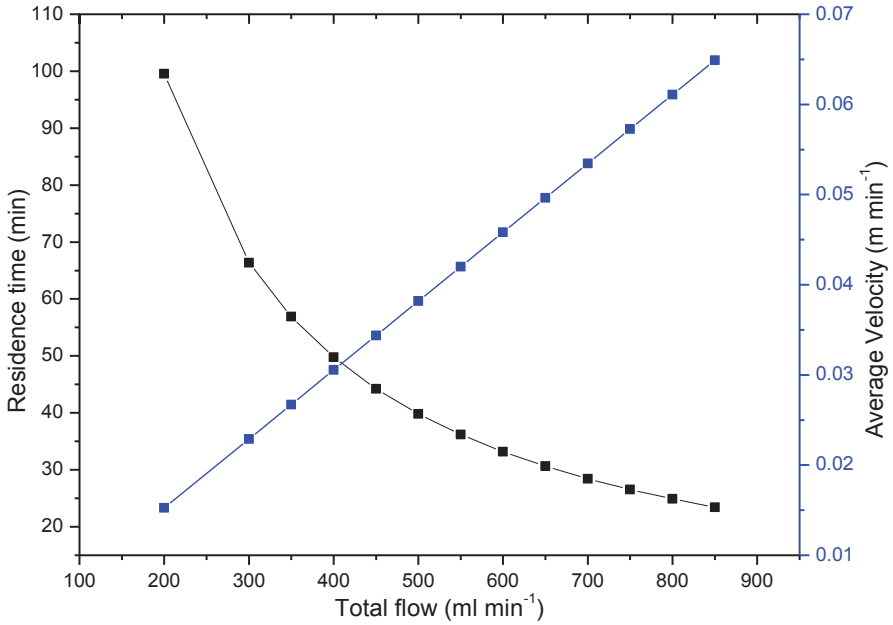

Figure 3-8 Gas/particle contact time (Black) and average velocity (Blue) as a function of total flow rate in the flow reactor.

Indeed two different type of flow reactor were used during this study. However, the difference is only in size, one with internal diameter of 8 cm and the other with 13 cm having the same length and irradiation system. These two different aerosol flow tubes allowed performing experiments in different contact time, and to attain more gas/ particle contact time, most of the results are presented here are from the bigger (i.d. 13 cm) flow tube.

Irradiation system

The fluorescence lamps mounted on the flow tube setup (Philips Cleo) emit a continuous spectrum in the near UV light ranging from 300–420 nm (Figure 3-9) with a total irradiance of 3.31×10^{16} photons cm^{-2} s^{-1}. The spectrum of actinic flux in the flow tube was measured using a calibrated radiometer connected to a receiver (Hofzumahaus et al., 1999).

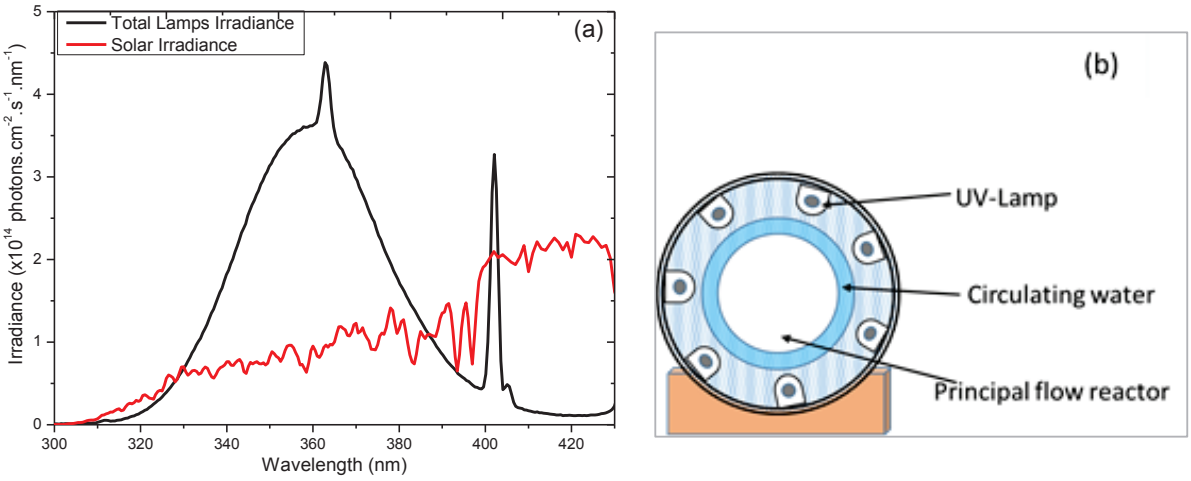

Figure 3-9 Irradiation system in the flow reactor: (a) with all 7 lamps irradiance in the flow tube (Black) when it is compared with solar light total irradiance (red); (b) Cross-sectional view for the arrangement of lamps around the flow reactor.

In Figure 3-9a, the total lamps intensity inside the aerosol flow tube compared with solar light intensity. The arrangement of lamps around the flow reactor is shown in Figure 3-9b. The intensity of each lamps in the flow reactor was measured by turning on and off the lamps.

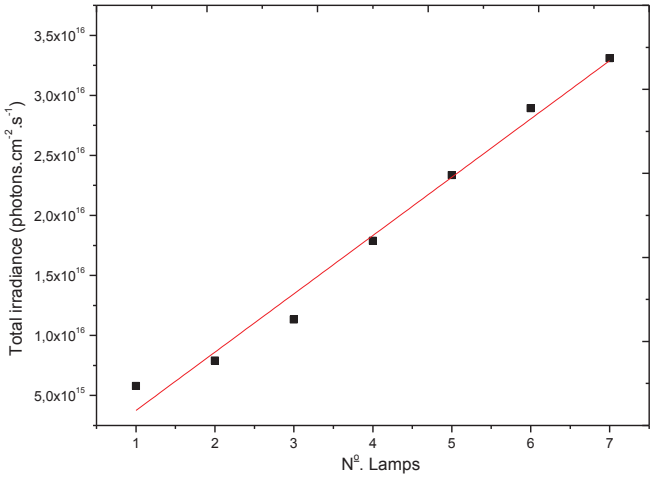

Figure 3-10 Total irradiance for different number of lamps in the flow tube.

Temperature and humidity control system

The temperature inside the flow reactor was controlled by water circulation through the outer jacket of the reactor using a thermostat (Model Huber CC 405). The temperature was kept constant at 293±2 K and is important to simulate atmospheric temperature.

The relative humidity of particles in the flow reactor was controlled using a device for saturating the carrier gas. The carrier gas, which is similar to particle carrier gas, was passed through a bubbler bottle containing pure water (Milli Q, 18 MΩ). The bubbler bottle is thermostated with a circulating water at the same temperature as the flow reactor. However, the temperature of circulating water might be changed depending on the amount of relative humidity needed.

The relative humidity (RH) in the system was varied by varying the flow rate of gas to the bubbler and by changing the temperature of circulating water around the outer jacket of the bubbler. A humidity sensor (Meltec UFT 75-AT, Germany) was connected at the exit of the flow reactor that allowed us to monitor and see the effect of the relative humidity and it also helps us to control the temperature of the flow reactor. Thus, in the flow reactor, the aerosol particles was exposed to the gas stream containing appropriate humidity that varied between 0 to 50 %.

3.1.4 The aerosol Instrumentation, SMPS-DMA-UCPC

The aerosol flow reactor was coupled with different aerosol analyzers, placed at the entrance and exit of the reactor (*Figure 3-1*), which will give us the necessary information on the number of aerosols (CPC) and their size distribution (SMPS). These instruments can give us information about the gas-particle surface interaction thereby to predict the growth and aging reaction mechanism of SOA.

Principles and function of Scanning Mobility Particle Sizer (SMPS)

Two SMPS were connected just after the seed generator and at the exit of the flow reactor. The first SMPS connected just after the seed generator allowed us to neutralize seed particles and select the particle size of interest for investigation. It also provides information about the flow rate of aerosol to the flow reactor. The polydispersed seed particles sample enters to SMPS that passes through Kr-85

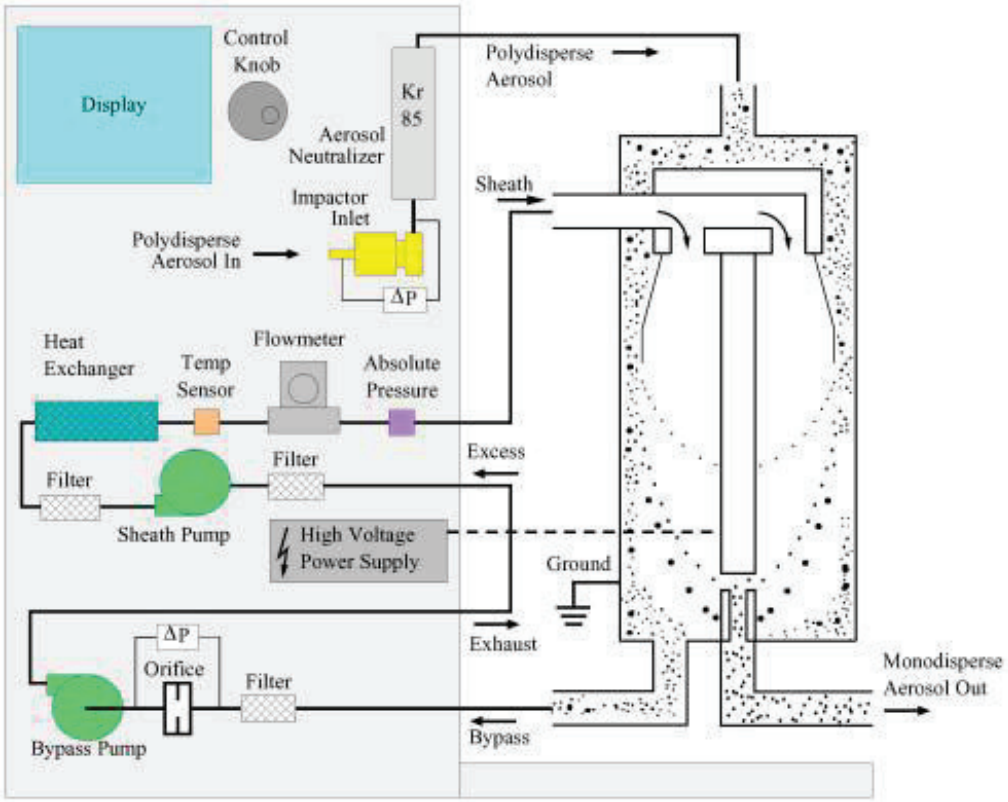

Figure 3-11 Scheme for operating principle of the SMPS with the DMA model 3081.

neutralizer to obtain equilibrium charge distribution of aerosol particles (Fuchs, 1963, Wiedensohler, 1988). The charge neutralized spray then enters to the DMA having two cylindrical column as seen in Figure 3-11. The seed particles and the sheath air are introduced at the top of the column downwardly through the space between the two columns. The clean sheath air flow used to ensure a laminar flow and to selectively protect the central electrode. The inner cylinder will be maintained at

a negative voltage controlled while the outer cylinder is connected to ground thereby creating an electric field between the two cylinders. This electric field will accelerate the positively charged particle along the field line. The particles are then precipitated along the column. Place of precipitation of these particles will depend on their electrical mobility, Zp, defined as:

$$Z_p = \frac{neC}{3\pi\mu D_p} \qquad \textit{(Eq. 3-12)}$$

where Z_p is the electrical mobility, n is the number of charge on the particles, e is the elementary charge, C is the Cunningham slip correction, μ is the dynamic viscosity of air, and D_p is the radius of the particles.

The electrical mobility of particle is dependent mainly on charge and particle size. Each voltage value corresponds to a certain electrical mobility of particles and therefore a certain diameter. Particles with a high electrical mobility (the smaller particles) will be collected on top and those having a lower electrical mobility (the larger particles) will be collected on the lower part of the bar (Figure 3-11). The particles comprised in the narrow range of mobility will be piloted to the output of the column giving a monodisperse aerosol stream. One can therefore draw monodispersed particles to the flow reactor for further analysis.

The second SMPS having the same working principle but operated differently was connected at the end of the flow tube to measure the size change in the range of 14 to 750 nm. It was then connected to the CPC to measure the concentration of particles.

Principles and function of Condensation Particle Counter (CPC)

The CPC we used for this study was UCPC (Ultrafine condensation particle counter). UCPC is the aerosol instrument that can continuously count particles ranging from 2.5 to 3000 nm in diameter in

real time. The working principle of this CPC is the aerosol sample drawn continuously through heated saturator in which the alcohol is vaporized and diffuses to the sample stream then pass into a cooled condenser where the alcohol vapor becomes supersaturated and ready to condense. The alcohol is then condense on the aerosol particles to obtain drops of the same size and large enough to be easily taken into account by the optical detector. The alcohol is pure 1-butanol.

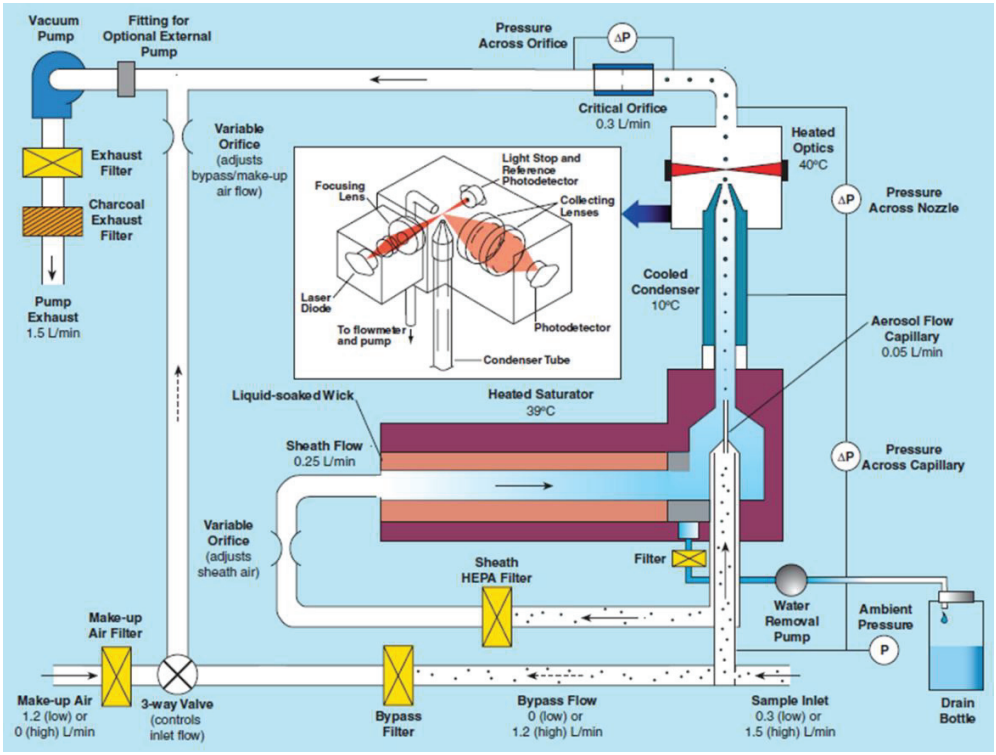

Figure 3-12 Schematic representation for the function of UCPC-3776.

When these droplets cross a laser beam of light optic, each droplet scatters light onto a nearby photo diode. These signals are continuously counted and are displayed in particles.cm^{-3} each second on the LCD. These particle counts were then stored and transmitted to an external data acquisition device.

3.1.5 Gas analyzer instruments

In order to control and analyze the evolution of gases, either by addition or production, in the aerosol flow tube, two types of gas analyzer was connected at the exit of the flow tube. These allowed us to monitor the presence or absence of oxidants (NO_x, and ozone) that contribute to the SOA aging. In addition to this, it is also important to monitor the evolution of gases in the presence of aerosol particles.

NO_x Analyzer

The CLD 88 nitrogen oxide analyzer (ECO PHYSICS CLD 88 cyp) or Thermo Environmental 42C was connected at the outlet of the flow reactor in order to make possible the continuous measurement and monitoring of NO-NO_2 concentration change during photochemical reactions. The NOx analyzer is based on the optional molybdenum convertor (Figure 3-13).

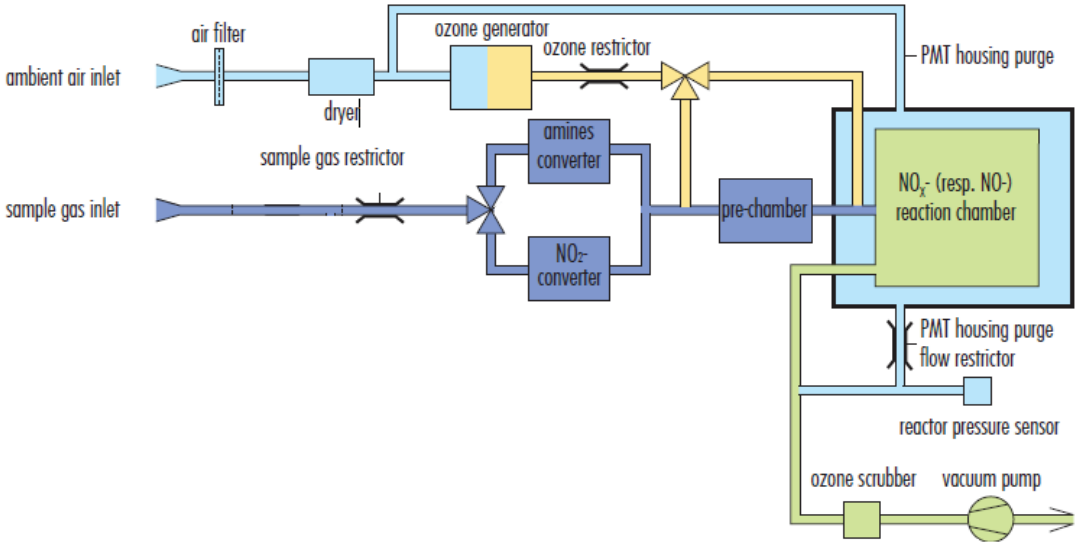

Figure 3-13 Scheme for working principles of NOx Analyzer (Eco physics CLD 88 cyp).

In this type of analyzer, the sample is introduced through the inlet and divided into two identical flows; amines convertor and NO_x convertor. On the other hand, dry ambient air passes through air filter to the ozonator that can generate the necessary concentration of ozone need for the chemiluminescent reaction. The ozone reacts with NO in the ambient air sample to produce electronically exited NO_2 molecules. The photomultiplier then detects the NO_2 luminescence. The minimum detection limit of this type of analyzer is 0.05ppb which mainly depends on the filter setting.

Ozone analyzer

THERMO ENVIRONMENTAL 49C model is a double-optical bench based on the principle of UV absorbance was used for this study. It comprises two sensors and two identical optical measuring cells, A and B, which each have a length of 37.84 cm (Figure 3-14). The UV radiation is emitted by a mercury vapor lamp at low pressure.

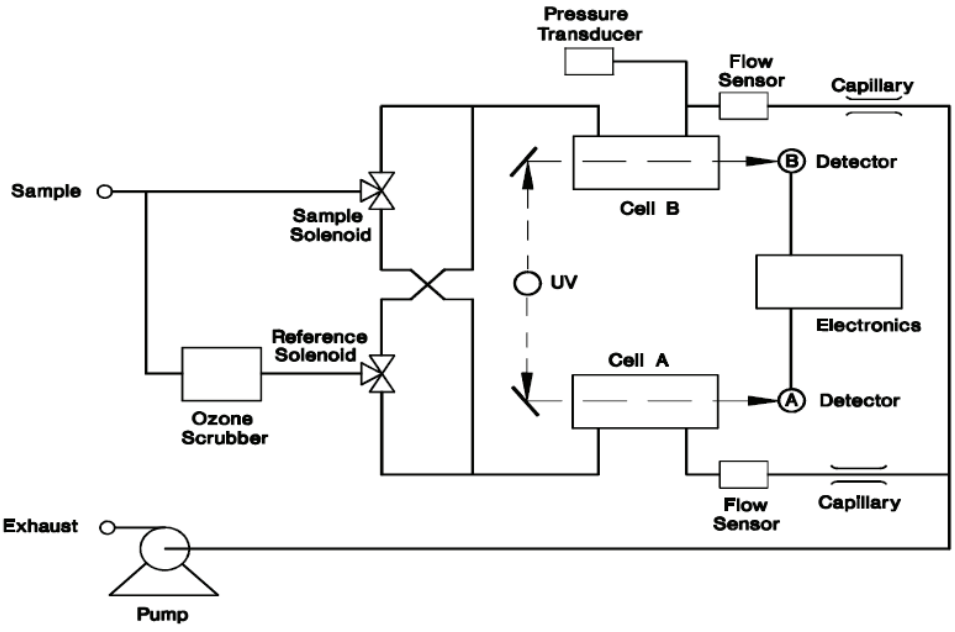

Figure 3-14 Flow schematic in the ozone analyzer (Thermo Environmental 49C).

The sample is separated from its entry into two identical streams, sampling being performed by an internal pump. The first pass through a trap for ozone in manganese oxide (also known as converter or scrubber) to become the reference sample. It is then passes through the "reference" solenoid. The second stream is sent directly to the "sample" solenoid. Both solenoid valves send the reference gas and the sample gas alternatively in the cell A and B by switching the two solenoid valves, with a periodicity of 10 s. Thus, when the cell A contains the "reference" gas, the cell B contains the "sample" gas and vice versa.

The UV light intensity of each cell are measured by detectors A and B, and calculate the ozone concentration for each cell and output the average concentration to both. The detection limits of this analyzer is 1ppbv.

3.1.6 Proton Transfer Reaction Mass Spectrometry (PTR-MS)

Proton-transfer-reaction mass spectrometry (PTR-MS) allows real-time measurements of volatile organic compounds (VOCs) in the aerosol flow tube with a high sensitivity and a fast time response. The advantage of PTR-MS is the possibility to rapidly measure online the VOCs which are not consumed while the photochemical reaction takes place. In this study, the PTR-MS was connected with the outlet of aerosol flow reactor to measure the amount of VOC consumed or condensed on the aerosol particles by performing dark and light measurement as well as direct measurement from VOC generator. For those three measurements, the amount of VOCs involved for aerosol growth feasibly estimated.

The simplified representation of PTR-MS is given in the following scheme, Figure 3-15:

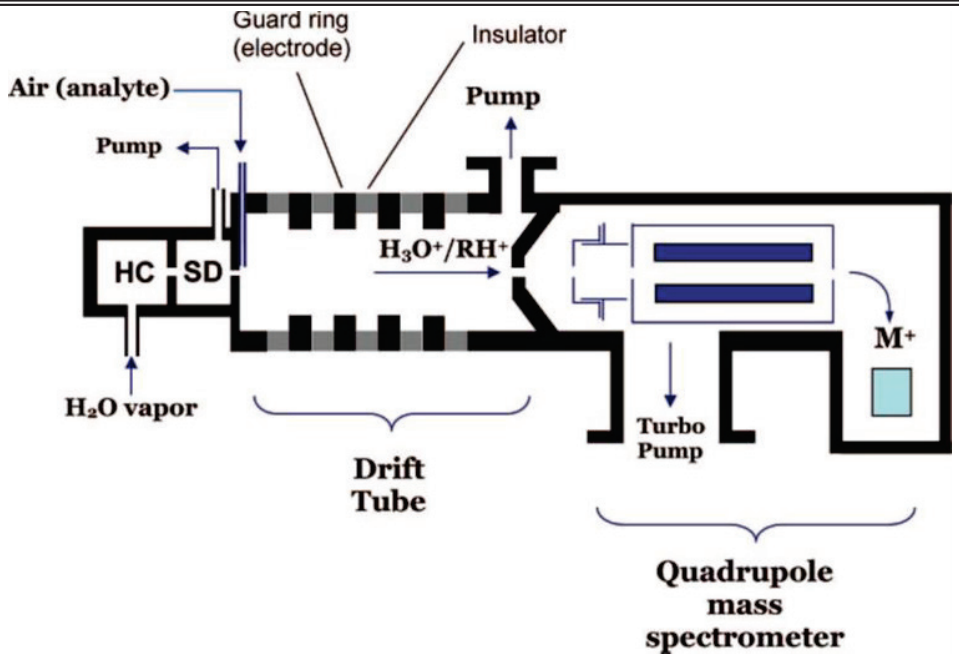

Figure 3-15 Simplified PTR-MS operational scheme utilizing a quadruple mass filter: HC - hollow cathode discharge source and SD - source drift region.

H_3O^+ is the proton donor most commonly employed in PTR-MS, ideally generated in the ion source as pure H_3O^+ and reaction of this ion and the organic gases in the analyte gas can only be considered. For the reaction with only single organic gas, for instance, designated by R, proton transfer to R can yield RH^+, only if the proton affinity of R is higher than the proton affinity of H_2O. However, unreacted water vapor may present in the ion source which inevitably leads to the formation of cluster ions of the type $H_3O^+(H_2O)_n$.

$$H_3O^+ + R \rightarrow RH^+ + H_2O \qquad (R.\ 3\text{-}13)$$

3.2 Aerosol composition analysis methods- Mass Spectrometry

It is crucial to know the aerosol composition to predict the reaction mechanism of SOA growth and aging in the flow tube.

The technique used for investigating the aerosol composition was filter sampling method which in turn bulk and flow tube experiments were performed to identify major products of the reaction by direct (±)ESI-HRMS and UPLC/(±)HESI-HRMS analysis. Two ways of investigation were employed: static bulk experiment and filter sampling by collecting aerosol particles at the flow tube outlet on a Teflon filter.

3.2.1 Static bulk method

A water/acetonitrile (50/50) solution containing VOC and photosensitizer was placed in a small cylindrical quartz reactor (Volume of 15 ml) and exposed to light in a box equipped with 7 UV lamps having the same range as seen in Figure 3-9 for 23 hr. At different time interval, samples were taken for direct analysis in (±)ESI-HRMS and analysis by UPLC/(±)HESI-HRMS.

3.2.2 Aerosol filter sampling

The aerosol filter sampling was performed by collecting particles on a Teflon filter (47 mm Fluoropore membrane filters, 0.45 μm FH, Merk Millipore, U.S.) using a stainless steel filter holder (Aerosol standard filter holder, 47 mm, Merk Millipore, U.S.). Two consecutive experiments were undertaken, the blank experiment where both seed particle containing photosensitizer and gaseous VOC are introduced in the absence of light, and the second sampled with UV light in the flow reactor in order to compare the composition variation in light and dark condition for the same other experimental conditions.

The collected aerosol samples were subsequently extracted using an appropriate solvent (water/acetonitrile) under ultra-sonication (40 min). The extraction was kept under low temperature in an ice bath to avoid temperature initiated distraction and reaction. The extracts were then

concentrated by gentle streaming of nitrogen over the solution followed by subsequent analysis by UPLC/(±)HESI-HRMS.

3.2.3 ESI-(±)HRMS and UPLC/(±)HESI-HRMS Analysis

The UPLC/(±)HESI-HRMS system comprised a Dionex Ultimate 3000 ultra-performance liquid chromatograph (UPLC, Thermo Scientific, U.S.) coupled to a Q-Exactive high resolution mass spectrometer (HRMS, Thermo Scientific, U.S.) equipped with a heated electrospray ionization (HESI) source. In this study, the sample solutions prepared in water/acetonitrile solvent were analyzed in two compartments. Half of the samples were analyzed by direct infusion of the diluted solutions into the non-heated electrospray ionization source (ESI-(±)HRMS analysis) at a flow rate of 30 μL min^{-1}. Source voltages of +3.5 kV and -2.6 kV were applied for the positive (+) and negative (-) ionization modes, respectively. The remaining fraction of the samples were analyzed by means of UPLC/(±)HESI-HRMS. The chromatograph was equipped with a HSS T3 Acquity UPLC column (1.8 μm, 2.1 × 100 mm). The mobile phase was (A) acidified water with 0.1%, v/v, formic acid, and (B) acidified acetonitrile with 0.1%, v/v, formic acid. A 16 min gradient was applied: eluent (B) was kept at 1% for 2 min and was then increased to 90% in 10 min, this ratio was maintained for 2 min before returning to the initial condition for 2 min. The flow rate was 0.3 mL min^{-1}.

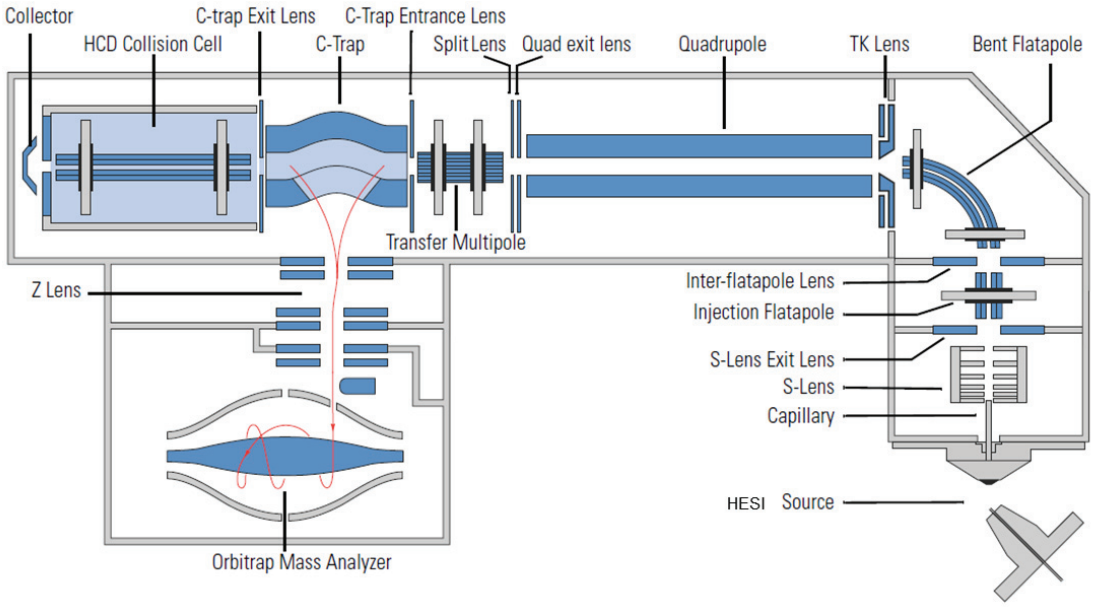

Figure 3-16 scheme for ESI-(±)HRMS and UPLC/(±)HESI-HRMS Analysis.

Source voltages of +3.7 kV and -3.0 kV were applied for the positive (+) and negative (-) ionization modes respectively. All acquisitions were performed in full MS mode with a scan ranging from m/z 50 to m/z 750 and a resolution set to 140 000. Specific MS2 spectra were acquired in direct infusion mode applying a normalized collision energy level of 35%. The data collected from both bulk and aerosol sample were processed using Xcalibur 2.2 software. The Q-Exactive mass spectrometer was calibrated achieve good accuracy for low masses.

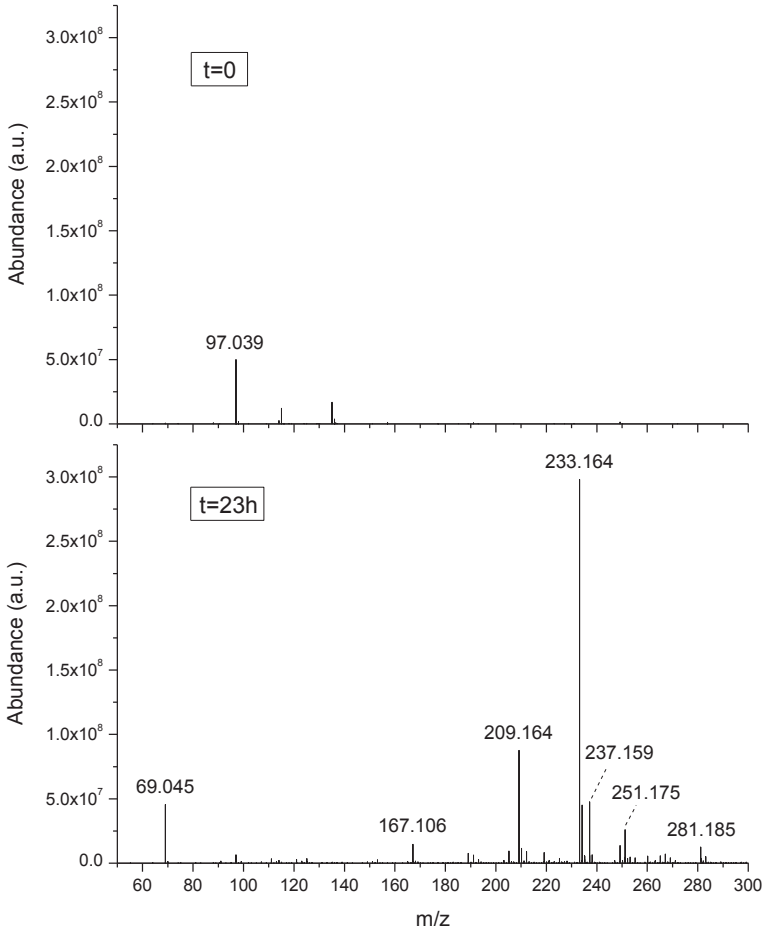

Figure 3-17 The typical average mass spectra obtained in (±)ESI-HRMS for bulk experiment at initial time and after 23 h of irradiation (average on ca. 70 spectra on 1 minute acquisition time in direct infusion). Inset: time evolution of m/z 233.164 abundance.

All of the exact mass assignments to chemical formula were done considering carbon, hydrogen, oxygen, nitrogen, sodium, and potassium as potential elements and with a mass accuracy below 4 ppm. All of the proposed chemical formulas comply with the octet rule for the related neutral compounds.

3.3 Organic coated flow tube

The organic coated flow tube, 1.1 cm i.d. x 20 cm length, was used to study the interaction between photosensitizer film and nitric oxide (NO) in the presence or presence of gaseous limonene. The organic film was prepared in a cleaned flow tube by pouring ethanol solution of 4-benzoylbenzoic acid (4-BBA) and adipic acid (AA) and rotating using a rotating machine. The sample was dried by evaporating the solvent at ambient temperature and pressure. The rotating machine helps to attain the homogeneity of the organic film throughout the flow reactor.

The mixing proportion and concentration of the organic compound in ethanol is given in Table 3-2.

Table 3-2 The mixture ratio of 4-BBA and AA used for preparing thin film in the flow reactor

No.	4-Benzoylbenzoic acid		Adipic acid	
	Mass (g)	Concentration (mM)	Mass (g)	Concentration (mM)
1	0.05	2.76	0	0
2	0.025	1.38	0.025	2.14
3	0.017	0.92	0.033	2.85

The amount of coated organic mass was obtained by weighing the tube before and after deposition. Masses from 0.5 to 2 mg were measured with an electronic balance (Mettler AG204 Deltarange).

Nitric oxide (NO, 1.01 ppmv) was passed through the photosensitizer coated flow tube using moveable injector.

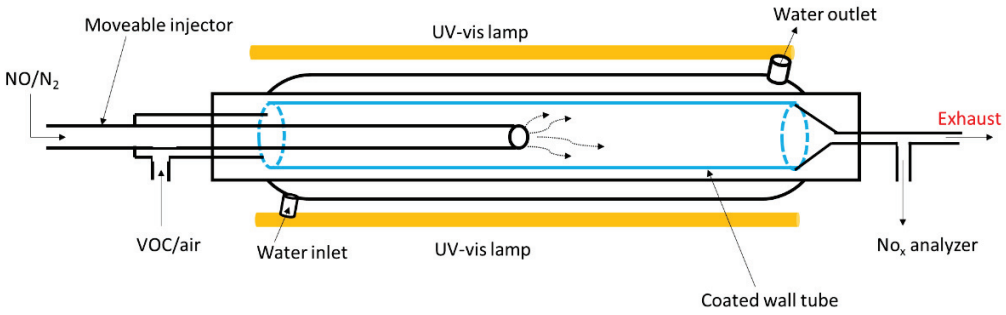

Figure 3-18 Schematic representation of the horizontal coated-wall flow tube experimental approach used to measure the NO concentration change on solid organic film (photosensitizer and/or organic acid.

The NO and NO_2 concentration change due to the interaction with the coated-wall of the flow tube in the presence of light and VOC was monitored using NO_x-analyzer ((ECO PHYSICS CLD 88 cyp). The change in concentration for NO and NO_2 due to surface reaction was measured for different residence time by the help of moveable injector.

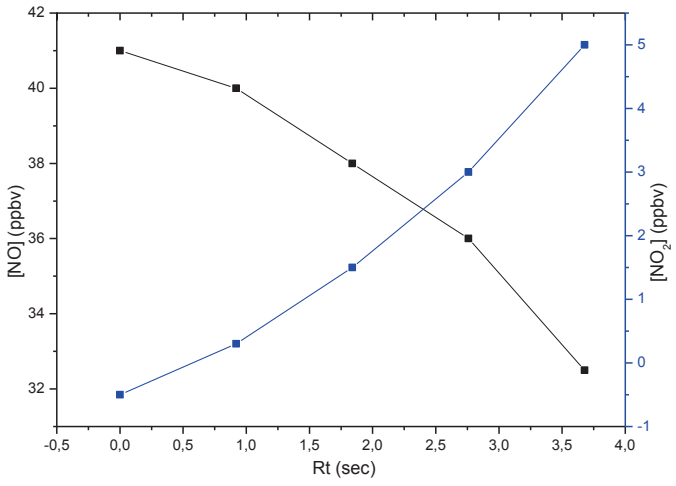

Figure 3-19 The NO/NO_2 conversion and concentration change for different contact time of NO gas to the solid organic film; black dot corresponds to [NO] change and blue dot represents [NO_2] change.

3.4 Laser Flash Photolysis (LFP)

The laser flash photolysis was a technique used to study the excited triplet state of a compound. It relies on the use of energetic fast pulsed laser that can cause photolysis and excitation of molecular entities. The duration of the laser pulse can vary between one microsecond and up to few femtoseconds.

3.4.1 Description of the experimental setup

The laser flash photolysis experimental setup used for our experiments consists of a high power Nd-YAG laser (II Surellite Continuum model Mark). It can work at 1064 nm and all its harmonics 632, 355 and 266 nm, the photolysis excitation source wavelength of 266 nm having a pulse width of 7 ns operated in the single-mode was, however, used in this study. The excitation wavelength was chosen depending on the absorption maximum of the compound used. For this study, IC that can absorb nearly at 290 nm coupled with other compound was studied using laser flash photolysis. The excitation energy of the laser was limited between ~ 15 – 20 mJ per pulse to have maximum possible photolysis of the compound used and to avoid interferences of its products. The laser power was monitored approximately before every experiments.

The Laser photolysis setup has two major components, the excitation laser and the analyzing lamp (Figure 3-20).

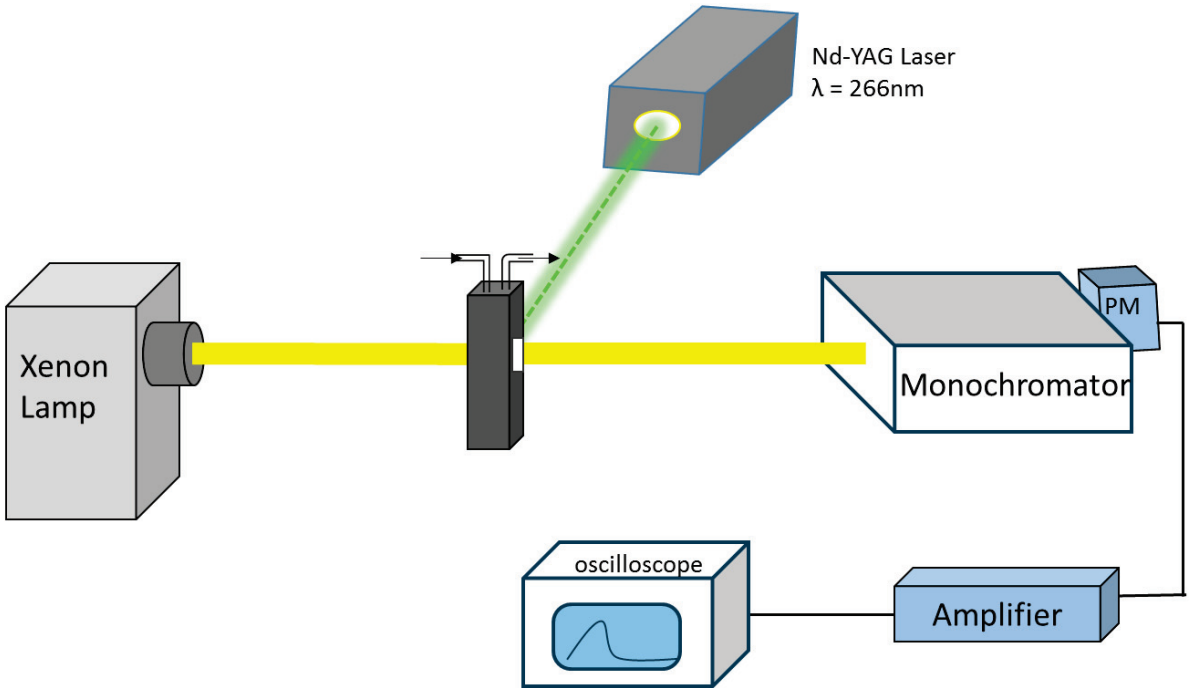

Figure 3-20 Experimental setup used for laser flash photolysis

The laser output passed through the aperture in the short axis (4 mm path length) of a fully masked quartz flow cell (1 cm x 1 cm), mounted at 13 cm of the laser output. The solution containing the compound of interest, IC, was introduced in the flow cell of 450 µL by means of a peristaltic pump, with a flow rate of 1.6 mL min^{-1}. This limited the exposition of the introduced solution to 3–4 laser shots and maintained a constant temperature in the flow cell. The flow connections were made by either glass or PTFE tubing. The analyzing light, provided by a 75 W high-pressure Xenon arc lamp (LOT-Oriel brand), passed through the two apertures of the long axis of the flow reaction cell of 1 cm optical path length. The light was then collected by a ¼-m monochromator (Spectral Products DK240) equipped with a 2400 grooves/mm grating and detected by a photomultiplier (Hamamatsu H7732-01). The signal was passed through a high-speed current amplifier (Femto) and the AC component recorded on a 300 MHz oscilloscope (Tektronix TDS3032c). The digitalized signal was then transferred to a computer for further processing.

The sample was prepared by dissolving known amount of the compound in pure water (Mili Q 18 MΩ) or pure water-acetonitrile (60/40 ratio) mixture depending on the compound we need to analyze. The freshly prepared sample solution was then degased with a continuous and constant streaming of nitrogen before (1 h) and during the experiment. All experiments were performed under ambient temperature and pressure.

3.4.2 Principles and data analysis

The raw data collected from the oscilloscope are treated based on Beer-Lambert law of absorption.

$$Abs = \log\left(\frac{I_o}{I}\right) \qquad \textit{(Eq. 3-14)}$$

By taking the proportionality between signal voltage amplitude and intensity, the absorbance was calculated from the signal amplitude of the measured value. By plotting the absorbance versus time, the absorption decay rate constant of excited triplet sate of the compound was estimated by using the following single exponential fitting function that correspond to the first order kinetics.

$$Abs_t = a + be^{-k^I t} \qquad \textit{(Eq. 3-15)}$$

where k^I is the first order rate constant and a and b represents the offset of absorbance and initial time, respectively.

The deactivation rate constant (k_Q) due to the presence of reactive excited triplet state quencher (Q) in the solution was determined by taking the pseudo-first order rate constant and the concentration of the quencher (Q). The decay rate under the influence of excited triplet state quencher is then defined by the triplet Stern-Volmer equation as follow:

$$k^I = k_q[Q] + {}^1/_{\tau_0} \qquad \textit{(Eq. 3-16)}$$

The decay rate constant of the observed intermediate (k^I) increases linearly with the quencher concentration [Q]. Thus, the quenching rate constant (k_q) and the lifetime in which the time spent by the molecule at its excited state (τ_0) are determined as slope and intercept, respectively, obtained from a series of kinetics experiments by varying [Q]. The solution was prepared at low concentration to reduce self-quenching of the compound called photosensitizer.

3.5 Chemicals

VOCs were generated from commercially available monoterpenes; limonene (Aldrich, 97%), α–pinene (Aldrich- 98%). and β–pinene (Aldrich- 98%), isoprene (Aldrich ≥ 99%) and toluene (Chimieplus ≥ 99%).

Different photosensitizers or sources of photosensitizers were used for this study. Glyoxal (0.1M Aldrich, 40% w/w in water) was used as a source of light absorbing later called photosensitizer. To identify the more efficient photosensitizer produced from the glyoxal condensed phase chemistry, 1H- imidazole (IM, Aldrich ≥99%), 1H-imidazole-2-caboxaldehyde (IC, Aldrich 99%), and 2,2-bi-1H-imidazole (BI) were used as photosensitizer. In addition to this, 4-Benzoylbenzoic acid (4-BBA, Aldrich 99%), the well-known photosensitizer, was used to compare the photosensitizing effect of glyoxal reaction products in the flow tube experiment.

In this study, commercially available AS (Aldrich, ≥ 99%), AN (Aldrich, ≥98%), succinic acid (Aldrich, ≥99%) and adipic acid (Aldrich, ≥99.5%) were used as source seed particles for the flow tube experiments.

To investigate the involvement of singlet oxygen for the aerosol growth reaction mechanism, singlet oxygen quencher, sodium azide (NaN_3, Aldrich ≥99%) and nickel chloride ($NiCl_2 \cdot 6H_2O$, Merck ≥98%) as used. Cyclohexane (Merck, >99%) was also used as OH radical quencher.

Carrier gases and ozone generation

Carrier gas is the gas flow that is used to generate and carry aerosol particles and sweeping the VOC from the VOC generator to the flow tube. Pure compressed N_2 contain 50 ppbv of O_2, pure compressed O_2 and synthetic air from a cylinder (purity 99.9990%) were used as a carrier gas.

Ozone is generated by a device using mercury lamp (185 nm) illuminating a quart tube in which pure oxygen or synthetic air circulating. Depending on the length of lamp exposure and flow rate of air used, the ozone concentration can be adjusted.

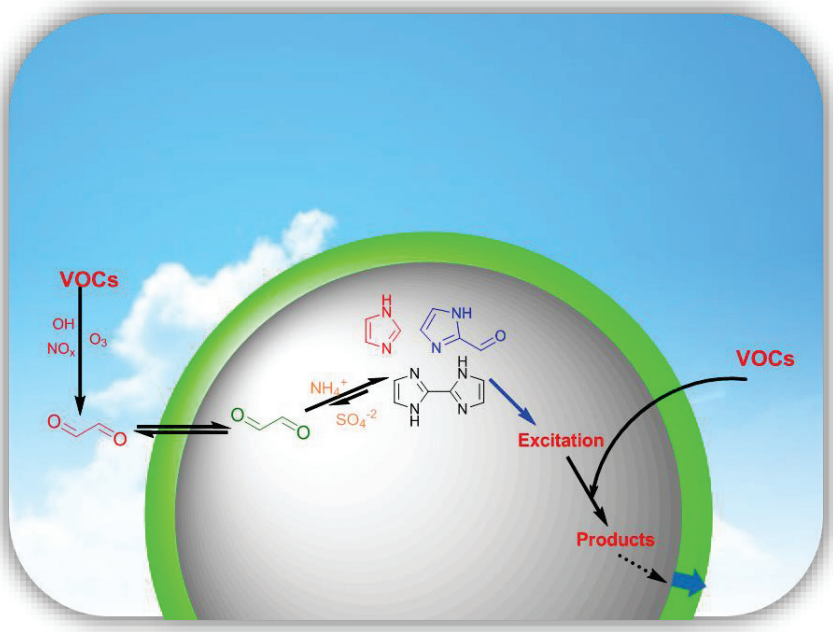

4 Investigation of IC photosensitized aerosol growth

In this chapter, we present an experimental study of the interaction of glyoxal and/or its condensed phase reaction products with atmospheric volatile organic compounds, and surfaces of aerosol particles that induce aerosol growth. The aerosol growth from glyoxal and/or its reaction products in the presence of VOCs was studied as a function of several parameters:

- glyoxal reaction time in the seed particles
- concentration of photosensitizer
- concentration of VOCs
- type of VOCs
- irradiation time and intensity
- relative humidity
- presence and concentration of NO-gas

The results allowed to propose a reaction mechanism to account for the photocatalytic SOA growth and estimate its potential impact in the atmospheric.

4.1 Glyoxal based Autophotocatalytic SOA growth

4.1.1 Photo-catalytic effect of Glyoxal

The UV – visible absorption spectra for IM, IC and BI have been measured in this study and are shown in Figure 4-1.

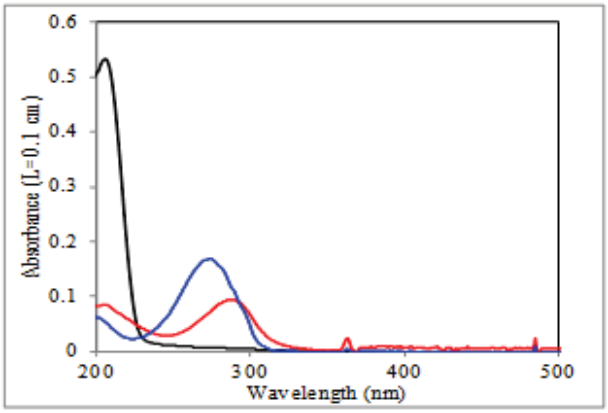

Figure 4-1 UV-VIS spectra of major light absorbing glyoxal condensed phase reaction products: IM (Black), IC (Red) and BI (Blue).

It is showed that IC is the compound absorbing at longer wavelength, with λ_{max} = 289 nm in solution. However, its absorption extends to 325 nm, making photo-induced reactions possible both in the real atmosphere and in the aerosol flow tube system used in this work, where light is emitted beyond 300 nm.

The growth of SOA on ammonium sulfate (and/or succinic acid) seeds was studied in the flow reactor. In the first series of experiment, glyoxal (Gly, 0.1 mM) was added to the seeds containing ammonium sulfate (AS, 0.95 mM) and succinic acid (SuA, 10.6 mM) to investigate its role in these

processes and the particles were exposed to 1.8 ppmv of limonene in the flow tube. In this experiment, succinic acid was used as a proxy for the organic fraction of atmospheric particles, thus allowing for more "realistic" conditions. In some experiments, the seeds were produced from freshly mixed solutions while in others the solutions were left to react for 24 h after the addition of glyoxal with continuous stirring, all other conditions being identical. According to the literature (Nozière et al., 2009, Shapiro et al., 2009, Yu et al., 2011), the condensed phase reaction between glyoxal and ammonium sulfate accelerated by higher pH. In most glyoxal experiments, the pH of the seed solution was adjusted to 9 by adding small amount of 2M NaOH solution. In some cases, the pH was left at 5.6 to study the effect of this parameter on SOA growth. The results are presented in Figure 4-2.

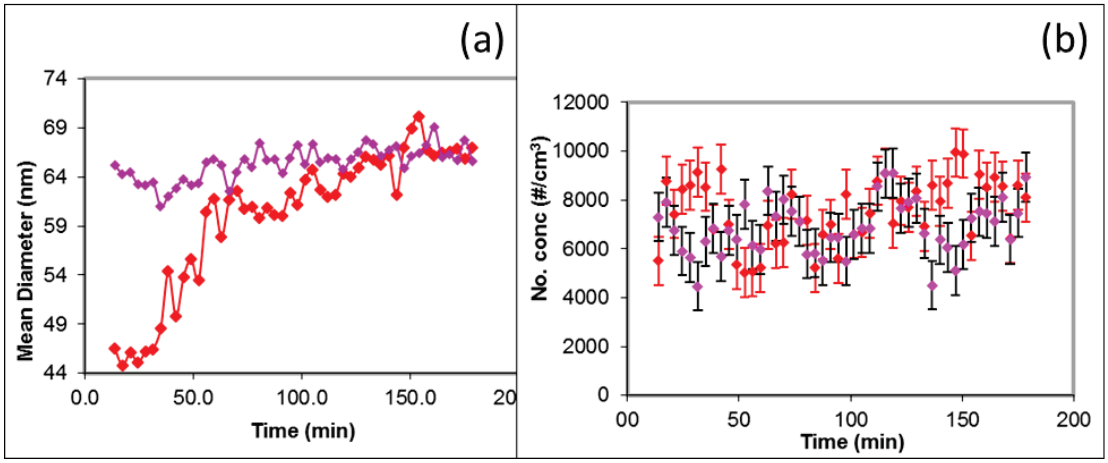

Figure 4-2 Particle growth from seeds containing AS (0.95 mM), SuA (10.6mM) and Gly (0.1M)at pH = 9 as a function of reaction time. From t=0 (fresh solution, Red) and after 24 hr (Pink); (a) diameter, (b) number concentration as a function of reaction time. It was exposed to 1.8 ppmv of limonene for 19 min.

As seen on Figure 4-2, the freshly mixed solutions showed significant growth of the particle diameter after an induction time of 30–45 min following the addition of glyoxal (time 0 in the experiments), and reached a constant value after about 100 min. Beyond this time and even after 24

h, the particle mean diameter remained constant. SOA growth was also found to be larger with the seeds at pH = 9 (24.9±3%) than at pH=5.6 (13.4±3%), indicating that this parameter directly affected the rate of formation of the relevant products.

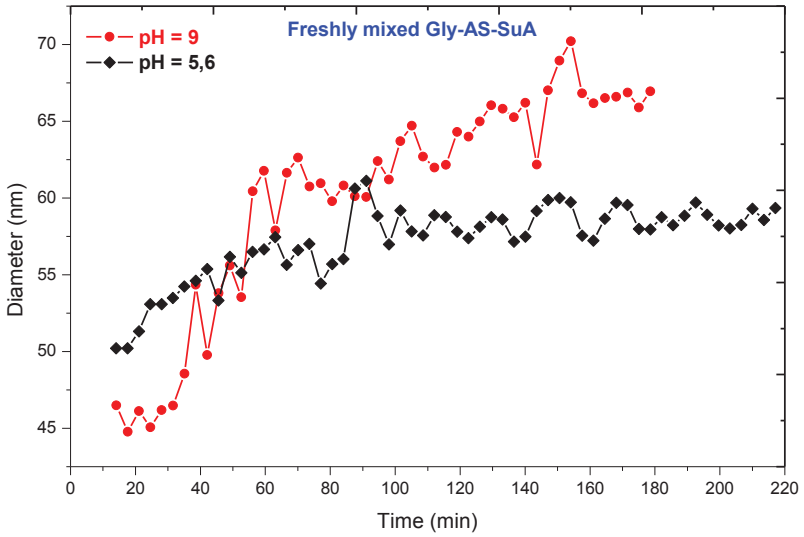

Figure 4-3 The effect of pH for the particle growth initiated by glyoxal/ammonium sulfate condensed-phase reaction (pH = 9, red and pH = 5.6, black).

The induction time observed before particle growth indicated that glyoxal itself does not take part in the photosensitization process, but one of its reaction products.

4.1.2 Role of imidazole in SOA growth

It is important to compare the contribution of products for SOA growth. In this section, the particle growth from glyoxal and some of the main light absorbing reaction products were compared.

Table 4-1 Experimental conditions and SOA Diameter Growth Factors (DGF, %) obtained for 1.8 ppmv of limonene with different photosensitizers (Gly = glyoxal, SuA = succinic acid and AS = Ammonium sulfate)

Composition	Photosensitizer Concentration (mM)	pH of a solution	Dry Particle diameter	Particle diameter after irradiation	Diameter growth factor
			Dpo (nm)	Dp (nm)	**DGF (%)**
Gly-AS-SuA	100	5.6	49.6	57.3	**13.4**
	100	9	49.6	66.1	**24.9**
IC-AS-SuA	1.3	5.6	49.6	68.5	**27.6**
	1.3	9	49.6	68.5	**27.6**
IM-AS-SuA	1.8	5.6	47.8	49.6	**3.6**
BI-AS-SuA	0.93	5.6	49.6	51.4	**3.5**
4-BBA-AS-SuA	0.4	5.6	49.6	55.2	**10.1**

In Table 4-1, the diameter grow factor, DGF (%) is defined as:

$$DGF(\%) = \frac{D_p - D_{p0}}{D_p} x100 \qquad \textit{(Eq. 4-1)}$$

where D_P is the diameter particle after irradiation, and D_{po} is the diameter of particle in the dark is calculated for different seed particles and photosensitizers.

In Table 4-1, glyoxal at higher pH and IC provided better SOA growth than compared to IM and BI. The observed particle growth from the condensation of glyoxal with ammonia is not directely from glyoxal and the yields of imidazole and its derivatives are generally low and unlikely contribute significantly to SOA mass (Galloway et al., 2009, Kampf et al., 2012, Nozière et al., 2009, Shapiro et al., 2009, Yu et al., 2011). However, it has been shown that these compounds have strong molar absorptivities and can thus significantly affect the optical properties of aerosol even at small concentration (Galloway et al., 2009, Kampf et al., 2012, Shapiro et al., 2009, Trainic et al., 2012, Trainic et al., 2011, Yu et al., 2011).

A series of experiments were performed to confirm the role of glyoxal reaction products and determine their efficiency in SOA formation and growth. Either IM, BI, or IC was added to ammonium sulfate seeds containing succinic acid by keeping other conditions constant. The seeds containing either of these products were exposed to gaseous limonene, at the same concentration as used in the glyoxal experiments.

From the observation above, IC is potentially the reaction product that drives a photosensitized growth in the glyoxal experiment. It contains an imidazole and carbonyl functional group, which may play role in its photosensitizing properties. According to Canonica et al., (Canonica et al., 1995), aromatic carbonyls are most likely photosensitizer that can support the result herein.

Thus, in the atmosphere, glyoxal and ammonium sulfate would attribute to produce an efficient photosensitizer, IC. IC is then an efficient photosensitizer that can initiate SOA growth by photo-induced reaction at the surface of particles in the atmosphere. From the production and reaction of glyoxal in the atmosphere, the SOA growth from gas phase glyoxal would be autophotocatalyzed.

4.2 Mechanistic investigation of SOA growth

This section is devoted to the experimental conditions and parameters that can potentially affect the SOA growth in the aerosol flow tube experiments. It is aimed to explore the factors affecting SOA growth and identify the possible reaction mechanism.

4.2.1 Photosensitizer type and concentration

As discussed in “Chapter 2” in detail, the nature of the photosensitizer plays a crucial role in the photosensitized SOA growth. Here we investigate the SOA growth initiated by different photosensitizers. In addition to condensed phase glyoxal reaction products, i.e. IC, IM and BI, 4-BBA,

the well-known photosensitizer, was used to compare the photosensitizing efficiency of other photosensitizer in SOA growth.

The SOA growth induced by IC, IM, BI, and 4-BBA are given in Table 4-1. There is remarkable SOA growth seen in the presence of IC and 4-BBA, and small growth due to IM and BI. In all of these compounds, aromatic ring is the characteristic feature. Imidazole is the common feature in IC, IM and BI, and carbonyl functional group is common feature for IC and 4-BBA. However, the molar concentration of those compounds were different which might less importantly affect the photo-catalysis processes (Figure 4-4).

The presence of a carbonyl functional group adds a great value for the photosensitizing nature of the compounds (Net et al., 2009, Nieto-Gligorovski et al., 2008). Intersystem crossing in aromatic carbonyl is efficient to have photochemically excited triplet state. The difference in SOA growth is, therefore, due to the presence and absence of carbonyl functional group attached to the aromatic ring of the photosensitizers.

Compounds having aromatic carbonyl have also different photosensitizing ability. They have different excitation efficiency, stability of triplet state, ability to transfer their excess energy to another molecule, rate and interaction with themselves or other molecule at their excited triplet state.

The influence of concentration change on the particle growth was investigated by varying the concentration of photosensitizer, IC. As can be seen in Figure 4-4, particles showed better growth for smaller IC concentration for the same concentration of limonene and irradiation time. However, there is small decrease in growth for relatively higher concentration of IC, which might be due to self-quenching of excited triplet state of IC. SOA growth could be initiated by minimal concentration of IC.

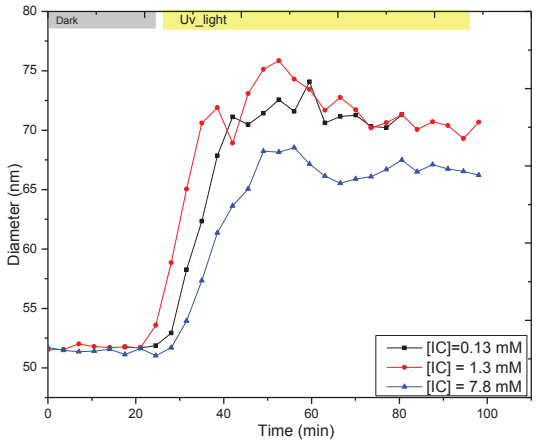

Figure 4-4 The aerosol particle growth composed of AS (0.95 mM) and different concentration of IC in the presence of 500 ppbv of limonene and 40 min of irradiation in the flow tube.

4.2.2 VOC Type and concentration

The influence of the type and concentration of VOCs on SOA growth were studied. The experiment was performed for 10 different VOCs depending on their structure, functional group and atmospheric relevance.

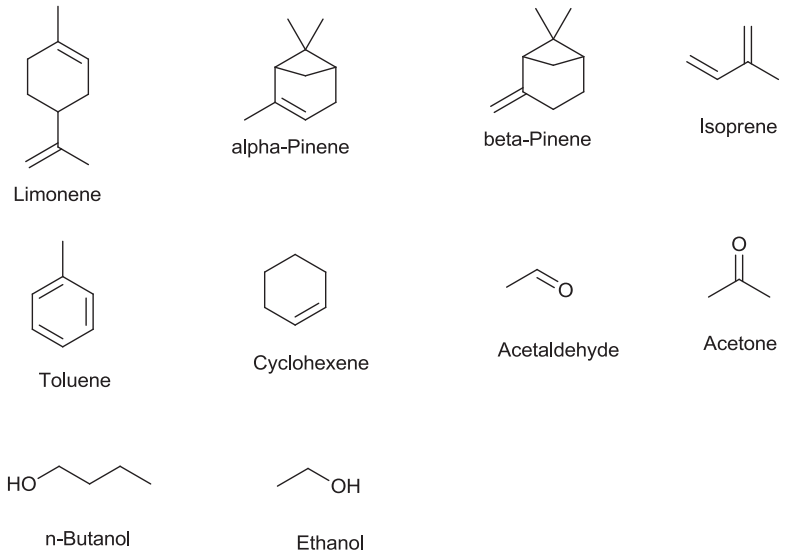

Figure 4-5 Molecular structure of different VOCs used in this study

The results are summarized in Table 4-2: only monoterpenes, isoprene, and toluene gave SOA growth, but the others not.

Table 4-2 Diameter growth factor of SOA particle composed of IC-AS-SuA for different VOCs in the aerosol flow tube experiment

Type of VOC	Vapor pressure @20°C (Bar)	Concentration (ppm)	pH of the solution	Residence time	Dry Particle diameter	Particle diameter after irradiation	Diameter growth factor
				Rt (min)	Dp_o (nm)	Dp (nm)	**DGF (%)**
Limonene	0.0017	1.8	5.6	19	49.6	68.5	**27.6**
Isoprene	0.622	4	5.6	19	49.6	51.4	**3.13**
		200	5.6	19	49.6	63.8	**22.26**
α-pinene	0.0051	63	5.6	19	49.6	61.5	**19.35**
β-pinene	0.00267	63	5.6	19	49.6	59.4	**16.5**
Toluene	0.028	352	5.6	19	49.6	51.4	**3.5**
Cyclohexene	0.2133	6	5.6	19	49.6	49.6	**0**
		>500	5.6	19	49.6	49.6	**0**
Ethanol	0.0551	688	5.6	19	49.6	49.6	**0**
n-Butanol	0.0063	470	5.6	19	49.6	49.6	**0**
Acetaldehyde	0.321	2.4	5.6	19	49.6	49.6	**0**
Acetone	0.066	4	5.6	19	49.6	49.6	**0**

From Table 4-2, limonene was found to be the most efficient SOA precursor, achieving a particle growth of 27.6 % within 19 min of particle-light-VOC exposure time. It provides better growth for the smallest concentration (1.8 ppmv). Particle growth from α-pinene and β-pinene are the second most efficient observed in the flow reactor. Isoprene and toluene also resulted SOA growth at higher concentration. These VOCs have unsaturated double bond in their structure. Furthermore, limonene has both endo and exocyclic unsaturation in its structure (Figure 4-5) that allows it to induce more SOA growth than other VOCs tested in this study. Although cyclohexene contains unsaturation in its structure, it does not provide SOA growth even at high concentration (>500 ppmv). However, the unsaturated carbon in limonene, α-pinene, β-pinene, isoprene and toluene is tertiary whereas secondary unsaturated carbon in cyclohexene. The hydrogen donating ability of unsaturated tertiary

carbon is better than secondary one so that the aryl or alkyl radical can stabilized by electron donating alkyl group.

VOC (i.e. Limonene) uptake by the surface of the particle in the aerosol flow tube was measured for a certain experiments using high resolution TOF PTR-MS (Ionicon Analytika Gmbh). The uptake was found to be very small (< 1 %) or below the detection limit. The result corresponds to the uptake coefficient of limonene equal or less than10^{-4}.

4.2.3 SOA irradiation time

Irradiation time of SOA is related to the residence time of particles in the aerosol flow tube. It is the exposure time of particles to light. Initially, the dry seed particles containing photosensitizer are only exposed to VOC in the dark. Under this condition, no change in particle size was observed. Once the particles are exposed to light, they started growing. The effect of irradiation time on SOA growth was studied in the flow tube by varying the residence time. Figure 4-6 represents the change in diameter of the particles due to irradiation as a function of irradiation time.

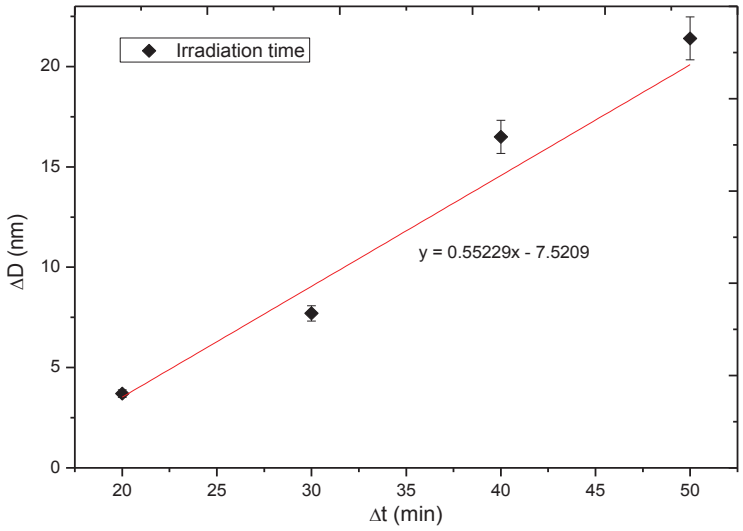

Figure 4-6 The dependence of SOA growth on irradiation time in the aerosol flow tube at constant limonene concentration (500 ppbv) and IC.

The result showed that SOA growth increased linearly with irradiation time. In the presence of appropriate photosensitizer, the size of aerosol particle increase when light-VOC-particle interaction time increases.

4.2.4 Irradiation Intensity

The seed particles composed of IC-SuA-AS (1:10:1 mass ratio) were irradiated in the flow tube with different light intensity for 19 min. This was studied by using different number of UV-lamps in the flow tube.

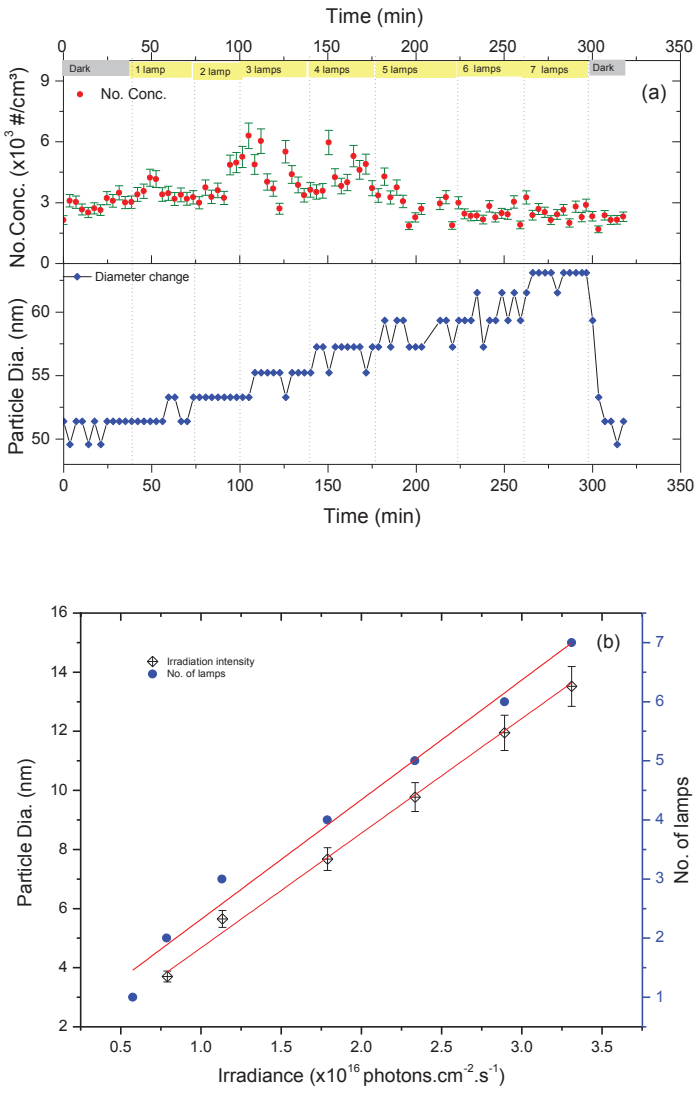

Figure 4-7 The influence of light intensity on SOA growth in the aerosol flow reactor; (a) The particle diameter change for different number of UV lamps and the corresponding particle number concentration; and (b) SOA diameter change with respect to irradiation intensity of UV lamps.

The results showed in Figure 4-7(b) clearly indicate that particle growth increased linearly with light intensity. As seen in Figure 4-7(a), the number of particle that corresponds to the particle diameter for different light intensity is nearly constant. No new particle formation and coagulation

during irradiation and particle growth. The higher the intensity the higher photosensitizer-VOC interaction the higher the particle growth will be.

4.2.5 Seed Composition

This section devoted to demonstrate the influence of seed composition of aerosol on their growth. The seed composition we used to investigate were ammonium sulfate (AS), succinic acid (SuA), ammonium nitrate (AN) and the photosensitizer (IC), and the resulted SOA diameter change is given in Table 4-3:

Table 4-3 Experimental conditions and SOA Diameter Growth Factors (DGF, %) obtained for 1.8 ppmv of limonene with different composition of seed aerosol (AN = Ammonium nitrate, SuA = succinic acid and AS = Ammonium sulfate) within 19 min of irradiation time

Composition	Photosensitizer Concentration (mM)	pH of a solution	Dry Particle diameter	Particle diameter in the dark	Particle diameter after irradiation	Diameter growth factor
			Dpo (nm)	Dp (nm)	Dp (nm)	**DGF (%)**
IC	1.3	7	50		Particle evaporates in the flow tube	**-**
AS	0	5.4	50	49.6	49.6	**0**
AN	0	3.5	50	49.6	49.6	**0**
SuA	0	5.6	50	49.6	49.6	**0**
AS-SuA	0	5.6	50	51.4	51.4	**0**
AN-SuA	0	5.6	50	51.4	51.4	**0**
IC-AS	1.3	5.6	50	51.4	63.8	**19.4**
IC-AS-SuA	1.3	5.6	50	49.6	68.5	**27.6**
IC-AN	1.3	5.6	50	37.4	46.4	**19.4**
IC-AN-SuA	1.3	5.6	50	51.4	61.5	**16.4**
IC-SuA	1.3	5.6	50	49.6	59.4	**16.5**

In the absence of IC, none of the seed particle composition exhibited any change in size in the dark and light conditions. However, in the presence of IC as a photosensitizer, these seed particles grew in light.

All seed particles containing photosensitizer (IC) revealed size change. AN seed aerosol behave differently with and without SuA. In the absence of SuA, the particle appeared at lower diameter in the dark even if the diameter was set at the entrance of the flow tube. This might show us AN particle evaporate or degraded in the flow tube. Nonetheless, when SuA was added to the AN seed, the particle behaves properly at the exit of the flow tube, that may improve its efflorescence relative humidity (Lightstone et al., 2000). The aerosol particle composed of AS or AN and SuA displayed better growth than otherwise.

4.2.6 Relative humidity

The relative humidity is one key factor for SOA growth in the flow tube experiment. The relative humidity of seed aerosol particle was varied between 0 and 50 %. It was controlled by the using a silica gel diffusion drier and humidifier Figure 3-1.

The relative humidity of a seed aerosol particle composed of IC-AS (1:1 mass ratio) was studied under constant limonene concentration (489 ppbv) and residence time (40 min), and the result is given in Figure 4-8.

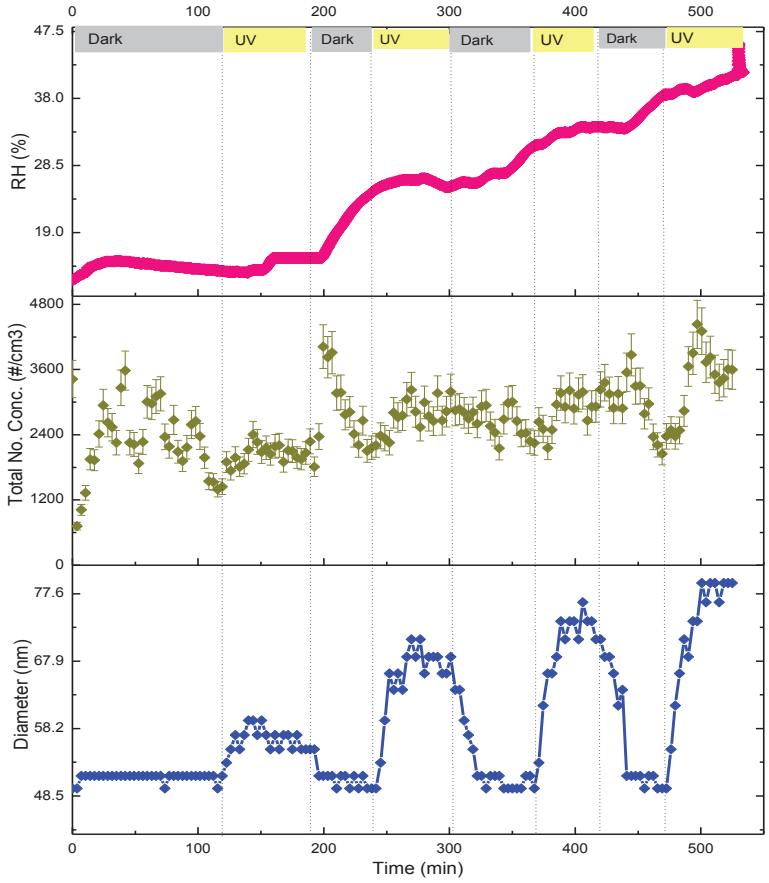

Figure 4-8 Effect of relative humidity (% RH) IC-AS particle growth at constant VOC concentration and residence time.

Increasing the relative humidity induces more particle growth, with relatively constant number concentration.

4.2.7 Type of Carrier gas

The type of carrier gas plays an important role for SOA growth in the flow tube. It is used as a medium of energy transfer, electron transfer, hydrogen transfer, radical formation and stability, and so on during photochemical reactions. The composition of carrier gas may control directly or indirectly the SOA growth. This influence was investigated by applying different carrier gases; pure oxygen, pure

nitrogen (containing upto 50 ppbv of oxygen) and air (20/80 synthetic air) on seed particles consisting of AS-SuA-IC in the presence of limonene. The subsequent SOA growth is shown in Figure 4-9.

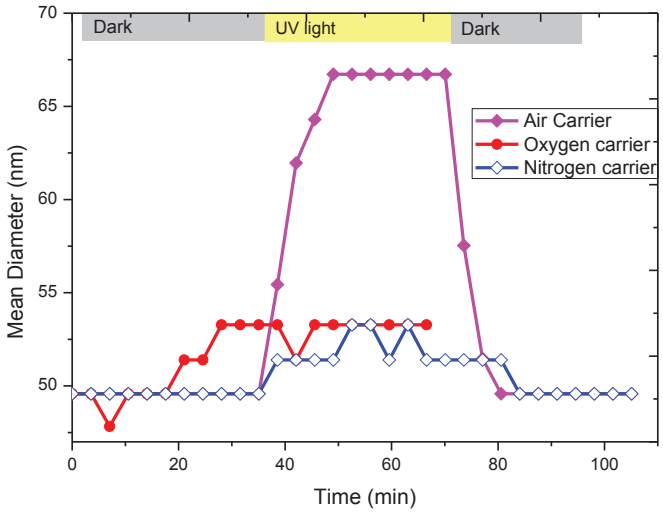

Figure 4-9 Particle growth obtained from seeds containing IC, SuA and AS exposed to 1.8 ppmv of limonene and UV-A light for 19min in different carrier gases: air (pink symbols), pure oxygen (Red), and pure nitrogen (contains 50ppbv of O_2) (Blue)

Using IC as photosensitizers and limonene as VOC (1.8 ppmv), the SOA growth resulted from pure nitrogen is very small (3.5%) and far better in air (27.6%). The very limited growth obtained in pure N_2 compared to in air indicated that O_2 plays an important role in the mechanism of SOA growth, possibly in the production of reactive species (radicals) resulting from the exchange between the photosensitizer and the VOCs. Oxygen is known to be essential in the photochemistry of dissolved organic matter with photosensitizers such as humic acids, which proceeds by the formation of singlet oxygen ($^1O_2$)(Aguer and Richard, 1996, You et al., 2011, Pospíšil et al., 2008) and superoxide (Baxter and Carey, 1983). In the contrary, very small SOA growth (6.9%) was observed in pure oxygen. This small SOA growth observed in pure oxygen carrier would seem to exclude the involvement of singlet

oxygen as the formation of this intermediate should be favored by large oxygen concentrations. But at high oxygen concentration, the relaxation and deactivation of the singlet oxygen by the ground triplet state might become significant (Afshari and Schmidt, 1991, Piötz and Maier, 1987, Wild et al., 1984) and could impede particle growth. On the other hand, ground triplet state of molecular oxygen is potently efficient to quench excited triplet state of photosensitizer (Clennan and Pace, 2005, Foote, 1968, Khan, 1976, Ogilby, 2010, Pospíšil et al., 2008, Ragone et al., 2013) that can deactivate before action.

The involvement of singlet oxygen in the mechanism of SOA growth was further investigated by performing experiments where different singlet oxygen quenchers, i.e. sodium azide (NaN_3, Aldrich ≥ 99.5%, 1.8 mM)(Canonica et al., 1995) and hydrated nickel chloride ($NiCl_2.6H_2O$, MERCK min 98%, 1 mM),(Carlsson et al., 1974, Monroe and Mrowca, 1979) were added to ammonium sulfate seeds containing imidazole-2-carboxaldehyde in air carrier. The SOA growth obtained in these experiments was identical to the one obtained in their absence. In addition to this, the action of singlet molecular oxygen is very low in the presence of water, provided that other experimental conditions kept constant, the increase in SOA growth by increasing RH (Figure 4-8) support the idea of excluding singlet oxygen involvement in the IC photosensitized SOA particle growth mechanism.

4.2.8 Photosensitized SOA growth mechanism

Based on the potential selective parameters studied in this work, the mechanism responsible for photosensitized SOA growth was proposed. Excited triplet state of a photosensitizer potentially interact with the VOCs having tertiary unsaturated carbon through hydrogen transfer and/or electron transfer to form ionic radicals as shown in Figure 4-10 below.

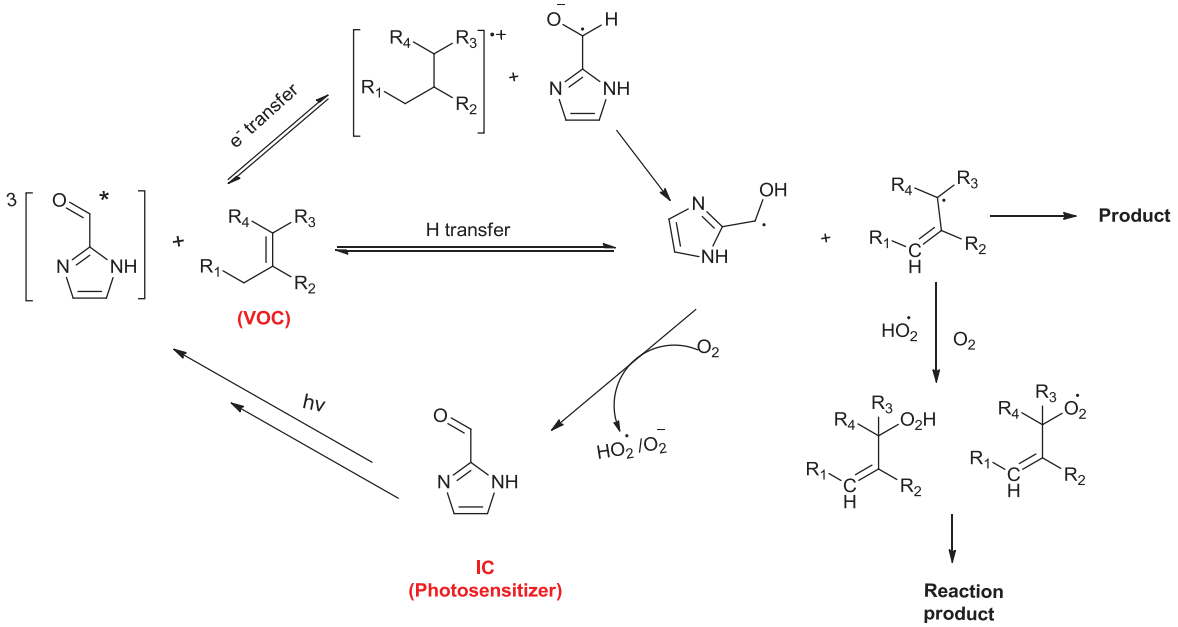

Figure 4-10 Proposed reaction mechanism for the photosensitized SOA growth.

The reaction mechanism proceeds most probably via hydrogen transfer leading to the formation of alkyl radicals. However, the hydrogen transfer can be either a direct transfer or proceed through an electron transfer followed by a proton transfer. In the oxygen rich system, the photosensitizer can regenerate to the ordinary molecule by the production of hydroperoxyl (HO_2). On the other hand, the allyl radical will undergo oxidation to form oxygenated products such as RO_2 radicals.

The reaction mechanism that involve in Photosensitized SOA growth and some other details are published in Faraday Discussion(Aregahegn et al., 2013).

Faraday Discussions

RSC Publishing

Cite this: *Faraday Discuss.*, 2013, **165**, 123

PAPER

View Article Online
View Journal | View Issue

Organic aerosol formation photo-enhanced by the formation of secondary photosensitizers in aerosols

Kifle Z. Aregahegn, Barbara Nozière* and Christian George

Received 20th March 2013, Accepted 26th April 2013
DOI: 10.1039/c3fd00044c

Secondary organic aerosols (SOA), which are produced by the transformations of volatile organic compounds in the atmosphere, play a central role in air quality, public health, visibility and climate, but their formation and aging remain poorly characterized. This study evidences a new mechanism for SOA formation based on photosensitized particulate-phase chemistry. Experiments were performed with a horizontal aerosol flow reactor where the diameter growth of the particles was determined as a function of various parameters. In the absence of gas-phase oxidant, experiments in which ammonium sulfate seeds containing glyoxal were exposed to gas-phase limonene and UV light exhibited a photo-induced SOA growth. Further experiments showed that this growth was due to traces of imidazole-2-carboxaldehyde (IC) in the seeds, a condensation product of glyoxal acting as an efficient photosensitizer. Over a 19 min irradiation time, 50 nm seed particles containing this compound were observed to grow between 3.5 and 30 ± 3% in the presence of either limonene, isoprene, α-pinene, β-pinene, or toluene in concentrations between 1.8 and 352 ppmv. The other condensation products of glyoxal, imidazole (IM) and 2,2-bi1H-imidazole (BI), also acted as photosensitizer but with much less efficiency under the same conditions. In the atmosphere, glyoxal and potentially other gas precursors would thus produce efficient photosensitizers in aerosol and autophotocatalyze SOA growth.

1 Introduction

Organic compounds are ubiquitous in ambient aerosols, accounting for up to 50% of the fine particulate mass.[1–4] The organic fraction plays an important role in determining their formation, growth, and removal of ambient aerosols.[5] Secondary Organic Aerosols (SOA), which are produced by the transformations of Volatile Organic Compounds (VOCs) in the atmosphere, have been the subject of sustained attention due to their importance in air quality, visibility, public health and climate.[6] Therefore, a good understanding of the formation and evolution of

Université de Lyon, université Lyon 1, CNRS, UMR5256, IRCELYON, Institut de recherches sur la catalyse et l'environnement de Lyon, Villeurbanne, F-69626, France

View Article Online
Faraday Discussions Paper

SOA in the atmosphere is necessary. However, gaining such an understanding poses a number of fundamental and practical challenges. For instance, it is difficult to directly observe SOA in the atmosphere as well as to differentiate between secondary and primary organic compounds that are present within SOA.[7] Investigations of SOA formation and growth processes are thus mainly based on laboratory experiments. Physical absorptive models based on volatility, such as the gas-to-particle partitioning model[8,9] and the Volatility Basis Set (VBS) model[10] are successful in describing SOA growth in a smog chamber but still largely underestimate SOA mass in the atmosphere.[11–14] Particulate-phase chemical reactions have recently been proposed as contributors to aerosol growth, thereby reducing such discrepancies.[15–18] It has been suggested that ionic reactions in the condensed phase, leading to the formation of C–C or C–O–C[15–17] bonds, can be catalyzed by strong acids,[18] amino acids,[19] or ammonium ions.[20] In particular, larger-than-expected yields of glyoxal SOA have recently been attributed to such reactions.[16,17] Indeed glyoxal is now expected to be an important source for SOA in the atmosphere due to its ubiquity and the fact that it is an oxidation product of a wide variety of biogenic and anthropogenic VOCs.[16,21–23]

Smog chamber experiments have shown, however, that a light-induced process is responsible for glyoxal SOA growth beyond that due to ionic reactions occurring in the dark.[17,24] The process(es) responsible for this light-induced SOA growth remain largely unknown, although several studies[25–27] have demonstrated that condensed phase glyoxal chemistry leads to the formation of light absorbing products. Recent work from our group has shown the existence of a photochemical growth pathway for aerosols containing a photosensitizer such as HULIS or 4-benzoyl benzoic acid (4-BBA). We have proposed that photosensitized reactions occurring on the particle surface give rise to the observed growth. Quite significantly, this growth does not require the presence of gas-phase oxidants. We believe that such a mechanism could also play an important role in the light-induced growth of glyoxal based SOA.[21,28]

In this work, we investigated photo-induced SOA growth associated with condensed phase glyoxal chemistry. Importantly, this allows us to identify atmospherically relevant photosensitizers. Aerosol flow tube experiments were performed in order to determine parameters affecting the observed SOA growth (precursor structure and concentration, seed composition, carrier gas, and UV-light intensity) and thereby elucidate a potential mechanism.

2 Experimental

SOA formation was investigated using a horizontal aerosol flow tube made of Pyrex (8 cm id × 152 cm length), thermostated and kept at 293 ± 1 K using a circulating water bath. This flow tube was surrounded by 7-UV lamps (Philips CLEO) with a continuous emission spectrum over 300–420 nm and a total irradiance of 3.7×10^{16} photon cm^2 s^{-1}. A complete description of this aerosol flow tube setup is given elsewhere.[28] First a monodispersed aerosol ("seeds") was generated from aqueous solutions using an atomizer (TSI 3076) and a Differential Mobility Analyzer (DMA) (TSI Model 3081, impactor size 0.0588 cm, aerosol flow = 0.3–0.5 lpm, sheath flow = 3–5 lpm). The seed aerosol particles were then dried with a silica gel diffusion drier and size selected to either 40 nm or 50 nm diameters using DMA. This monodispersed aerosol typically contained 5 000

View Article Online
Paper Faraday Discussions

particles cm ^{3} and corresponded to a total mass of a few μg m ^{3}. The seed particles were then directed into the flow tube reactor where they were exposed to a constant VOC flow and UV light. The VOC concentration was generated with a permeation tube in a temperature controlled oven (Dynacal, Valco instruments Co.inc. using VICI metronics dynacalibrator, model 150). The carrier gas used in all the experiments was synthetic air from a cylinder (purity 99.9990%) (total flow = 0.4–0.5 lpm), except when stated otherwise (section 3.3). The temperature and Relative Humidity (RH) inside the reactor were monitored at the inlet and at the outlet using a SP UFT75 sensor. The particle size distribution and concentration were monitored at the exit of the flow tube using a Scanning Mobility Particle Sizer (SMPS) (TSI 3080), consisting of a DMA, (TSI 3081) and a Condensation Particle Counter (CPC, TSI 3776). In the size measurements the bin width was 0.8 nm. For the particles studied in this work (typical size ~50 nm), this represented 1.6% uncertainty on each size measurement and a little less than 3% uncertainty on the determination of each diameter growth factor.

Several series of experiments were performed to characterize the photosensitized SOA growth where the composition of the seeds, type and concentration of VOC, relative humidity, irradiation time, and residence time of the aerosol in the reactor were varied. The seeds were made of ammonium sulfate (Aldrich ≥ 99%) and/or organic acid (Succinic acid, Aldrich ≥ 99%) to which was added glyoxal (0.1 M, Aldrich, 40% w/w in water) or a photosensitizer such as 1*H*-Imidazole-2-carboxaldehyde ("IC", Aldrich 98%), 1*H*-Imidazole ("IM", Aldrich ≥ 99%) and 4-Benzoylbenzoic acid ("4BBA", Aldrich 99%) in a 1 : 10 : 1 weight ratio. The seed solutions were prepared with 18 MΩ distilled water (Millipore). The VOCs investigated for this study were limonene, α-pinene, β-pinene, isoprene, toluene, cyclohexene, ethanol, acetaldehyde, acetone and n-butanol.

To verify that the SOA produced in this work resulted specifically from the presence of photosentisizers, "blank" experiments were routinely performed in which the seed particles did not contain any photosensitizer, and all other conditions were the same. Furthermore, control experiments were carried out to 1) investigates the potential production of organic particles from the irradiation of the VOCs in the absence of seed particles, 2) check for the potential generation of gas-phase oxidant during the experiments, and 3) determine the photo-stability of the seed particles. For these, a NO_x detector (Thermo 42C chemiluminescent analyser, detection limit of 0.4ppbv) and an O_3 monitor (Thermo 49C, detection limit is 1ppbv) were connected to the outlet of the reactor.

3 Results and discussion

The control experiments showed that no particles were produced when VOCs were irradiated in the absence of seed particles in the reactor. They also showed that neither NO_x species nor O_3 were produced inside the reactor during the irradiation experiments, thus confirming the absence of gas-phase oxidants and thereby excluding gas-phase oxidation of the VOC in the experiments.

3.1 Autophotocatalytic SOA growth from glyoxal

In a first series of experiments, seed particles were produced from atomizing aqueous solutions containing a mixture of ammonium sulfate (0.95 mM),

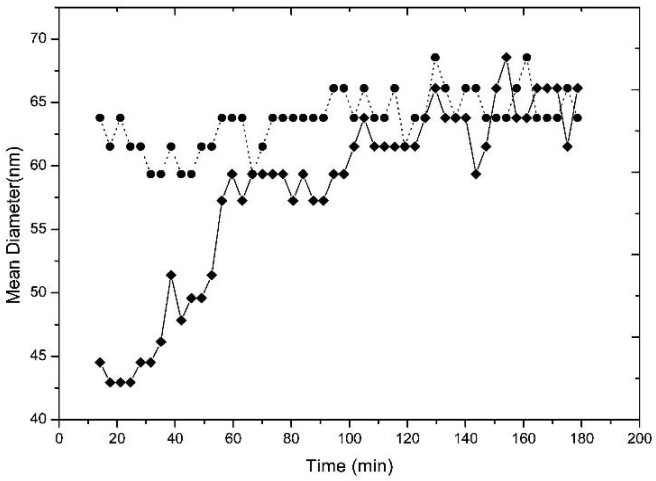

Fig. 1 Diameter growth of particles containing ammonium sulfate (0.95 mm), succinic acid (10.6 mm), Glyoxal (Gly) (0.1 M) at pH = 9 and exposed to UV-A light and 1.8 ppmv of limonene for 19 min. in the flow reactor. Experiments with freshly mixed seeds (solid line) are compared with those where the solution was left to react for 24 h after the addition of glyoxal (dotted line).

succinic acid (10.6 mM) and glyoxal (0.1 M). The dried and size selected particles were exposed to 1.8 ppmv of limonene and near-UV light in the reactor, and the particle diameter obtained at the end of the reactor was monitored in real time (Fig. 1). In this experiment, succinic acid was used as a proxy for the organic fraction of atmospheric particles, thus allowing for more "realistic" conditions. In some experiments, the seeds were produced from freshly mixed solutions while in others the solutions were left to react for 24 h after the addition of glyoxal with continuous stirring, all other conditions being identical. In most glyoxal experiments, the pH of the seed solution was adjusted to 9 by adding small amount of 2M NaOH solution. In some cases, the pH was left at 5.6 to study the effect of this parameter on SOA growth.

With the freshly mixed solutions, a significant growth of the particle diameter was observed after an induction time of 20–45 min following the addition of glyoxal (time 0 in the experiments), and reached a constant value after about 100 min. Beyond this time and even after 24 h, the particle mean diameter remained constant (Fig. 1). The seeds produced with the aged mixtures exhibited

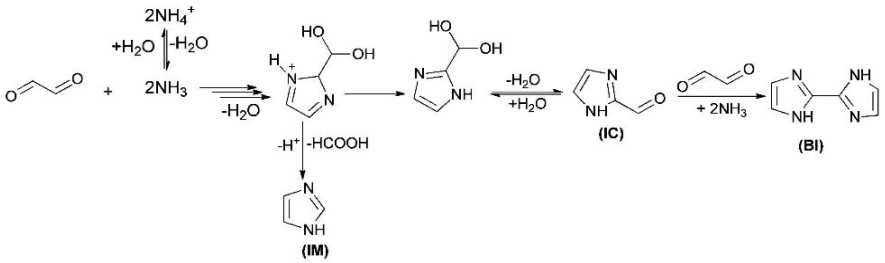

Fig. 2 Formation mechanisms for the different imidazoles produced in the Glyoxal/AS/water system proposed by Yu *et al.*[30] and Kampf *et al.*[25]

View Article Online
Paper Faraday Discussions

Table 1 Experimental conditions and SOA Diameter Growth Factors (DGF, %) obtained for 1.8 ppmv of limonene with different photosensitizers (Gl – glyoxal, SuA – succinic acid and AS – Ammonium sulfate)

Composition	Photosensitizer concentration (mM)	pH of solution	Dry particle diameter	Particle diameter after irradiation	Diameter growth factor
			Dp_o (nm)	Dp (nm)	**DGF (%)**
IC	1.3	7	49.6	Particle evaporates in the flow tube	—
AS	0	5.4	49.6	49.6	**0**
AS–SuA	0	3.5	49.6	49.6	**0**
GL–AS–SuA	100	5.6	49.6	57.3	**13.4**
	100	9	49.6	66.1	**24.9**
IC–AS–SuA	1.3	5.6	49.6	68.5	**27.6**
	1.3	9	49.6	68.5	**27.6**
IM–AS–SuA	1.8	5.6	47.8	49.6	**3.6**
BI–AS–SuA	0.93	5.6	49.6	51.4	**3.5**
4BBA–AS–SuA	0.4	5.6	49.6	55.2	**10.1**

some photochemical properties directly and led to particle growth in the flow tube, identical to those obtained with the freshly mixed seeds after 100 min, within the uncertainties (Fig. 1). The total diameter growth observed with the freshly mixed seeds (lowest to highest average mean diameter) was about 24.9 ± 3%. The 20–45 min induction time observed before particle growth indicated that glyoxal was not directly responsible for the SOA growth, but rather some of its reaction products. SOA growth was also found to be larger with the seeds at pH = 9 (24.9 ± 3%) than at pH = 5.6 (13.4 ± 3%), indicating that this parameter directly affected the rate of formation of the relevant products.

The condensation of glyoxal with ammonia in condensed-phase ammonium is known to produce light-absorbing compounds,[20,24–26,29,30] potentially acting as photosensitizers. These products have been identified as imidazole (IM),[31] imidazole-2-carboxaldehyde (IC),[24,27] and 2,2-bi1H-imidazole (BI)[25] and their proposed formation mechanism in aerosols shown Fig.2.[25,27]

In atmospheric related studies, the yields of this imidazole and its derivatives are generally low and unlikely to contribute significantly to SOA mass.[20,24–27] However, these compounds have strong molar absorptivities and can thus significantly affect the optical properties of solutions or aerosols even at small concentrations.[24–27,29,30] These compounds could thus be the photosensitizers responsible for SOA growth in the experiments in this work. This is reinforced by the timescale and effect of pH on the observed SOA growth, which are in very good agreement with the rate constant of the reaction for glyoxal in NH_4^+ salts[20] producing the imidazoles and with the timescales for particle-phase imidazole formation in other flow tube experiments.[29,30]

To confirm the role of imidazoles as photosensitizers and determine their efficiency in SOA formation a second series of experiments was performed in which either (IM), (IC) or (BI) was added to the ammonium sulfate seeds containing succinic acid. These seeds were flown into the reactor to be exposed to 1.8 ppmv of limonene and UV-A light at a relative humidity (RH) of 15%. Table 1 summarizes the seed composition and particle growth obtained in these experiments.

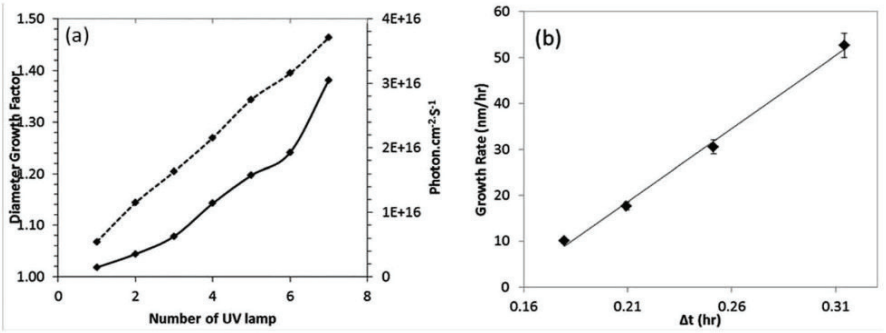

Fig. 3 Effect of light intensity and irradiation time on SOA growth in the reactor: (a) growth factor as function of number of lamps (solid line) and lamp intensities (dotted line), (b) growth rate as function of time of exposure (concentration × irradiation time). In both cases, the seeds contained IC (1.3 mM)-SuA (10.5 mM)-AS (0.95 mM) and constant limonene concentration.

In Table 1, the Diameter Growth Factor (DGF(%) = ((Dp − Dp_o)/Dp) × 100) where Dp is the particle diameter after irradiation and Dp_o is particle diameter in the dark) is calculated for different seed particles and photosensitizers.

The aqueous solutions containing only a photosensitizer (IC) evaporated over the timescale of our experiments, thus did not produce any stable seeds to perform SOA experiments. The seeds containing only ammonium sulfate or ammonium sulfate/succinic acid but no glyoxal or photosensitizer and exposed to limonene and UV-A light ("control experiments") led to no particle growth. This confirmed that the SOA growth observed in the other experiments was not due to the gas-phase oxidation of the VOCs. By contrast, all the experiments where the seeds contained a photosensitizer displayed some particle growth, evidencing the

Table 2 Diameter growth factors of SOA particle composed of IC–SuA–AS in Milli-Q water. The bin width on each particle size measurement is 0.8nm

Type of VOC	Vapour pressure[a] @20 °C (Bar)	Concentration (ppm)	pH of the solution	Residence time Rt (min)	Dry particle diameter Dp_o (nm)	Particle diameter after irradiation Dp (nm)	Diameter growth factor **DGF (%)**
Limonene	0.0017	1.8	5.6	19	49.6	68.5	**27.6**
Isoprene	0.622	4	5.6	19	49.6	51.4	**3.13**
		200	5.6	19	49.6	63.8	**22.26**
α-Pinene	0.0051	63	5.6	19	49.6	61.5	**19.35**
β-Pinene	0.00267	63	5.6	19	49.6	59.4	**16.5**
Toluene	0.028	352	5.6	19	49.6	51.4	**3.5**
Cyclohexene	0.2133	6	5.6	19	49.6	49.6	**0**
		>500	5.6	19	49.6	49.6	**0**
Ethanol	0.0551	688	5.6	19	49.6	49.6	**0**
n-Butanol	0.0063	470	.6	19	49.6	49.6	**0**
Acetaldehyde	0.321	2.4	5.6	19	49.6	49.6	**0**
Acetone	0.066	4	5.6	19	49.6	49.6	**0**

[a] CAMEO chemical datasheet.

critical role of this photosensitizer. The most efficient particle growth was observed with IC and was even slightly larger (27.6%) than in the glyoxal experiments (24.9%). With the two other imidazoles studied (IM) and (BI), the SOA growth observed was small, <5% or below the detection limit. IC was thus identified as the glyoxal product most likely to act as a photosensitizer in the glyoxal experiments. This efficiency could be due to a combination of the aromatic group of the imidazole and the carbonyl group, the latter being known to have strong photosensitizing properties.[32]

Thus, in the atmosphere, the partitioning and reaction of glyoxal in ammonium sulfate particles would produce an efficient photosensitizer, IC, which, in turn would trigger SOA growth by photo-induced reactions in or at the surface of the particles. SOA growth from gas-phase glyoxal in the atmosphere would thus be autophotocatalyzed.

3.2 Investigating the mechanism

The effect of various experimental conditions on the particle growth was characterized by further experiments. The effect of light intensity on SOA growth was studied in the reactor by using different numbers of UV lamps. The results showed that particle growth increased linearly with light intensity (Fig. 3a).

Particle growth was also found to depend on VOC concentration and the residence time (Rt) of the particles in the flow tube. For instance, an increase in isoprene concentration from 4 to 200 ppmv led to an increase in particle size from 3.13 to 22.3% (Table 2). These parameters affected the SOA growth from limonene, α-pinene, and β-pinene in the same way.

The growth rate of SOA, GR, was also determined as the ratio $\Delta D_m/\Delta t$, where ΔD_m is the difference of the mean particle diameter in the dark and under irradiation, and Δt their residence time in the reactor. Different residence times between 5 and 20min were thus tested. The results are presented in Fig. 3b and

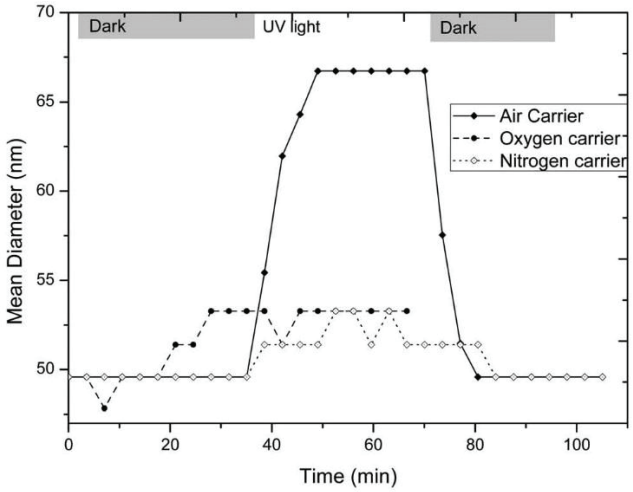

Fig. 4 Particle growth obtained from seeds containing imidazole-2-carboxaldehyde, succinic acid and ammonium sulphate exposed to 1.8 ppmv of limonene and UV-A light in different carrier gases: air (solid line), pure oxygen (dashed dotted line), and pure nitrogen (dotted line).

show that GR, the particle growth in the flow tube, increases linearly with time of exposure. These results allow us to extrapolate our laboratory experiments to smog chambers and even atmospheric time scales.

In a limited series of experiments, the uptake of limonene from the gas in the flow tube was tentatively measured using a high resolution TOF PTR-MS (Ionicon Analytika, Gmbh). This uptake was found to be below the detection limit, which would correspond to an uptake coefficient equal or lower than 10^{-4}. In spite of this, seemingly small uptake, the increase of particle mass and volume in similar experiments was shown with an Aerosol Mass Spectrometer (AMS, Aerodyne) to result exclusively from the trapping of non-condensable organic species, here the VOC.[28]

3.3 Investigating the mechanism: effect of the VOCs molecular structure

The potential selectivity of the mechanism responsible for SOA growth towards certain molecular structures was studied by performing experiments with 10 different VOCs. The results are summarized in Table 2: SOA growth was only observed with limonene, isoprene, α-pinene, β-pinene and toluene, but not with cyclohexene, n-butanol, ethanol, acetaldehyde and acetone within the residence time of our experiments.

Limonene was found to be the most efficient SOA precursor, achieving a particle growth of 27.6% for the smallest concentration (1.8 ppmv). Isoprene, α-pinene, β-pinene, and toluene resulted in particle growth ranging from 22.3 to 3.5%, but for larger concentrations than limonene (6–352 ppmv). The results in Table 2 would suggest that photo-induced SOA growth is associated with unsaturated VOCs. However, no growth is observed for cyclohexene, even when it is at concentration exceeding 500 ppmv. The results thus suggest that, more specifically, the photo-induced reaction mechanism is favoured for compounds containing unsaturated tertiary carbon atoms (isoprene, terpenes with endocyclic and/or exocyclic unsaturated tertiary sites, and toluene), over those containing secondary carbons only.

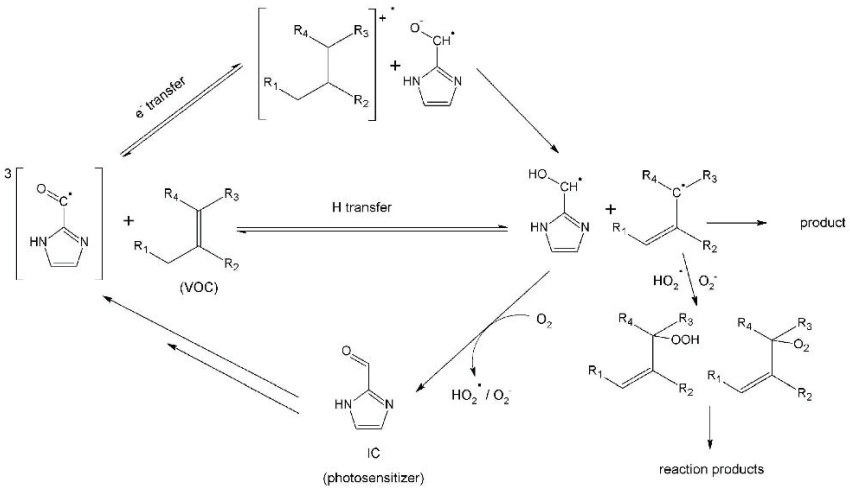

Fig. 5 Proposed reaction mechanism for the formation of active radicals in the photosensitized SOA growth.

View Article Online
Paper Faraday Discussions

3.4 Investigation of mechanism: role of carrier gas

To investigate the role of oxygen in the mechanism responsible for the observed SOA growth, a few experiments were performed using pure oxygen or pure nitrogen (containing $\leq$ 50 ppmv of O_2) as a carrier gas instead of air. Using IC as photosentisizers and limonene as VOC (1.8 ppmv), the SOA growth obtained was much more limited in both pure nitrogen (3.5%) and pure oxygen (6.9%) than in air (27.6%) (Fig. 4).

The very limited growth obtained in pure N_2 compared to in air indicated that O_2 plays an important role in the mechanism of SOA growth, possibly in the production of reactive species (radicals) resulting from the exchange between the photosensitizer and the VOCs. Oxygen is known to be essential in the photochemistry of dissolved organic matter with photosensitizers such as humic acids, which proceeds by the formation of singlet oxygen ($^1O_2$)[33–35] and superoxide.[36] Singlet oxygen is known to be produced by the electronic energy transfer between the excited triplet state of the photosensitizer, produced upon UV-vis light absorption, and the ground triplet state of molecular oxygen. Singlet oxygen would react with all unsaturated hydrocarbons and aromatic compounds.[37] But both singlet oxygen and superoxide could potentially be involved in the mechanisms responsible for SOA growth in this work.

The very small SOA growth observed in a pure oxygen carrier would seem to exclude the involvement of singlet oxygen as the formation of this intermediate should be favoured by large oxygen concentrations. But at high oxygen concentrations the relaxation and deactivation of the singlet oxygen by the ground triplet state might become significant[38–40] and could impede particle growth.

The involvement of singlet oxygen in the mechanism was further investigated by performing experiments where different singlet oxygen quenchers, sodium azide (NaN_3, Aldrich, $\geq$99.5%, 1.8 mM)[32] and hydrated nickel chloride ($NiCl_2 \cdot 6H_2O$, MERCK, min 98%, 1 mM),[41] were added to ammonium sulfate seeds containing imidazole-2-carboxaldehyde in air carrier. The SOA growth obtained in these experiments was identical with the one obtained in their absence.

The lack of SOA growth from cyclohexene (Table 2) and the lack of effects of the singlet oxygen quenchers seem to exclude the involvement of singlet oxygen in the mechanisms. An alternative mechanism, shown in Fig. 5, could involve the direct interaction of the triplet state of the photosensitizer with the VOC[34] to produce radicals on the surface of the aerosol particle. This mechanism is similar to the one proposed by Canonica *et al.*[32] The radicals produced would then be stabilized by proton transfer and reaction with ground state oxygen. The proton transfer may also directly be produced by the abstraction of α-hydrogen to leave an allyl radical that is then stabilized by the tertiary carbon. In this redox reaction, molecular oxygen would create more reactive radicals for SOA growth, which would be limited in pure nitrogen. The excited triplet state of the photosensitizer could also potentially be quenched by ground state molecular oxygen which would account for the lower SOA growth in pure oxygen carrier.

3.5 Atmospheric relevance

Both glyoxal and ammonium sulphate containing particles are ubiquitous in the atmosphere. SOA formation from glyoxal is thus expected to occur *via* ionic reactions in the aerosol particles, resulting in an exceptionally large apparent

Henry's law constant[17,42] as well as *via* photosensitized reactions triggered by the condensed phase production of IC, as demonstrated by this work.

The SOA growth obtained in this work can be compared with those observed in the atmosphere, such as the one observed in the MCMA-2003 campaign in Mexico City, which was largely attributed to glyoxal reactions in the aerosols.[43] On 9 April 2003 a steady SOA growth corresponding of 3.3 μg m $^{-3}$ h $^{-1}$ [12,43] was observed over 6 h of sunlight, and varying between ~2 and 5.2 μg m $^{-3}$ h $^{-1}$. In our experiments, a SOA mass growth of 3.2 μg m $^{-3}$ hr $^{-1}$ was obtained when exposing seed particles to 1.8 ppm of limonene for 19 min. As the total concentration of VOCs expected to contribute to these processes (tertiary alkenes, branched aromatic…) in Mexico City might not exceed 100 ppbv[44,45] the new processes might account for 5 to 10% of the SOA growth observed at this location. This estimate indicates that these new processes might make a significant contribution to SOA mass in the atmosphere. But further investigation is now needed, in particular of the SOA mass produced as a function of VOC concentrations, in order to refine this estimate.

4 Conclusions

In this work, photo-induced SOA growth resulting from the interaction of glyoxal with ammonium sulfate seeds was demonstrated and investigated. Among the different light-absorbing products formed by the reactions of glyoxal in ammonium salts, imidazole-2-carboxaldehyde was found to be the most efficient photosensitizer for initiating SOA growth. SOA formation from glyoxal in the atmosphere is thus expected to be autophotocatalytic: the partitioning and reactions in ammonium-containing seeds producing photosensitizers, which, in turn, leads to further photo-induced growth of SOA.

In this study we found that SOA growth from seeds containing IC was linearly dependent on VOC concentration, and irradiation time and intensity. Different VOCs also gave very different SOA growth, those having unsaturated tertiary carbon, such as terpenes, isoprene and toluene, having the highest yields. The potential role of singlet oxygen or the photosensitizer triplet state as the key species controlling the SOA growth was investigated but needs to be studied further. The SOA mass obtained in the experiments suggests that these photo-induced processes could account for most of the SOA growth attributed to glyoxal chemistry in regions such as Mexico City. These processes need, however, to be further characterized, especially over longer time scales.

Acknowledgements

Support by the FP7 project PEGASOS (EU–FP7 project under grant agreement no. 265307) is gratefully acknowledged. C.G. thanks Olivier Piva for fruitful discussions having stimulated this work and Sumi Wren for her stylistic inputs.

References

1 M. C. Jacobson, H. C. Hansson, K. J. Noone and R. J. Charlson, *Rev. Geophys.*, 2000, **38**, 267–294.
2 M. Kanakidou, J. H. Seinfeld, S. N. Pandis, I. Barnes, F. J. Dentener, M. C. Facchini, R. Van Dingenen, B. Ervens, A. Nenes, C. J. Nielsen, E. Swietlicki, J. P. Putaud, Y. Balkanski, S. Fuzzi, J. Horth, G. K. Moortgat, R. Winterhalter, C. E. L. Myhre,

K. Tsigaridis, E. Vignati, E. G. Stephanou and J. Wilson, *Atmos. Chem. Phys.*, 2005, **5**, 1053–1123.
3 J. H. Seinfeld and J. F. Pankow, *Annu. Rev. Phys. Chem.*, 2003, **54**, 121–140.
4 Q. I. Zhang, C. O. Stanier, M. R. Canagaratna, J. T. Jayne, D. R. Worsnop, S. N. Pandis, Jimenez and J. L., *Environ. Sci. Technol.*, 2004, **38**, 4797–4809.
5 M. Prather, D. Ehhalt, F. Dentener, R. Derwent, E. Dlugokencky, E. H. I. Isaksen, J. Katima, V. Kirchhoff, P. Matson, P. Midgley and M. Wang, in *Climate Change 2001: The Scientific Basis, Contribution of WG1 to the Third Assessment report of the IPCC*, ed. J. T. Houghton, Y. Ding, D. J. Griggs, M. Noguer, P. J. Van der Linden, X. Dai, K. Maskell and C. A. Johnson, Cambridge University Press, UK, 2001.
6 V. Perraud, E. A. Bruns, M. J. Ezell, S. N. Johnson, Y. Yu, M. L. Alexander, A. Zelenyuk, D. Imre, W. L. Chang, D. Dabdub, J. F. Pankow and B. J. Finlayson-Pitts, *Proc. Natl. Acad. Sci. U. S. A.*, 2012, **109**, 2836–2841.
7 M. Hallquist, J. C. Wenger, U. Baltensperger, Y. Rudich, D. Simpson, M. Claeys, J. Dommen, N. M. Donahue, C. George, A. H. Goldstein, J. F. Hamilton, H. Herrmann, T. Hoffmann, Y. Iinuma, M. Jang, M. E. Jenkin, J. L. Jimenez, A. Kiendler-Scharr, W. Maenhaut, G. McFiggans, T. F. Mentel, A. Monod, A. S. H. Prévôt, J. H. Seinfeld, J. D. Surratt, R. Szmigielski and J. Wildt, *Atmos. Chem. Phys.*, 2009, **9**, 5155–5236.
8 J. F. Pankow, *Atmos. Environ.*, 1994, **28**, 185–188.
9 J. R. Odum, T. Hoffmann, F. Bowman, D. Collins, R. C. Flagan and J. H. Seinfeld, *Environ. Sci. Technol.*, 1996, **30**, 2580–2585.
10 A. L. Robinson, N. M. Donahue, M. K. Shrivastava, E. A. Weitkamp, A. M. Sage, A. P. Grieshop, T. E. Lane, J. R. Pierce and S. N. Pandis, *Science*, 2007, **315**, 1259–1262.
11 C. L. Heald, D. J. Jacob, R. J. Park, L. M. Russell, B. J. Huebert, J. H. Seinfeld, H. Liao and R. J. Weber, *Geophys. Res. Lett.*, 2005, **32**, L18809.
12 R. Volkamer, J. L. Jimenez, F. San Martini, K. Dzepina, Q. Zhang, D. Salcedo, L. T. Molina, D. R. Worsnop and M. J. Molina, *Geophys. Res.Lett.*, 2006, **33**, L17811.
13 R. Bergström, H. A. C. Denier van der Gon, A. S. H. Prévôt, K. E. Yttri and D. Simpson, *Atmos. Chem. Phys.*, 2012, **12**, 8499–8527.
14 M. Kuwata and S. T. Martin, *Aerosol Sci. Technol.*, 2012, **46**, 937–949.
15 M. Jang, N. M. Czoschke, S. Lee and R. M. Kamens, *Science*, 2002, **298**, 814–817.
16 J. H. Kroll, N. L. Ng, S. M. Murphy, V. Varutbangkul, R. C. Flagan and J. H. Seinfeld, *J. Geophys. Res.*, 2005, **110**, D23207.
17 R. Volkamer, P. J. Ziemann and M. J. Molina, *Atmos. Chem. Phys.*, 2009, **9**, 1907–1928.
18 J. L. Duncan, L. R. Schindler and J. T. Roberts, *Geophys. Res. Lett.*, 1998, **25**, 631–634.
19 B. Noziere and A. Cordova, *J. Phys. Chem. A*, 2008, **112**, 2827–2837.
20 B. Nozière, P. Dziedzic and A. Córdova, *J. Phys. Chem. A*, 2009, **113**, 231–237.
21 S. Myriokefalitakis, M. Vrekoussis, K. Tsigaridis, F. Wittrock, A. Richter, C. Brühl, R. Volkamer, J. P. Burrows and M. Kanakidou, *Atmos. Chem. Phys.*, 2008, **8**, 4965–4981.
22 P. Lavvas, R. V. Yelle, T. Koskinen, A. Bazin, V. Vuitton, E. Vigren, M. Galand, A. Wellbrock, A. J. Coates, J.-E. Wahlund, F. J. Crary and D. Snowden, *Proc. Natl. Acad. Sci. U. S. A.*, 2013, **110**, 2729–2734.
23 S. M. Saunders, M. E. Jenkin, R. G. Derwent and M. J. Pilling, *Atmos. Chem. Phys.*, 2003, **3**, 161–180.
24 M. M. Galloway, P. S. Chhabra, A. W. H. Chan, J. D. Surratt, R. C. Flagan, J. H. Seinfeld and F. N. Keutsch, *Atmos. Chem. Phys.*, 2009, **9**, 3331–3345.
25 C. J. Kampf, R. Jakob and T. Hoffmann, *Atmos. Chem. Phys.*, 2012, **12**, 6323–6333.
26 E. L. Shapiro, J. Szprengiel, N. Sareen, C. N. Jen, M. R. Giordano and V. F. McNeill, *Atmos. Chem. Phys.*, 2009, **9**, 2289–2300.
27 G. Yu, A. R. Bayer, M. M. Galloway, K. J. Korshavn, C. G. Fry and F. N. Keutsch, *Environ. Sci. Technol.*, 2011, **45**, 6336–6342.
28 M. E. Monge, T. Rosenørn, O. Favez, M. Müller, G. Adler, A. Abo Riziq, Y. Rudich, H. Herrmann, C. George and B. D'Anna, *Proc. Natl. Acad. Sci. U. S. A.*, 2012, **109**, 6840–6844.
29 M. Trainic, A. Abo Riziq, A. Lavi and Y. Rudich, *J. Phys. Chem. A*, 2012, **116**, 5948–5957.
30 M. Trainic, A. A. Riziq, A. Lavi, J. M. Flores and Y. Rudich, *Atmos. Chem. Phys.*, 2011, **11**, 9697–9707.
31 H. Debus, *Justus Liebigs Ann. Chem.*, 1858, **107**, 199–208.
32 S. Canonica, U. Jans, K. Stemmler and J. Hoigne, *Environ. Sci. Technol.*, 1995, **29**, 1822–1831.
33 J. P. Aguer and C. Richard, *J. Photochem. Photobiol., A*, 1996, **93**, 193–198.
34 K. You, D. Yin, L. Mao, P. Liu and H. a. Luo, *J. Photochem. Photobiol., A*, 2011, **217**, 321–325.
35 J. Pospíšil, S. Nešpůrek and J. Pilař, *Polym. Degrad. Stab.*, 2008, **93**, 1681–1688.
36 R. M. Baxter and J. H. Carey, *Nature*, 1983, **306**, 575–576.

37 E. L. Clennan, *Tetrahedron*, 2000, **56**, 9151–9179.
38 E. Afshari and R. Schmidt, *Chem. Phys. Lett.*, 1991, **184**, 128–132.
39 J. Piötz and M. Maier, *Chem. Phys. Lett.*, 1987, **138**, 419–424.
40 E. Wild, H. Klingshirn and M. Maier, *J. Photochem.*, 1984, **25**, 131–143.
41 D. J. Carlsson, T. Suprunchuk and D. M. Wiles, *Can. J. Chem.*, 1974, **52**, 3728–3737.
42 H. S. S. Ip, X. H. H. Huang and J. Z. Yu, *Geophys. Res. Lett.*, 2009, **36**, L01802.
43 R. Volkamer, F. San Martini, L. T. Molina, D. Salcedo, J. L. Jimenez and M. J. Molina, *Geophys. Res. Lett.*, 2007, **34**, L19807.
44 E. Velasco, B. Lamb, H. Westberg, E. Allwine, G. Sosa, J. L. Arriaga-Colina, B. T. Jobson, M. L. Alexander, P. Prazeller, W. B. Knighton, T. M. Rogers, M. Grutter, S. C. Herndon, C. E. Kolb, M. Zavala, B. de Foy, R. Volkamer, L. T. Molina and M. J. Molina, *Atmos. Chem. Phys.*, 2007, **7**, 329–353.
45 E. C. Fortner, J. Zheng, R. Zhang, W. Berk Knighton, R. M. Volkamer, P. Sheehy, L. Molina and M. André, *Atmos. Chem. Phys.*, 2009, **9**, 467–481.

5 Excited triplet state study of IC

The photophysical and photochemical properties of IC were investigated by means of a laser flash photolysis setup to better characterize the mechanism of photosensitization in the presence of limonene. Different parameters were studied based on the experimental setup stated in section 3.4 such as:

- concentration;
- quencher (such as limonene, halides, nitrate);
- effect of degasing.

This method relies on the use of high-energy laser pulse of short duration photolysing molecular entities.

5.1 Laser flash photolysis of IC

The transient absorption spectrum of ^{3}IC* was obtained between 300 and 500 nm. ^{3}IC* absorbs strongly between 310 and 400 mm. The Solvent does not contribute absorption to ^{3}IC* at least in the range of absorption maxima. The absorption maximum of ^{3}IC* falls at 330 nm. ^{3}IC* exhibits the some absorption in both water and water-acetonitrile mixed solvent regardless of solubility and degasing process and duration.

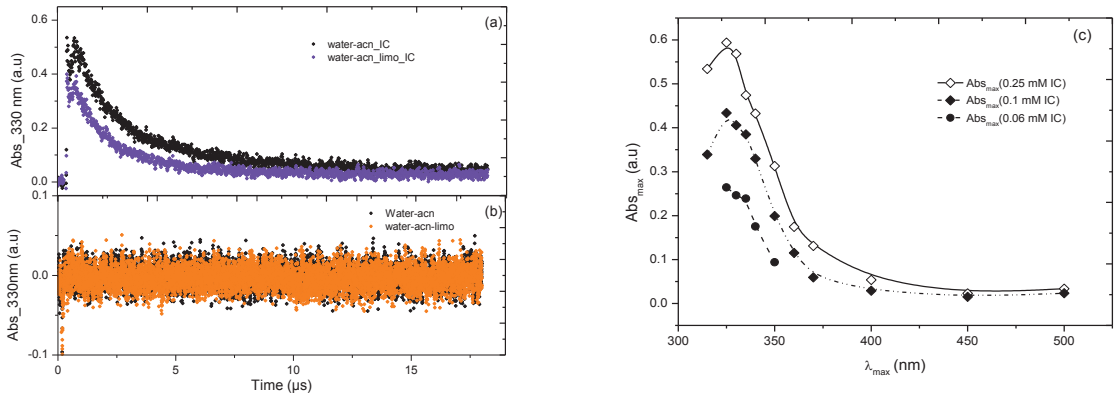

Figure 5-1 Transient absorption spectra observed after flash excitation of 0.25 mM IC; (a) with and without limonene in water-acetonitrile (3:2); (b) solvents with and without limonene; (c) absorption maxima at λ_{max} = 330 nm for different concentration of IC.

No transient absorption peak appear during solvent excitation with in the excitation wavelength range. Even if, limonene is present in the Solvent without IC, no absorption peak was observed.

The spectrum has been drawn to obtain the first order kinetics for each wavelength by means a mono-exponential function. The excited triplet state decay of IC follows first order kinetics with a corresponding rate constant of (7.73 ± 0.04) x 10^5 s^{-1}. The corresponding lifetime of the triplet state of IC, according to the equation:

$$\tau = \frac{1}{k^1} \qquad \text{(Eq. 5-1)}$$

was found to be (1.29 ± 0.007) µs in a deoxygenated IC solution for which the longer triplet lifetime allows for the reaction with a reactant molecule (Zhao et al., 2013). The result agreed with the recently published result about the triplet lifetime of IC (Tinel et al., 2014).

5.2 Triplet state quenching of IC

The influence of potential quencher, i.e., limonene and cyclohexene, on the lifetime of the triplet state were studied. The addition of limonene to the IC solution resulted in the faster decrease of the triplet state absorption of IC, while the addition of cyclohexene had no effect. Increasing concentration of limonene resulted in a decreasing triplet state lifetime. Furthermore, Figure 5-2a showed that degasing a solution affects the triplet lifetime of IC.

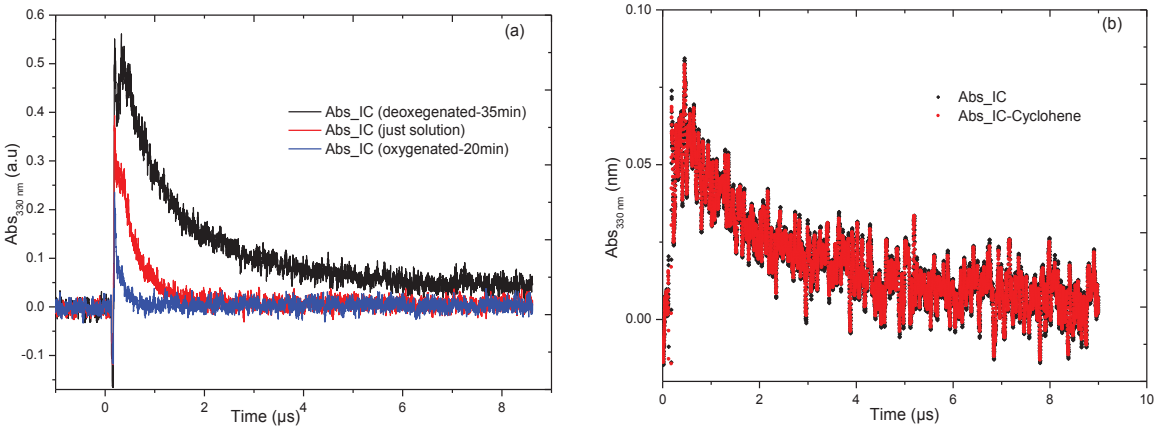

Figure 5-2 Triplet-triplet absorption of IC in water-acetonitrile (3:2); (a) effect of degasing, (b) in the presence of cyclohexene.

Ground state molecular oxygen can indeed quench the excited triplet state of IC. In other word, the excited triplet state of IC can react with ground state molecular oxygen and hence degasing the aqueous solution of IC play a role to determine the reaction rate constant and its lifetime.

The relative absorption spectrum of ^{3}IC* in the absence and presence of cyclohexene is given in Figure 5-2b. Cyclohexene can therefore react only very slowly with excited ^{3}IC explain its poor contribution in photosensitized SOA growth.

In the contrary, limonene interacts strongly with the excited triplet state of IC. Addition of different limonene concentration to a solution of 0.25 mM IC, in Figure 5-3a, showed that the transient

absorption of the excited triplet state and its lifetime decreased. The triplet lifetime of IC follows the concentration of limonene in the solution, decrease with increasing limonene concentration. The rate of deactivation of triplet state of IC by limonene is (1.8 ± 0.065) x 10^7 s^{-1} (Figure 5-3b).

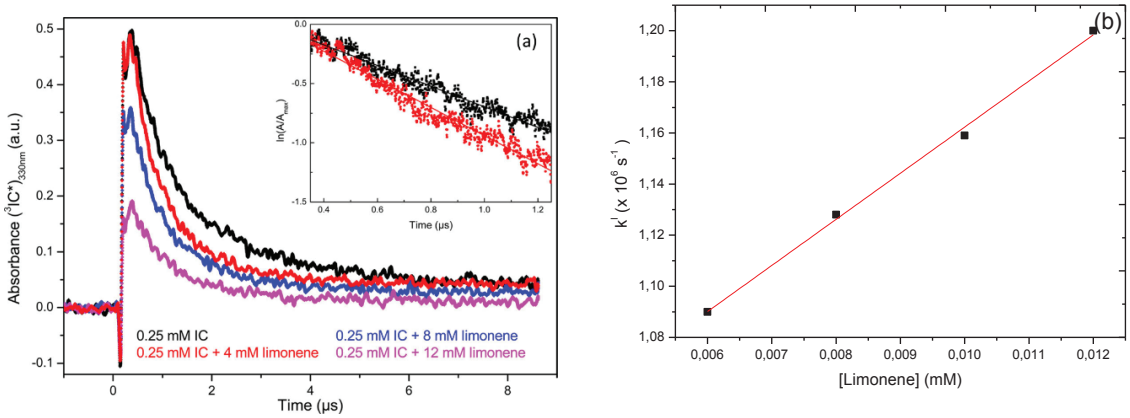

Figure 5-3 The change in the first order rate constant of IC for different limonene concentration in a degassed solution; (a) transient absorption of excited triplet state of IC (0.25 m M). In the presence of (4 mM-Red), (8 mM – Blue) and (12 mM-pink) limonene; (b) first order rate constant as a function of limonene concentration.

6 Photosensitized NO/NO_2 conversion in the SOA growth

The nitrogen oxides, nitric oxide (NO) and and nitrogen dioxide (NO_2), are extremely important in the atmospheric chemistry of radicals and the production and destruction of tropospheric ozone (Crutzen, 1979). Photolysis of NO_2 is one of the most important conversion pathways in this regards. Moreover, atmospheric radical reactions with NO can also contribute to the NO/NO_2 conversion. From Table 1-2, the conversion is very fast according to the reaction HO_2 + NO → NO_2 + OH, and very slow in NO + O_2 → NO_2 reaction. Such processes in the atmosphere could affect NO_x concentration by converting NO into NO_2 (Figure 6-1), and in turn affect the SOA growth. This study was aimed to investigate the formation of HO_2 during photosensitized SOA growth as it was proposed in Figure 4-10.

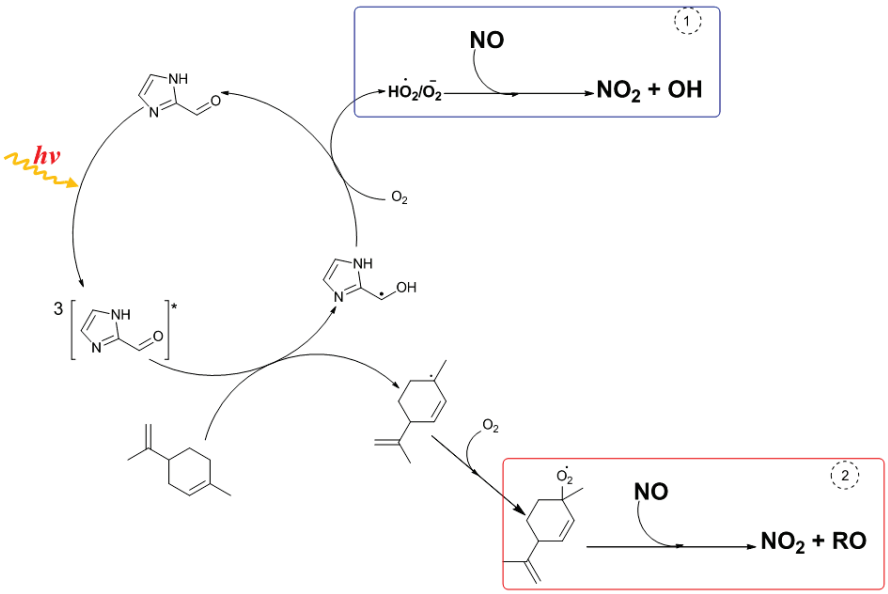

Figure 6-1 Simplified photosensitized reaction mechanism for SOA growth.

6.1 Effect of photosensitized SOA growth on NO concentration

To investigate the formation of HO_2 during photosensitized SOA growth in the aerosol flow tube, NO gas was used by taking the following assumptions. 1) NO is stable towards aerosol flow tube light wavelength range. 2) The reaction with molecular oxygen and VOCs such as limonene is almost negligible. 3) The NO_2 formation from the reaction of HO_2 and NO is substantial, and hence the NO_2 concentration would increase. The gaseous HO_2 produced via triplet state chemistry of photosensitizer (IC) on the aerosol surface is thus reacted with NO in NO containing environment. The NO reaction can also proceed with other peroxyl radicals depending on the reactivity of peroxyl radical. 4) Photolysis of NO_2 can occur in the flow tube. As a result, aerosol flow tube experiments were performed, which were identical to those presented in chapter 4, but where NO was added in the gas (1.01 ppmv in N_2, the linde group). In these experiments, the seed particle was composed of IC and AS, and the VOC used was limonene (500 ppbv).

The concentrations of NO, NO_2 and NO_x were monitored in real-time using the NO_x analyzer described in Section 3.1.5.

As shown in Figure 6-2, the irradiation of aerosol particles containing a photosensitizer (IC) performed in the absence of limonene (VOC), led to no change in the NO and NO_2 concentration. By adding limonene, rapid consumption of NO and production of NO_2 was observed. The conversion of NO and formation of NO_2 on the IC containing aerosol is not only strongly activated by light but also by the presence of limonene.

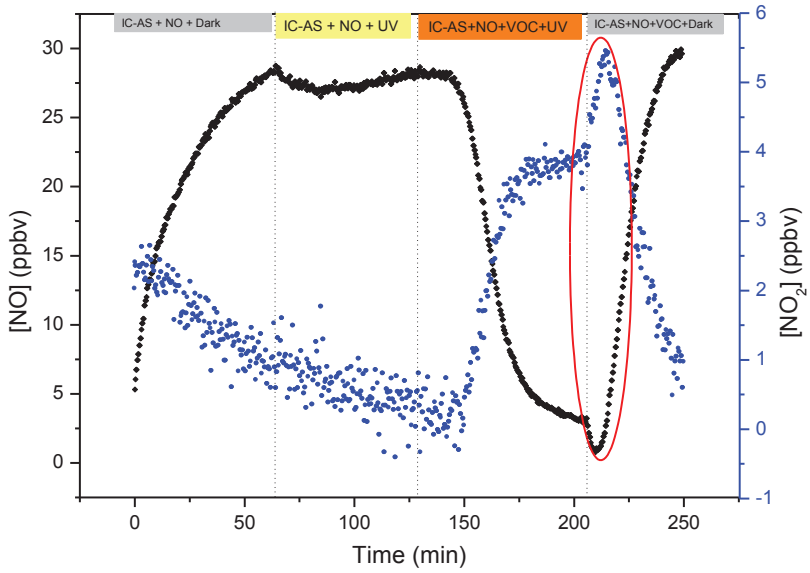

Figure 6-2 The concentration change of NO (black dots) and NO2 (blue dots) during photosensitized reaction on the surface of aerosol particle. The red in the graph showed the instantaneous reaction in the dark which proceed without NO_2 photolysis.

On the contrary, there is an immediate increase in NO_2 concentration and extra decrease in NO concentration followed by rapid decrease and increase, respectively, after UV light is turned off. This might be because of the instantaneous chemical reaction between the already produced radicals and oxidants, and NO, but without photolysis of NO_2.

The photolysis rate coefficient, J_{NO2}, of NO_2 in the flow tube was calculated from its quantum yield (Gardner et al., 1987, Troe, 2000) and absorption cross-section (Sander et al., 2002), and actinic flux of the UV lamps measured inside the flow tube at specific wavelength and temperature using the following equation (Eq. 6-1):

$$J_{NO_2} = \int \Phi(\lambda)\,\sigma(\lambda)F(\lambda)d\lambda \qquad \textit{(Eq. 6-1)}$$

where J_{NO2} is the first order photolysis rate coefficient of NO_2 (s^{-1}), $\Phi(\lambda)$ is the quantum yield of NO_2, $\sigma(\lambda)$ is the absorption cross-section of NO_2 (cm^2 $molecule^{-1}$), and $F(\lambda)$ is the spectral actinic flux density of lamps in the flow tube (photon cm^{-2} s^{-1}) at a given wavelength.

For the quantum yield and absorption cross-section of NO_2, we used the already available data from the literature ((www.uv-vis-spectral-atlas-mainz.org) but the actinic flux of the lamps in the flow reactor was measured using calibrated iDUS CCD camera.

$$NO_2 + hv\ (\lambda < 420\ nm) \rightarrow NO + O(\ ^3P) \qquad \textit{(R. 6-2)}$$

For a given temperature, T = 293 ± 2 K, the first order photolysis rate coefficient, J_{NO2}, was calculated in the wave length range of the flow tube emission (300 – 420 nm) and found to be 6.75 x 10^{-3} s^{-1} and corresponds to a photolysis lifetime with respect to $O(^3p)$ formation of 2.5 minutes. The average NO_2 concentration in the flow tube could be lowered due to photolysis.

$$O + HO_2 \rightarrow OH + O_2 \qquad \textit{(R. 6-3)}$$

$$O + O_2 \overset{M}{\rightarrow} O_3 + M \qquad \textit{(R. 6-4)}$$

$$O + NO \overset{M}{\rightarrow} NO_2 + M \qquad \textit{(R. 6-5)}$$

where M in (R. 6-4 and R. 6-5) is any third molecule that stabilizes the excited intermediate before it dissociate back to the reactant.

6.2 Investigation of photosensitizer thin film in the coated-wall reactor

The interaction between photosensitized reaction product and NO gas was further investigated using the coated-wall reactor, where photosensitizer and/or organic matrix was placed as a thin film, as described in section 3.3. The thin film consisting of a photosensitizer and/or an organic acid as a matrix was evenly coating the inner walls of small reactor (20 cm x 1.1 cm id), placed in a temperature controlled reactor. The temperature of the reactor was kept at 293 ± 2 K. 790 ppbv of gaseous limonene

and NO gas were passed through it. The maximum contact time, depend on the maximum flow, was 3.6 s. As it was done in the aerosol flow tube, the first order photolysis rate of NO_2 was calculated and it is found to be 2.5 x 10^{-3} s^{-1}. The contact time is, however, very fast, photolysis of NO_2 in a coated flow tube might not be happened. Besides, the extra peak appeared in aerosol flow tube (Figure 6-2) while turned off the light. Further more, the coated flow tube is used to increase the surface area interaction.

The composition of organic thin film for different ratio of photosensitizer and organic acid matrix was used as specified in Table 3-2 and 1 mg of photosensitizer, and/or adipic acid that behaves similarly with succinic acid in SOA, were typically coated onto the inner flow tube wall.

During the irradiation we observed a substantial loss of NO and a corresponding formation of NO_2 on the surface of thin film (Figure 6-3a). The high conversion of NO indicates that NO is oxidized by photochemically produced radicals in the organic film. This indirectly confirms that there might be hydroperoxyl radical production during irradiation of photosensitizer in the presence of hydrogen or electron donor, VOC. The blank experiment in a clean flow reactor (Figure 6-3b) attested that the interaction only happened when photosensitizer and hydrogen donor (VOC) were present at the same time.

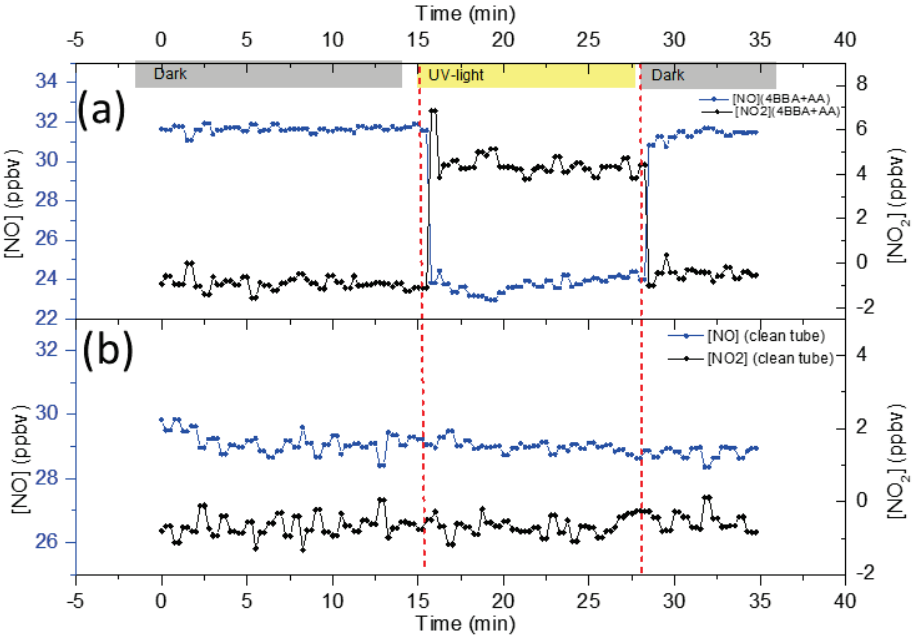

Figure 6-3 Nitric oxide profile in the flow reactor in the presence of 790 ppbv of gaseous limonene, (a) Coated flow reactor (4-BBA + AA, 1:1); (b) clean flow reactor.

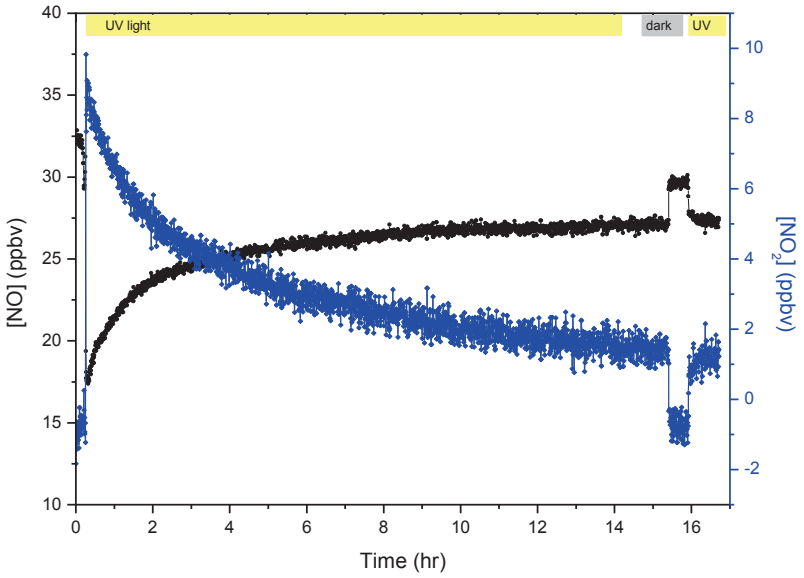

Figure 6-4 The [NO] and [NO_2] change on the solid 4-benzoylbenzoic acid coated film in the presence of 790 ppbv of gaseous limonene and light; Blue – [NO_2] and black – [NO].

The NO/NO_2 conversion due to photosensitizer (4-BBA) coated film persist for longer time. As seen in Figure 6-4, the conversion continued for more than 15 h in the presence of gaseous limonene and light. The photosensitization processes can proceeds throughout the day. However, 4-BBA was used in the coated flow tube instead of IC because of it solubility and solvent interaction in water and ethanol, respectively.

6.3 Photosensitized aerosol surface reaction and HO_2 flux

It is evidenced that photosensitized surface reaction might induces HO_2 in the system. The HO_2 flux that could be produced from the surface reaction according to the mechanism proposed in Figure 4-10 will be now calculated.

To deduce the HO_2 flux during photosensitized SOA growth, two approachs were used; the bottom-up approach for which the particle size change is due to limonene consumption and NO/NO_2 approach in which NO_2 is produced from $NO\text{-}HO_2$ reaction.

The HO_2 flux from the surface of the particle was calculated from the change in size of the particle due to VOC condensation. The change in volume of particle during SOA growth, assume particles are spherical in shape, is given by:

$$\Delta V = \frac{4}{3}\pi(r_1^3 - r_0^3) \qquad \textit{(Eq. 6-6)}$$

where ΔV is the change in volume (cm^3), and r_1 and r_0 are particle diameter after and before growth, respectively (cm).

The total ΔV for the change in diameter from 51.4 nm to 68.5 nm in the presence of 500 ppbv of gaseous limonene and 40 min of residence time is equal to 1.46×10^{-12} cm^3/cm^{-3}.

The number of VOC molecule (limonene in this case) interacted with the triplet state of IC in order to induce this volume change is proportional to the number of HO_2 molecule comes out from this volume change, and thus the number of HO_2 molecules produced (n) is then defined by:

$$n(molecule\ cm^{-3}) = \frac{\Delta V.d.n_p.\mathcal{N}}{M} \qquad \textit{(Eq. 6-7)}$$

where d is the average density of aerosol (g/cm^3), n_p is the number of particles involved ($\#/cm^3$), N is the Avogadro number (molecule/mole), and M is the molecular weight of VOC used limonene (g/mol).

The flux of HO_2 (molecule cm^{-2} s^{-1}) resulting from the photosensitizer-VOC interaction in light is 2.78 $x10^{+12}$ molecule cm^{-2} s^{-1}. The measured value of VOC (limonene) taken by the surface using PTR-MS was negligible or below the detection limit and was assumed to be less than 1% and the calculated value here is nearly 0.1%.

Likewise, the HO_2 flux from the photosensitizer coated flow reactor surface is calculated by assuming that the number of NO_2 molecule produced during $NO + HO_2 \rightarrow NO_2 + OH$ is proportional to the HO_2. Consequently, the HO_2 flux is calculated from the concentration of NO_2 by taking the surface area of thin film in to account for a give contact time. The resulting HO_2 flux is then equal to 4.62 x 10^{+11} molecule cm^{-2} s^{-1}.

The photosensitized emission of HO_2 in the atmosphere is estimated by taking the typical SOA surface in the atmosphere is ca. 10^{-6} cm^2 cm^{-3} (Seinfeld and Pandis, 2006). The estimated HO_2 emission from photosensitized process is therefore 2.8 × 10^{+6} cm^{-3} s^{-1}, which is comparable to the typical HO_2 emission in the atmosphere ca. 1.4 × 10^{+5} cm^{-3} s^{-1} (Hofzumahaus et al., 2009).

The result obtained from both condition showed us, there is significantly large amount of HO_2 production during photosensitized reaction.

6.4 Contribution of NO for SOA mass

The photo-induced reaction between excited triplet state photosensitizer and VOC produces large enough amount of HO_2 radicals and hence SOA growth, and a lot more besides in the presence of NO in the system (Figure 6-5). In addition to the consumption of NO due to photosensitized SOA growth (Figure 6-2), additional aerosol growth was also observed.

Through the reaction:

$$HO_2 + NO \rightarrow NO_2 + OH \qquad \textit{(R. 6-8)}$$

sources of HO_2 are potential sources of OH radical (Finlayson-Pitts and Pitts, 1997). As a result of the formation of OH radical in the system, extra SOA growth is expected.

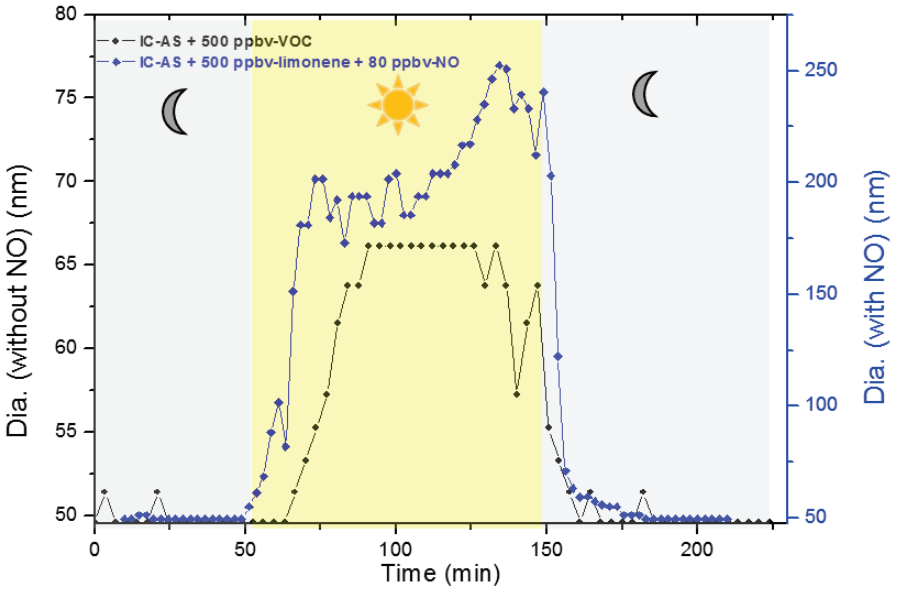

Figure 6-5 Comparative SOA growth with (Blue) and without (Black) NO in the system for the seed containing IC and AS in the presence of 500 ppbv of gaseous limonene, the residence time for both condition was 40 min.

Moreover, the photolysis of NO_2 produce atomic oxygen $O(^3p)$ which will react with molecular oxygen to produce ozone in the system according to the reaction (R.6-4).

The ozone formed in the flow tube can possibly react with VOCs, NO, NO_2 and other radicals which potentially affect the measurement at the exit of the flow tube. However, the formation of ozone in the system, and the unreacted ozone was measured at the exit of the flow reactor. The measurement result is shown in the following figure (Figure 6-6).

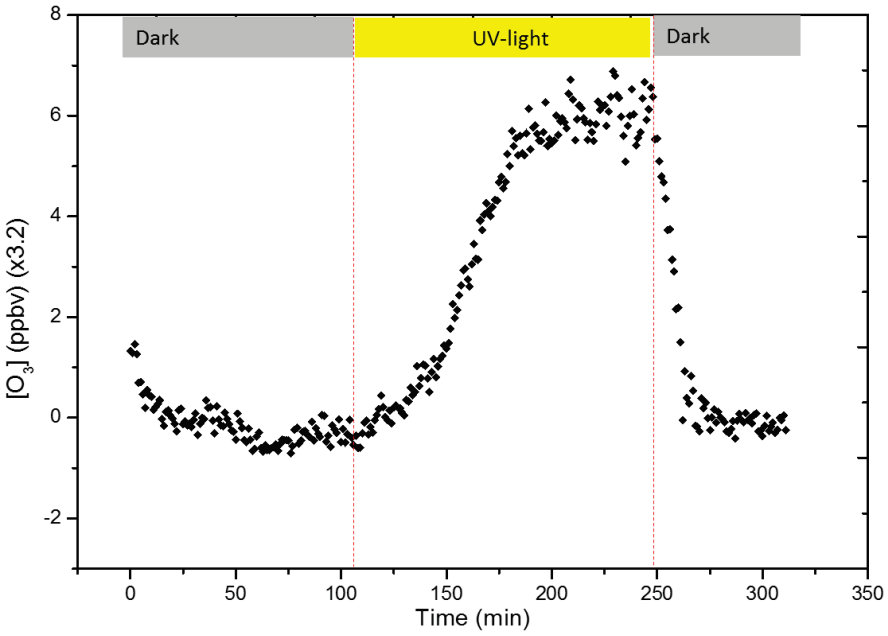

Figure 6-6 The unreacted ozone produced during SOA growth in the presence of NO.

Ozone production during photochemical reaction in the presence of NO is significant, ~20 ppbv, to make change in the system. However, this value corresponds to the unreacted O_3 in the flow tube with limonene and/or something else, and hence the actual value must be higher in this regard.

The extra SOA growth is therefore due to the cumulative effect of the products during photosensitized aerosol surface reaction. The SOA growth in the presence of NO initiated not only by HO_2 and RO_2 radicals but also by OH radicals, O_3, NO and other possible radicals. The contribution of radicals and ozone to the extra SOA growth in the presence of NO was summarized in the following table (Table 6-1).

Table 6-1 Summary of particle growth in different conditions, Rt = 40min

Seed composition	VOC	External oxidant	Cyclohexane as OH	Particle Size		DGF (%)
				D_{p0}	D_p	

Photosensitized NO/NO2 conversion in the SOA growth

	Type	Conc. (ppm)	Type	Conc. (ppb)	scavenger (ppm)		Dark	UV	
IC-AS	limonene	0.5	-	-	-	49.6	49.6	68.5	27.6
IC-AS	limonene	0.5	-	-	1000	49.6	49.6	68.5	27.6
IC-AS	limonene	0.5	NO	80	-	49.6	49.6	200	75.2
IC-AS	limonene	0.5	NO	80	1000	49.6	49.6	$\geq$250	$\geq$80.2
IC-AS	limonene	0.5	O_3	87	-	49.6	105.5	105.5	53
IC-AS	Toluene	225	-		-	49.6	49.6	53.3	6.9
IC-AS	Toluene	225	O_3	100	-	49.6	57.3	57.3	13.4
IC-AS	Toluene	225	O_3	100	1000	49.6	49.6	53.3	6.9

These experiments were to examine the relative contributions of O_3 and the OH radical to the aerosol growth and formation. In Table 6-1 the SOA growth in the presence of gaseous limonene and cyclohexane as OH radical scavenger, behaved the same in the absence of OH radical scavenger. The photosensitized SOA growth is due to HO_2 radical.

The presence of NO induced a considerably large SOA growth regardless of the presence of OH scavenger. Addition of OH scavenger in the NO containing system does not decreased the particle diameter in light rather it increased. OH scavenger does not behave as usual in NO containing environment. The reaction of the OH radical with cyclohexane in the presence of NO leads to the formation of cyclohexanone and cyclohexyl nitrate that potentially contribute for more SOA mass loading (Aschmann et al., 1997b, Takagi et al., 1981).

On the other hand, the SOA growth induced by O_3 in the absence of NO is not proportional with that of NO induced growth. It prompts less SOA growth, indicating that the growth in NO containing environment is not only due to O_3.

Addition of OH scavenger does not affect O_3 induced growth in the presence of limonene but the O_3 induced growth for toluene hindered by OH scavenger. This suggests that there is no direct (or very slow) reaction between toluene and O_3 inducing SOA growth. Ozonolysis of aromatic compounds in ambient atmosphere is very slow (Izumi and Fukuyama, 1990, Atkinson, 2000). Indeed,

the extra growth in toluene-O_3 system in the absence of OH scavenger is due to the formation of OH radical through the reaction $HO_2 + O_3 \rightarrow OH + 2O_2$, and OH is important aerosol formation pathway for aromatic compounds (Atkinson, 2000). The RH of particles in the flow tube during NO and O_3 experiment was < 15%.

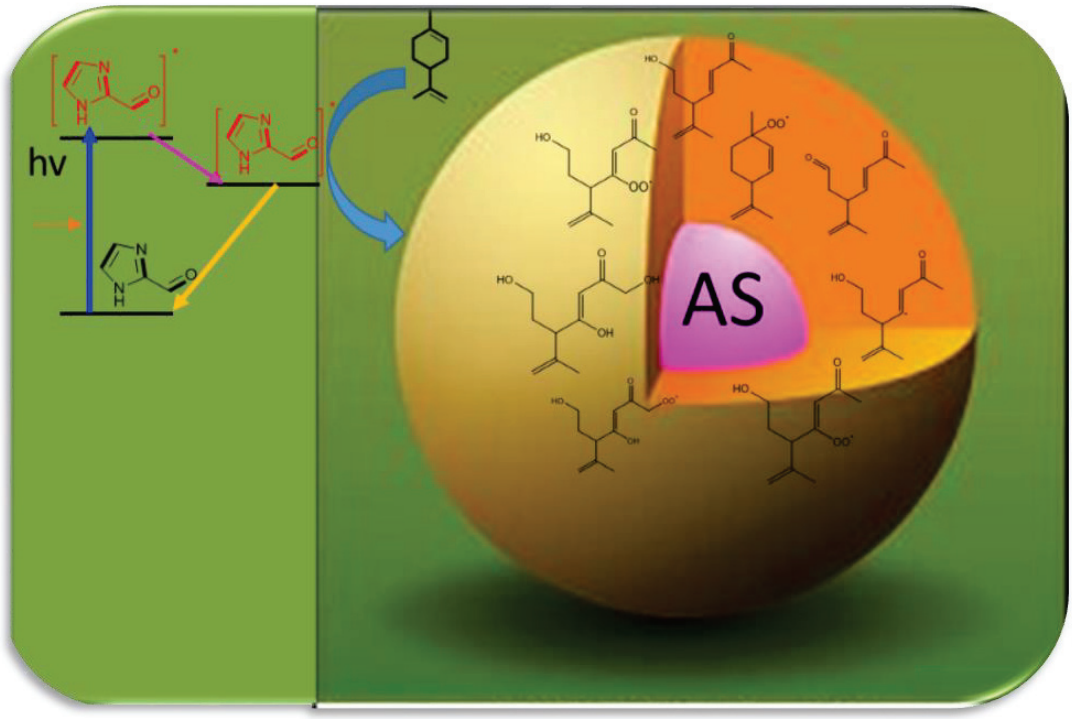

7 Aerosol composition: Contributing Reaction for SOA aging

The composition of SOA depends on the chemical compounds involved during their formation and growth. The light-particle contact time and light intensity is another parameter for the aged aerosol composition in our experiments. This chapter mainly focuses on the chemical composition of aged aerosol in the flow tube, and consists of mostly on the article published by "Environmental Science and Technology"(Rossignol et al., 2014), on the chemical compounds that are formed during photosensitized chemistry leading to organic aerosol growth.

A sample of aerosol particles was collected from the out let of the flow tube and prepared for the ESI-(±)HRMS and UPLC/(±) HESI-HRMS analysis based on the procedure given in section 3.2. In addition to this, bulk experiments using small cylindrical quartz reactor were also performed in order to compare the major products identified from the aerosol sample.

7.1 General consideration

Five important conditions have taken in to consideration to analyze the composition of aged aerosol in aerosol flow tube.

1. ***Composition of seed particles:*** The experiments were started with a known concentration and composition of seed particles. In most of our experiments, the seeds composed of AS (0.95mM) and IC (1.3mM) unless otherwise specified. Furthermore, the blank experiments were performed in a solution containing IC (1mM) and limonene (10 mM).
2. ***Gas phase oxidants****:* it is shown that the SOA growth in the flow tube is purely photosensitized, without any gas phase oxidants (OH, O_3, NO_x).
3. ***Light conditions:*** light intensity and irradiation time plays a role in photosensitized SOA growth. There was a significant difference in aerosol size when exposed to light. The aerosol samples were collected in both dark and light conditions.
4. ***VOC****:* the type and concentration of VOC can be used to assess the role of individual hydrocarbon precursors in secondary organic aerosol growth mechanism and thus to the composition analysis. VOCs having unsaturated tertiary carbon induced growth (section 4.2). Limonene was preferentially used to study the composition because of its possible contribution for SOA growth.
5. ***Oxygen content****:* the oxygen content of the carrier gas has taken in to consideration in identifying the major products that contribute for aerosol growth.

On top of these conditions, the photochemistry of IC also considered towards different VOCs, as is explained in Chapter 5.

7.2 Results and discussion

7.2.1 Photosensitized radical formation

Bulk and flow tube experiments were performed to identify major products of the reaction between the IC triplet state and limonene. In the bulk experiments, direct (±)ESI-HRMS analysis showed the formation of nitrogen-containing products as well as a range of oxygenated species. Among them, the formation of a major product at m/z 233.1643 ± 0.0001 was observed in the positive ionization mode. The high resolution of the instrument coupled with a mass accuracy estimated to be below 4 ppm under our experimental conditions allowed us to identify $C_{14}H_{21}ON_2^+$ (exact mass 233.1648, Δppm = −2.3) as the unique matching positive ion, which corresponds to a $C_{14}H_{20}ON_2$ neutral compound. The compound detected at the exact mass m/z 233.164 might thus be a radical−radical recombination product of IC ($C_4H_4ON_2$) and limonene ($C_{10}H_{16}$). This would be consistent with the expected reactivity of the IC triplet state, proceeding most probably via a hydrogen transfer leading to the formation of alkyl radicals (section 4.2.8). This hydrogen transfer can be either a direct transfer or proceed via an electron transfer followed by a proton transfer. To account for these results, formation mechanisms proceeding via the photosensitized formation of two radicals, an IC and limonene radical, are hereby suggested Figure 7-1. Due to the presence of endo and exocyclic unsaturated tertiary carbon in limonene, the UPLC/(+)HESI-HRMS analysis of bulk samples was broad and correspond to the formation of several isomers. However, the detection of such recombination product(s) highlights the photosensitized formation of radicals from limonene and IC bulk solutions.

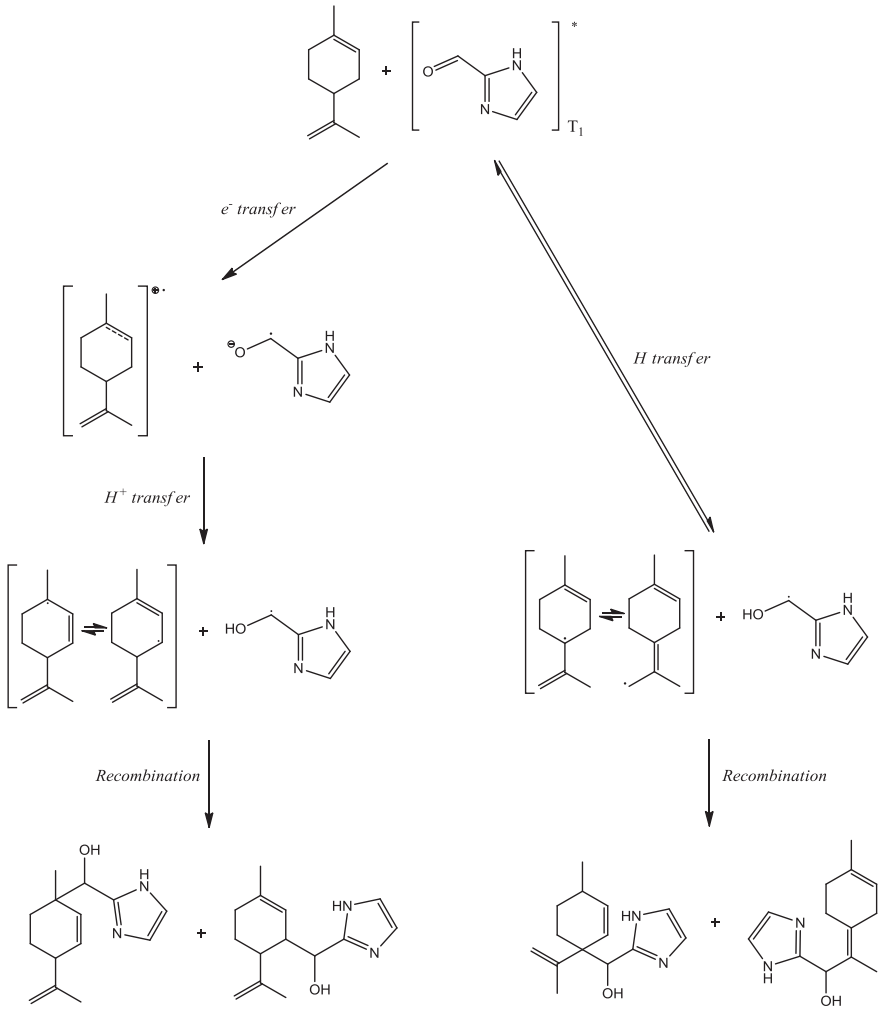

Figure 7-1 potential formation mechanisms of the recombination product of IC and limonene detected at mass m/z 233.164 in the bulk experiments from molecular limonene and IC triplet state.

In the flow tube aerosol samples, the mass at m/z 233.164 was also observed by means of UPLC/(+)HESI-HRMS analysis, but at a lower level, which precluded a direct quantitative comparison with the bulk experiments. However, two additional masses were also detected i.e., at m/z 193.072 and m/z 191.056. These masses only match with neutral compounds having as chemical formulas $C_8H_8O_2N_4$ and $C_8H_6O_2N_4$, respectively, and could therefore correspond to recombination products of IC ($C_4H_4ON_2$) with itself via hydrogen transfer from the fundamental state of IC to its

triplet state. These two recombination products of IC were not detected in bulk experiments. The high IC concentration in the seed particles in the flow tube experiments, results in a high probability of the IC triplet state reacting with another IC molecule as compared to the bulk experiments in which IC was 10 times less concentrated than limonene. It is difficult to infer from these experiments if the formation of IC-limonene and IC-IC recombination products is atmospherically relevant as the IC and limonene concentrations used here are high compared to expected atmospheric concentrations. However, the presence of these recombination products both in the bulk and in the flow tube samples indicates that the photosensitized chemistry of IC initiates radical chemistry in the aerosol phase and/or at the gas/particle interface under realistic irradiation conditions. In addition, the results of the bulk experiments showed explicitly that the IC triplet state is able to react with limonene through hydrogen abstraction as seen in Figure 7-2.

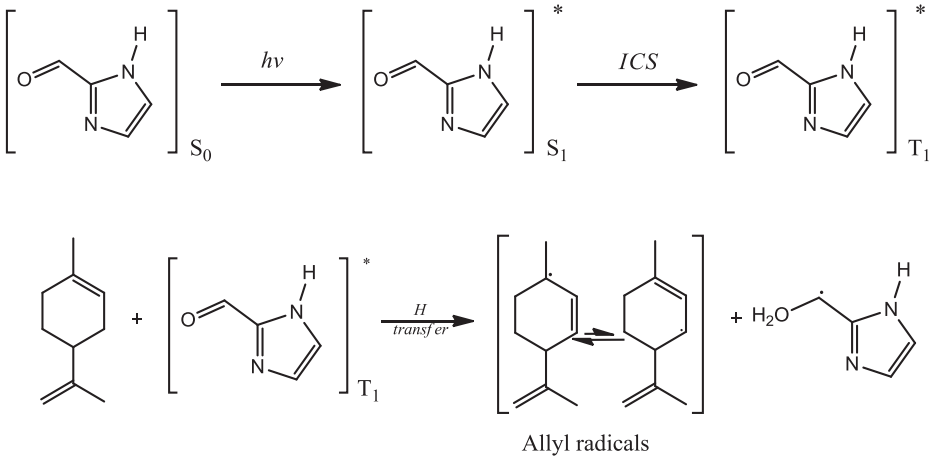

Figure 7-2 Quenching reaction of 3IC by limonene which leads to the formation of peroxyl radicals.*

7.2.2 Photosensitized limonene oxidation products

In addition to the recombination products, the SOA analysis by means of UPLC/(-)HESIHRMS revealed the formation of a range of highly oxygenated products with a majority of compounds bearing

between C_8 and C_{10} carbon chains and up to 6 oxygen atoms. These oxygenated compounds kept the C_{10} carbon skeleton of limonene and contained 4 to 6 oxygen atoms, which are remarkable in that they cannot be explained by classical gas-phase ozonolysis or photo-oxidation chemistry (Leungsakul et al., 2005).

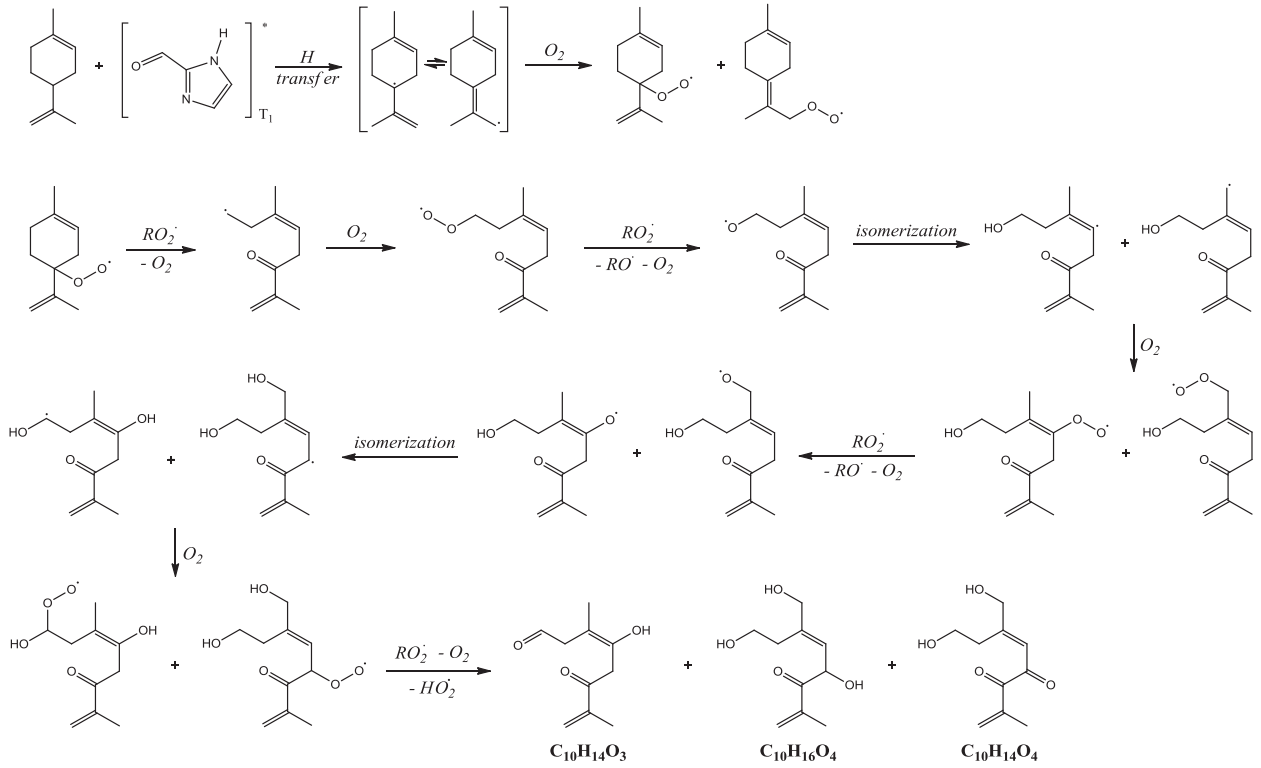

Figure 7-3 Photosensitized limonene oxidation mechanism initiated by hydrogen abstraction from limonene molecule by the IC triplet state and based on peroxy radical chemistry.

In Figure 7-3, allylic radical stabilized by electron donor alkyl group. Oxygen reacts with allylic radicals to form peroxyl radicals, which will condense o the seed aerosol. Depending on the presence of oxygen in the system, the radicals formed at the first stage will further oxidize to form more oxygenated products. The presence of such compounds clearly shows that limonene reacts in the

particle upon uptake and not in the gas phase. The formation of similar oxygenated products was confirmed in the analysis of bulk experiments.

This study showed that the presence of such photosensitizer in the ambient atmosphere could affect the daytime SOA growth, the C/O ratio and volatility of organic fraction of the aerosol via the formation of highly oxidized products.

Experimental conditions, Results and further discussion are given the paper (Rossignol S., Aregahegn K.Z., et al., 2014)

Environmental Science & Technology

Article

pubs.acs.org/est

Glyoxal Induced Atmospheric Photosensitized Chemistry Leading to Organic Aerosol Growth

Stéphanie Rossignol, Kifle Z. Aregahegn, Liselotte Tinel, Ludovic Fine, Barbara Nozière, and Christian George*

Université de Lyon, Université Lyon 1, Lyon, F-69626, France and CNRS, UMR5256, IRCELYON, Institut de Recherches sur la Catalyse et l'Environnement de Lyon, Villeurbanne, F-69626, France

ABSTRACT: In recent years, it has been proposed that gas phase glyoxal could significantly contribute to ambient organic aerosol (OA) mass through multiphase chemistry. Of particular interest is the reaction between glyoxal and ammonium cations producing light-absorbing compounds such as imidazole derivatives. It was recently shown that imidazole-2-carboxaldehyde (IC) can act as a photosensitizer, initiating aerosol growth in the presence of gaseous volatile organic compounds. Given the potential importance of this new photosensitized growth pathway for ambient OA, the related reaction mechanism was investigated at a molecular level. Bulk and flow tube experiments were performed to identify major products of the reaction of limonene with the triplet state of IC by direct (±)ESI-HRMS and UPLC/(±)HESI-HRMS analysis. Detection of recombination products of IC with limonene or with itself, in bulk and flow tube experiments, showed that IC is able to initiate a radical chemistry in the aerosol phase under realistic irradiation conditions. Furthermore, highly oxygenated limonene reaction products were detected, clearly explaining the observed OA growth. The chemistry of peroxy radicals derived from limonene upon addition of oxygen explains the formation of such low-volatile compounds without any traditional gas phase oxidant.

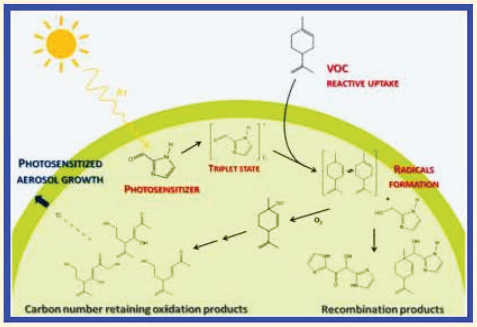

INTRODUCTION

Organic aerosol (OA) represents an important fraction (20 to 90% in mass) of the total budget of atmospheric aerosols, and its oxygenated fraction, considered as mainly of secondary origin, is significant in many locations.[1,2] A detailed knowledge of the formation and aging pathways of secondary organic aerosol (SOA) is thus critical to accurately assess their impact on visibility, health and climate. Traditionally, SOA formation has been described as proceeding only through gas phase oxidation of volatile organic compounds (VOC) forming low volatility products, which then partition between gas and particulate phases. However, in recent years it has become increasingly apparent that this simple model was not sufficient to accurately reproduce the OA mass observed and its oxidation state.[2,3] Important efforts were thus made to explain and close the gap between observations and modeling. The classical approach including only anthropogenic and biogenic VOCs (aromatic compounds, isoprene, limonene, pinene, and so forth) has been widened to include semi- and low-volatile precursors, thus bringing the calculated SOA masses closer to observations.[4−7] However, in addition to these condensation processes, it has also been pointed out that very volatile compounds such as glyoxal can significantly contribute to SOA mass through multiphase chemistry. As glyoxal and other small dicarbonyl species are emitted in large amounts during oxidation of VOCs,[8] the existence of condensed phase sinks for these gases is indeed able to explain an important part of the missing SOA mass in models,[9−12] for example, at least 15% of the SOA mass in the specific case of glyoxal uptake in Mexico city (MCMA-2003 campaign).[10]

It was shown that glyoxal uptake into droplet and water containing aerosol particles leads to the formation of low volatility species, and thus to SOA formation, through three main processes: (1) oligomer formation, (2) photochemical radical oxidation, and (3) condensation with ammonium cations (NH_4^+) and amines leading to nitrogen-containing products.[13,14] Oligomer formation occurs via acetal formation (C−O−C bond formation).[13,15−17] Photochemical oxidation of glyoxal is initiated by hydrogen abstraction by OH radical and leads to the formation of small organic acids, such as glyoxylic acid or formic acid, but also to the formation of larger oxygenated products through organic radical recombination in concentrated solutions.[13] These two pathways (oligomerization and photochemical oxidation), are particularly interesting as they form low volatility products that can match with the high oxygen to carbon ratio (O/C) detected in ambient aerosols, not yet well reproduced in models. Although this condensation pathway is certainly minor relative to SOA mass formation,[18] glyoxal reactivity toward ammonium cations and amines has

Received: December 17, 2013
Revised: February 11, 2014
Accepted: February 20, 2014
Published: February 20, 2014

dx.doi.org/10.1021/es405581g | Environ. Sci. Technol. 2014, 48, 3218−3227

Environmental Science & Technology Article

gained interest in recent years due to the fact that it leads to the formation of compounds absorbing in the UV−visible region.[17,19,20] Nozière et al.[17] showed that the reaction of glyoxal with NH_4^+ ions indeed forms light-absorbing nitrogen-containing species. Among these nitrogen-containing products, Galloway et al.[21] have identified 1H-imidazole-2-carboxaldehyde (IC), which absorbs UV radiation at λ = 290 nm. A number of laboratory studies have further confirmed the formation of products bearing an imidazole ring,[22,23] including IC.[18,24] It was also shown that these minor products were nevertheless able to impact optical and radiative properties of ambient aerosols.[23]

However, the formation of such light absorbing species can also induce new photochemical processes within the aerosol particles and/or at the gas/particle interfaces. Monge et al.[25] found experimental evidence of a photoinduced pathway for organic aerosol growth. The growth was observed when seeds containing light absorbing material [e.g., humic acid or 4-(benzoyl)benzoic acid] were exposed to light and gaseous VOCs, suggesting a reactive uptake for the latter under irradiation. Interestingly, a similar observation was made with IC-containing seeds by Aregahegn et al.[26] who, based on the works of Canonica et al.,[27] suggested a photosensitized mechanism where radical chemistry is initiated by the reaction of a VOC with the triplet state of IC.

Given of the potential importance of this new photosensitized pathway for SOA production and aging, we aimed to understand the reaction mechanism leading to the aerosol growth as reported by Aregahegn et al.[26] A first series of experiments investigated the reactivity of the IC triplet state toward limonene, chosen as a key VOC compound, using laser flash photolysis. Bulk experiments were then carried out to identify the products of the reaction between the IC triplet state and limonene, using direct electrospray ionization (positive and negative modes) coupled to high resolution mass spectrometry [(±)ESI-HRMS] and ultraperformance liquid chromatography coupled with heated (±)ESI-HRMS [UPLC/(±)HESI-HRMS]. Finally, aerosols produced in flow tube experiments, similar to those of Aregahegn et al.,[26] were analyzed by UPLC/(±)HESI-HRMS and compared with the bulk experiments to identify the organic products responsible for SOA growth.

■ EXPERIMENTAL SECTION

Laser Flash Photolysis Experiment. The reactivity of excited IC toward limonene was investigated using a classical laser flash photolysis apparatus.[28] IC triplet state was produced upon excitation under UV irradiation and its deactivation over time was followed by monitoring its absorption in the presence or absence of limonene. The photolysis excitation source was the third harmonic (266 nm, pulse width ~7 ns) of an Nd:YAG laser (Surelite II 10, Continuum, U.S.) operated in a single-shot mode. During these experiments, the laser pulse energy was limited at 20 mJ per pulse to reduce photolysis of the photosensitizer. It was experimentally observed that under this energy threshold the upper limit of the fraction of IC depleted by each pulse was negligible (<0.14 μM). Ground state IC extinction coefficient was calculated as $\varepsilon_{266\ nm}$ = 4698 M^{-1} cm^{-1}. The laser output passed through the aperture in the short axis (4 mm path length) of a fully masked quartz flow cell. The working water-acetonitrile (1:1) solutions containing IC (0.25 mM, 97%, Sigma-Aldrich, U.S.) and various amounts of limonene (0 mM, 4 mM, 8 mM and 12 mM, (*R*)-(+)-limonene 97%, Sigma-Aldrich, U.S.) were deoxygenated for at least 1 h. They were introduced into the flow cell (volume of 450 μL) by means of a peristaltic pump, with a flow rate of 1.6 mL min^{-1}, ensuring a complete purge of the exposed volume every 17 s. This limited the exposure of the introduced solution to 3−4 laser shots and maintained a constant temperature in the flow cell. All connections on the apparatus were made from either glass or PTFE tubing, ensuring a clean liquid flow. The transient absorption of the excited IC produced upon 266 nm excitation was followed by means of time-resolved absorption spectroscopy at 330 nm in the absence and presence of limonene. The analyzing light, provided by a 75 W high-pressure Xenon arc lamp (LOT-Oriel, Germany), passed through the two apertures of the long axis of the flow cell (1 cm path length). The light was then collected by a 1/4 m monochromator (DK240, Spectral Products, U.S.) equipped with a 2400 grooves/mm grating and detected by a photomultiplier (PMT, H7732-10, Hamamatsu, Japan). The PMT signal was passed through a high-speed current amplifier/discriminator (Femto, Germany) and the AC and DC component recorded on a 300 MHz oscilloscope (TDS3032c, Tektronix, U.S.). The digitalized signal was then transferred to a computer for further processing. The analysis of transient absorbance decays as well as the fitting was performed on OriginPro (version 8.5).

Bulk Experiments. A water-acetonitrile solution (1:1, v/v, Elga ultrapure water, France/Fischer Chemical, U.K.) containing IC (1 mM, 97%, Sigma-Aldrich, U.S.) and limonene (10 mM, (*R*)-(+)-limonene 97%, Sigma-Aldrich, U.S.) was placed in a small cylindrical quartz reactor (volume of 15 mL) and exposed to light in a box equipped with 7 UV-lamps (Cleo 20 W, emission range 280−400 nm, Philips, Netherlands) for 23 h. At different intervals, two 400 μL samples were diluted by a factor 25, in a water−acetonitrile solution (1:1, v/v) or pure water for direct analysis in (±)ESI-HRMS and analysis by UPLC/(±)HESI-HRMS, respectively.

Flow Tube Experiments. Photosensitized growth of aerosols was carried out using a horizontal double wall aerosol flow tube made of Pyrex (13 cm i.d. ×152 cm length) kept at 293 ± 1 K by means of a circulating water bath. The carrier gas was dry air (purity 99.9990%, Air Liquide, France), introduced at a total flow rate of 0.4 L min^{-1} allowing an aerosol residence time of 50 min. The flow tube was surrounded by 7 UV-lamps (Cleo, Philips, Netherlands) with a continuous emission spectrum over 300−420 nm and a total irradiance of 3.7 × 10^{16} photon cm^{-2} s^{-1}. A complete description of this aerosol flow tube setup is given elsewhere.[25]

For physical characterization of the aerosol growth, a monodispersed aerosol ("seed particles") was generated from an aqueous solution containing IC (1.3 mM, 97%, Sigma-Aldrich, U.S.) and ammonium sulfate (0.95 mM, 99.0%, Sigma-Aldrich, U.S.). The atomized solution (atomizer 3076, TSI, U.S.) was then dried using a Silica gel 20 diffusion drier and an initial seed particles diameter of 50 nm was selected using a Differential Mobility Analyzer (DMA 3081, TSI, U.S., impactor size 0.0588 cm, aerosol flow = 0.3 L min^{-1}, sheath flow = 3 L min^{-1}). This monodispersed aerosol contained typically 5000 particles cm^{-3} and corresponded to a total mass of a few μg m^{-3}. It was flown into the reactor where it was exposed to gaseous limonene and, when required, to UV light. A limonene concentration of around 0.9 ppm was generated using a permeation tube placed in a temperature controlled oven (Dynacal, Valco Instruments Co. Inc., U.S., using VICI

Environmental Science & Technology Article

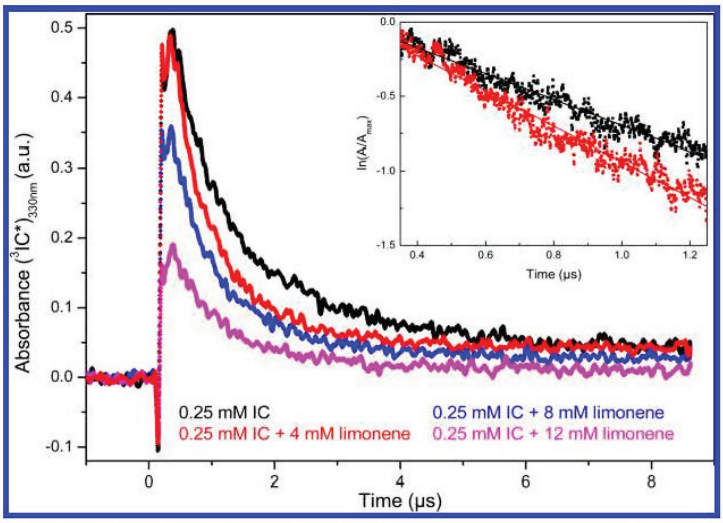

Figure 1. Transient triplet−triplet absorption of the excited IC followed at 330 nm in a water−acetonitrile (1:1) mixture in the absence of limonene as a quencher (black), in the presence of 4 mM of limonene (red), 8 mM of limonene (blue) and 12 mM of limonene (pink). Inset: linear fitting of corresponding $\ln(A/A_{max}) = f(t)$. A_{max}: maximum absorbance observed for each data series.

Metronics, U.S., Dynacalibrator, model 150). The particle size distribution and concentration obtained at the outlet of the flow tube were monitored using a Scanning Mobility Particle Sizer (SMPS 3080, TSI, U.S.), consisting of a DMA (TSI 3081) and a Condensation Particle Counter (CPC, TSI 3776).

For the aerosol sampling and subsequent chemical analysis, we decided to increase the seed particles concentration in order to improve the signal-to-noise ratio of the ESI-HRMS. At the flow tube inlet, the DMA was removed to generate a polydispersed dry aerosol. Particles were then collected at the flow tube outlet on a Teflon filter (47 mm Fluoropore membrane filters, 0.45 μm FH, Merk Millipore, U.S.) using a stainless steel filter holder (Aerosol standard filter holder, 47 mm, Merk Millipore, U.S.). Two experiments of 16 h were systematically and consecutively performed; first, a "blank" consisting of introducing both seed particles and gaseous limonene but without light, and second, a "sample" was collected with the light on. The filters were subsequently solvent extracted under ultrasonication (40 min) in 7 mL of a water-acetonitrile solution (4:6, v/v) in an Erlenmeyer, maintained at low temperature in an ice bath. Extracts were then concentrated to 1 mL under a gentle stream of nitrogen and were subsequently analyzed by UPLC/(±)HESI-HRMS.

ESI-(±)HRMS and UPLC/(±)HESI-HRMS Analysis. The UPLC/(±)HESI-HRMS system comprised a Dionex Ultimate 3000 ultraperformance liquid chromatograph (UPLC, Thermo Scientific, U.S.) coupled to a Q-Exactive high resolution mass spectrometer (HRMS, Thermo Scientific, U.S.) equipped with a heated electrospray ionization (HESI) source. Half of the bulk samples (diluted in water−acetonitrile mixture) were analyzed by direct infusion of the diluted solutions into the nonheated electrospray source (ESI-(±)HRMS analysis) at a flow rate of 30 μL min^{-1}. Source voltages of +3.5 kV and −2.6 kV were applied for the positive (+) and negative (−) ionization modes, respectively. The remaining bulk fraction and the flow tube samples were analyzed by means of UPLC/(±)HESI-HRMS. The chromatograph was equipped with a HSS T3 Acquity UPLC column (1.8 μm, 2.1 × 100 mm). The mobile phase was (A) acidified water (Fischer Chemical, U.K., + 0.1%, v/v, formic acid, Sigma-Aldrich, U.S.) and (B) acidified acetonitrile (Fischer Chemical, U.K., + 0.1%, v/v, formic acid, Sigma-Aldrich, U.S.). A 16 min gradient was applied: eluent (B) was kept at 1% for 2 min and was then increased to 90% in 10 min, this ratio was maintained for 2 min before returning to the initial condition for 2 min. The flow rate was 0.3 mL min^{-1}. Source voltages of +3.7 kV and −3.0 kV were applied for the positive (+) and negative (−) ionization modes respectively. All acquisitions were performed in full MS mode with a scan ranging from m/z 50 to m/z 750 and a resolution set to 140 000. Specific MS^2 spectra were acquired in direct infusion mode applying a normalized collision energy level of 35%. The data were processed using Xcalibur 2.2 software. The Q-Exactive mass spectrometer was mass calibrated using commercial Calmix solutions (Thermo Scientific, U.S.). To achieve good accuracy for low masses (<4 ppm) commercially used mass lists were completed with mass 74.09643 for the positive mode and masses 59.013 85 and 514.284 40 for the negative mode. All of the exact mass assignments to chemical formula were done considering carbon, hydrogen, oxygen, nitrogen, sodium, and potassium as potential elements and with a mass accuracy below 4 ppm. All of the proposed chemical formulas comply with the octet rule (i.e., an integer double bond equivalent) for the related neutral compounds.

RESULTS AND DISCUSSION

Triplet State Chemistry of IC. This first series of experiments was performed to verify the hypothesis proposed by Aregahegn et al.[26] that the excited triplet state of IC could react with limonene. The formation of an IC triplet state under UV-irradiation was demonstrated elsewhere by Tinel et al.[29] The triplet−triplet IC absorption monitored at 330 nm showed a monoexponential decay. By adding increasing amounts of limonene to the IC containing solution, the decay of the transient absorption was observed to be faster (Figure 1). These results confirmed that limonene quenches the IC triplet state, i.e., introducing a reaction that may proceed via electron or hydrogen transfer in agreement with Aregahegn et al.[26]

Environmental Science & Technology Article

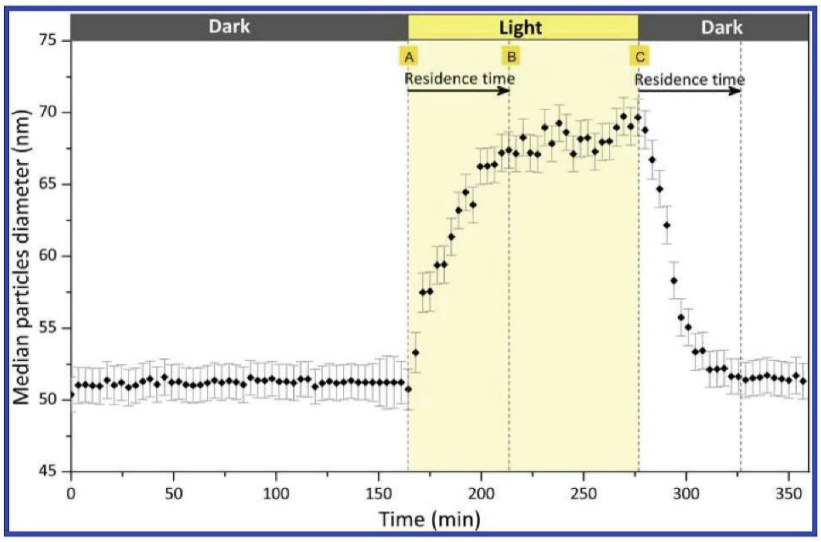

Figure 2. Temporal evolution of the median diameter of particles during a flow tube experiment. Monodisperse seed particles (IC/ammonium sulfate) were exposed to gaseous limonene continuously (0.9 ppmv) and to UV light between 165 and 277 min. Error bars correspond to 2 times the geometrical standard deviation. Arrows and dotted vertical lines mark the theoretical aerosol residence time at two critical points: when the lamps were switched on (A) and off (C).

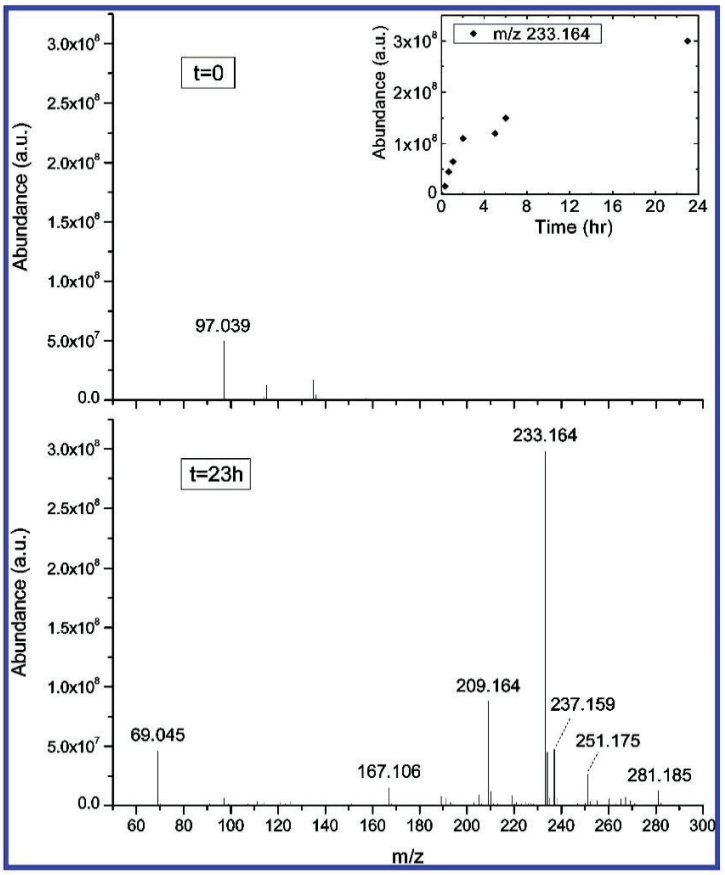

Figure 3. Average mass spectra obtained in (+)ESI-HRMS for bulk experiment at initial time and after 23 h of irradiation (average on ~70 spectra on 1 min acquisition time in direct infusion). Inset: time evolution of m/z 233.164 abundance.

Photosensitized Aerosol Growth. In order to produce SOA from photosensitization for chemical analysis, flow tube experiments similar to those presented by Aregahegn et al.[26] were performed. Monodisperse IC/ammonium sulfate aerosol seeds and gaseous limonene were first injected and irradiated. A typical profile for the evolution of the median diameter of the particles at the flow tube outlet is shown in Figure 2. As expected, a significant particle growth was observed when seed particles were exposed to both limonene and UV light. In the dark (from initial time to A in Figure 2), the median diameter was constant and very close to the seed particle diameter selected at the inlet of the flow tube (50 nm). Under irradiation, this diameter increased during a period corresponding to the residence time of the aerosol in the flow tube (50 min, from A to B in Figure 2), to reach a value of 68 nm, corresponding to a diameter growth factor of around 25% (calculated as the ratio of the difference between the final and the initial and final diameters). When the lamps were subsequently turned off (from C in Figure 2), the median diameter decreased, during a period corresponding to the residence time, returning to its initial value, confirming the key role of light in the growth of IC containing particles exposed to gaseous limonene. The observed growth was consistent with that obtained by Aregahegn et al.[26] The experimental parameters (seeds composition, limonene concentration, irradiation, and residence time) were consequently chosen to explore the composition of the grown aerosols from an initial polydisperse seed aerosol. This grown aerosol was collected and extracted by the method described in the Experimental Section for chemical analysis.

Photosensitized Radical Formation from ^{3}IC*. Bulk and flow tube experiments were performed to identify the major products of the reaction between the IC triplet state and limonene. In the bulk experiments, direct (±)ESI-HRMS analysis showed the formation of nitrogen-containing products as well as a range of oxygenated species. Among them, the formation of a major product at m/z 233.1643 ± 0.0001 was observed in the positive ionization mode (Figure 3). The signal intensity for this ion rose faster during the first 2 h of the experiment than during the last 21 h, however still increasing with time (Figure 3 inset). The high resolution of the instrument coupled with a mass accuracy estimated to be below 4 ppm under our experimental conditions allowed us to identify $C_{14}H_{21}ON_2^+$ (exact mass 233.1648, Δppm = −2.3) as the unique matching positive ion, which corresponds to a $C_{14}H_{20}ON_2$ neutral compound. An MS^2 mass spectrum of m/z 233.164 was acquired (Figure 4) and its fragmentation pattern reveals the formation of a major fragment at m/z 97.0394 ± 0.0001. This fragment corresponds to a $C_4H_5ON_2^+$ chemical formula (exact mass 97.0396, Δppm = −2.5) and can consequently be attributed to an IC fragment ($C_4H_4ON_2$). The compound detected at the exact mass m/z 233.164 might thus be a radical−radical recombination product of IC ($C_4H_4ON_2$) and limonene ($C_{10}H_{16}$). This would be consistent with the expected reactivity of the IC triplet state, proceeding most probably via a hydrogen transfer leading to the formation of alkyl radicals.[26] This hydrogen transfer can be either a direct transfer or proceed via an electron transfer followed by a proton transfer. To account for these results, formation mechanisms proceeding via the photosensitized formation of two radicals, an IC and limonene radical, are hereby suggested (Figure 5). The position of the transferred hydrogen on the limonene structure could be mechanism dependent. In

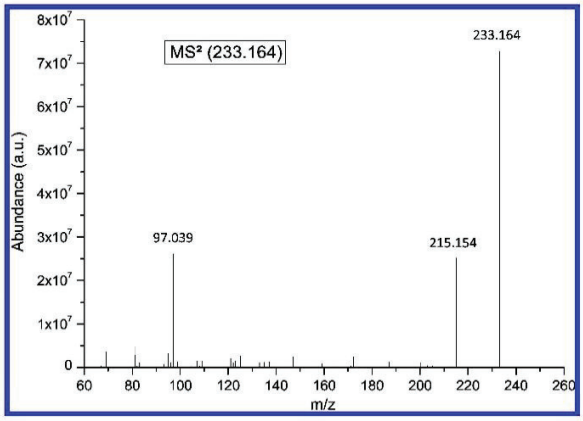

Figure 4. MS^2 mass spectrum of m/z 233.164 in (+)ESI-HRMS.

principle, the weaker C−H bond in the limonene molecule should be on the secondary allylic carbons or on the tertiary allylic carbon.[30] Accordingly, these hydrogen atoms will be preferentially transferred in case of a direct transfer. If the mechanism proceeds first via an electron transfer, then the abstracted electron will preferentially be located on the endocyclic double bond as the corresponding radical cation is stabilized by both tertiary and secondary carbons. Using the available data, it remains difficult to suggest which of the proposed pathways is most dominant. Furthermore, the chromatographic peak obtained for m/z 233.164 by UPLC/(+)HESI-HRMS analysis of bulk samples was broad and bore shoulders that could correspond to the formation of several isomers. In any case, the detection of such recombination product(s) highlights the photosensitized formation of radicals from limonene and IC the bulk solutions.

In the flow tube aerosol samples, the mass at m/z 233.164 was also observed by means of UPLC/(+)HESI-HRMS analysis, but at a lower level, which precluded a direct quantitative comparison with the bulk experiments. However, two additional masses were also detected i.e., at m/z 193.072 and m/z 191.056 (Table 1). These masses only match with neutral compounds having as chemical formulas $C_8H_8O_2N_4$ and $C_8H_6O_2N_4$, respectively, and could therefore correspond to recombination products of IC ($C_4H_4ON_2$) with itself via a pathway depicted in Figure 6. The high IC concentration in the seed particles in the flow tube experiments, results in a high probability of the IC triplet state reacting with another IC molecule leading to hydrogen transfer from the fundamental state to the triplet state. This hydrogen transfer likely involves the carbonyl hydrogen as the corresponding C−H bond dissociation energy is in the same order of magnitude as an allylic transfer.[30] This hydrogen transfer subsequently leads either directly to the recombination of the two just formed radicals to give the recombination product detected at m/z 193.072, or to the recombination of two radicals having undergone hydrogen abstraction to give the compound detected at m/z 191.056. These two recombination products of IC with itself were not detected in bulk experiments. A simple concentration effect can be invoked here, as in the bulk experiments, IC was 10 times less concentrated than limonene. On the contrary, in flow tube experiments, seed particles were only composed of dry IC and ammonium sulfate exposed to 0.9

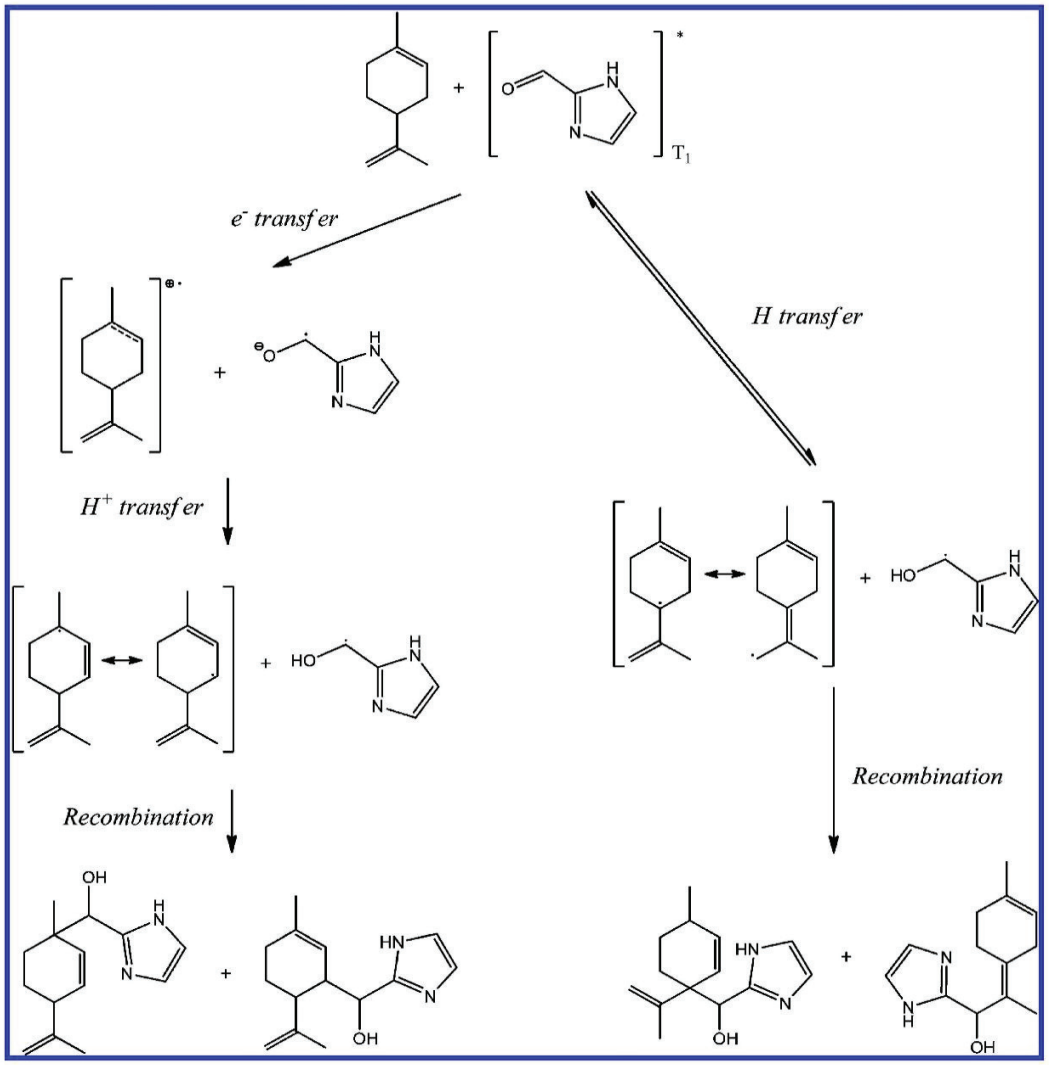

Figure 5. Potential formation mechanisms of the recombination product of IC and limonene detected at mass m/z 233.164 in the bulk experiments from molecular limonene and IC triplet state.

ppm of gaseous limonene leading to the predominance of IC-IC recombination products over IC-limonene ones.

It is difficult to infer from these experiments if the formation of IC-limonene and IC-IC recombination products is atmospherically relevant as the IC and limonene concentrations used here are high compared to expected atmospheric concentrations. However, the presence of these recombination products both in the bulk and in the flow tube samples indicates that the photosensitized chemistry of IC initiates radical chemistry in the aerosol phase and/or at the gas/particle interface under realistic irradiation conditions. In addition, the results of the bulk experiments showed explicitly that the IC triplet state is able to react with limonene through hydrogen abstraction.

Highly Oxygenated Limonene Oxidation Products. Both bulk and flow tube experiments provided evidence of radical formation from the IC triplet state. Here, results of the flow tube experiments will be preferentially discussed to explain the observed aerosol growth. In addition to the recombination products, the SOA analysis by means of UPLC/(-)HESI-HRMS revealed the formation of a range of highly oxygenated products with a majority of compounds bearing between C_8 and C_{10} carbon chains and up to 6 oxygen atoms (Table 1). No attempt was made here to elucidate their chemical structure nor to quantify them. However, the fact that these oxygenated products were formed in only 50 min without any gas phase oxidant is noteworthy. Of particular interest are the compounds that kept the C_{10} carbon chain of limonene and contained 4 to 6 oxygen atoms, which are remarkable in that they cannot be explained by classical gas-phase ozonolysis or photooxidation chemistry; the terminal double bond of limonene implying necessarily some fragmentation reducing the carbon number.[31−33] The presence of such compounds clearly shows that limonene reacts in the particle upon uptake and not in the gas phase. The formation of similar oxygenated products was confirmed in the analysis of bulk experiments, with

Environmental Science & Technology Article

Table 1. Detected Exact Masses in the Grown Aerosols Coming from a Flow Tube Experiment by UPLC/(±)HESI-MS

ionization mode	detected mass (m/z)	chemical formula[a]	R_t (min)	area[b] (× 10^5 a.u.)	light/dark ratio[c]
(+)	233.164	$C_{14}H_{20}ON_2$	7.53	26	459
(+)	193.072	$C_8H_8O_2N_4$	6.61	1100	101
(+)	191.056	$C_8H_6O_2N_4$	5.27	820	380
(−)	151.113	$C_{10}H_{16}O$	8.99−9.41	1.7 (9.41)	344
(−)	167.108	$C_{10}H_{16}O_2$	7.06−7.31−7.60	7.6 (7.31)	89
(−)	183.102	$C_{10}H_{16}O_3$	8.05−8.14	36 (8.05)	97
(−)	181.087	$C_{10}H_{14}O_3$	8.35	10	40
(−)	199.098	$C_{10}H_{16}O_4$	6.88	280	14
(−)	197.082	$C_{10}H_{14}O_4$	6.64	26	73
(−)	215.092	$C_{10}H_{16}O_5$	5.80−6.15	86 (6.15)	203
(−)	213.077	$C_{10}H_{14}O_5$	6.10−6.46−6.65	19 (6.65)	37
(−)	231.087	$C_{10}H_{16}O_6$	4.91−5.14	49 (4.91)	1245
(−)	229.072	$C_{10}H_{14}O_6$	5.89	11	106
(−)	185.082	$C_9H_{14}O_4$	7.26	330	130
(−)	183.066	$C_9H_{12}O_4$	5.19−5.31−5.84	15 (5.19)	333
(−)	169.087	$C_9H_{14}O_3$	7.73	26	40
(−)	155.071	$C_8H_{12}O_3$	6.33	23	9
(−)	187.061	$C_8H_{12}O_5$	5.53	220	340

[a]Neutral chemical formula corresponding to the positively or negatively charged chemical formula determined form detected exact mass. [b]In case of several retention times, the area of the main peak is given (peak retention time in brackets). [c]Ratio of the peak area detected in the irradiated sample on the peak (or the noise) area detected at the same retention time in the nonirradiated sample.

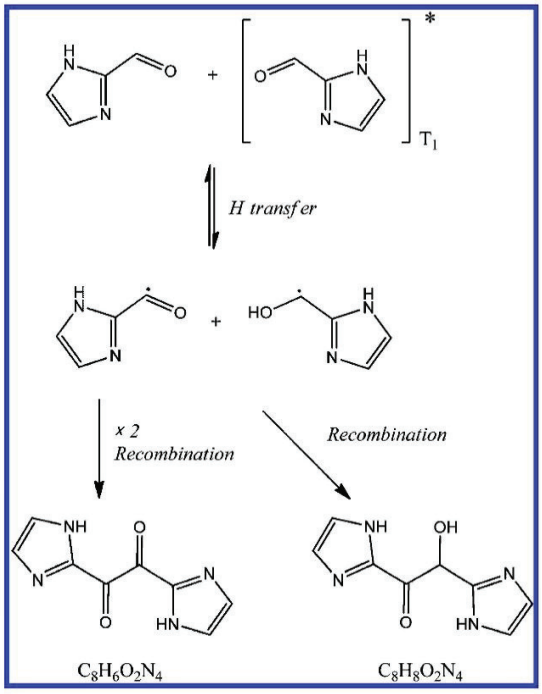

Figure 6. Potential formation mechanisms of the recombination products of IC with itself detected in flow tube sample.

corresponding ion intensities increasing with time. Because of their expected low volatility, due to the presence of up to 6 oxygen atoms on the limonene structure, these oxygenated products are expected to participate to the observed SOA growth.

On the basis of the IC radical chemistry evidenced in this work and the previous observation that molecular oxygen is necessary for SOA growth,[26] a mechanism explaining the formation of such compounds and based on peroxy radical chemistry is suggested. This mechanism is initiated by the direct abstraction of a hydrogen atom on limonene by the IC triplet state leading to the formation of a stable allylic radical. The addition of molecular oxygen leads to a peroxy radical that can evolve toward a large range of oxidation products,[34] including compounds retaining the same number of carbons as limonene. As an illustration, the formation mechanism of the three compounds $C_{10}H_{16}O_4$, $C_{10}H_{14}O_4$ and $C_{10}H_{14}O_3$, detected at m/z 199.098, m/z 197.082, and m/z 181.087, respectively, is presented in Figure 7. This mechanism underlines that the observed products are the result, after ring-opening, of intramolecular isomerization (1,5 hydrogen shift[35]) which are particularly favored in the case of limonene. The number of possible 1,5 hydrogen shifts is indeed numerous in the limonene structure because of the chain of 7 carbons and the isopropene side chain. Furthermore, the first step of the mechanism is controlled by the formation of an allylic radical, especially stable in the case of limonene and any other VOC bearing unsaturated tertiary carbon. This mechanism would thus be consistent with the previous observations of Aregahegn et al.[26] that aerosol growth was mostly observed with this type of compounds.

Atmospheric Implications. Light-induced reactive uptake of VOCs was previously observed and presented as a potentially important atmospheric pathway, but still unaccounted for in SOA mass budget, by Monge et al.[25] and Aregahegn et al.[26] However, the data reported here is, to our knowledge, the first proposed photosensitized mechanism based on actual reaction products. In this work, the identification of various recombination products has clearly shown that the presence of IC in the aerosol phase can initiate radical chemistry under near-UV irradiation. The IC triplet state is able to abstract hydrogen from limonene molecules leading to their reactive uptake with subsequent oxidation, and similar mechanisms can be inferred for the other unsaturated and branched VOCs studied by Aregahegn et al.[26] Such VOCs (i.e., bearing a branched allylic or a branched aromatic

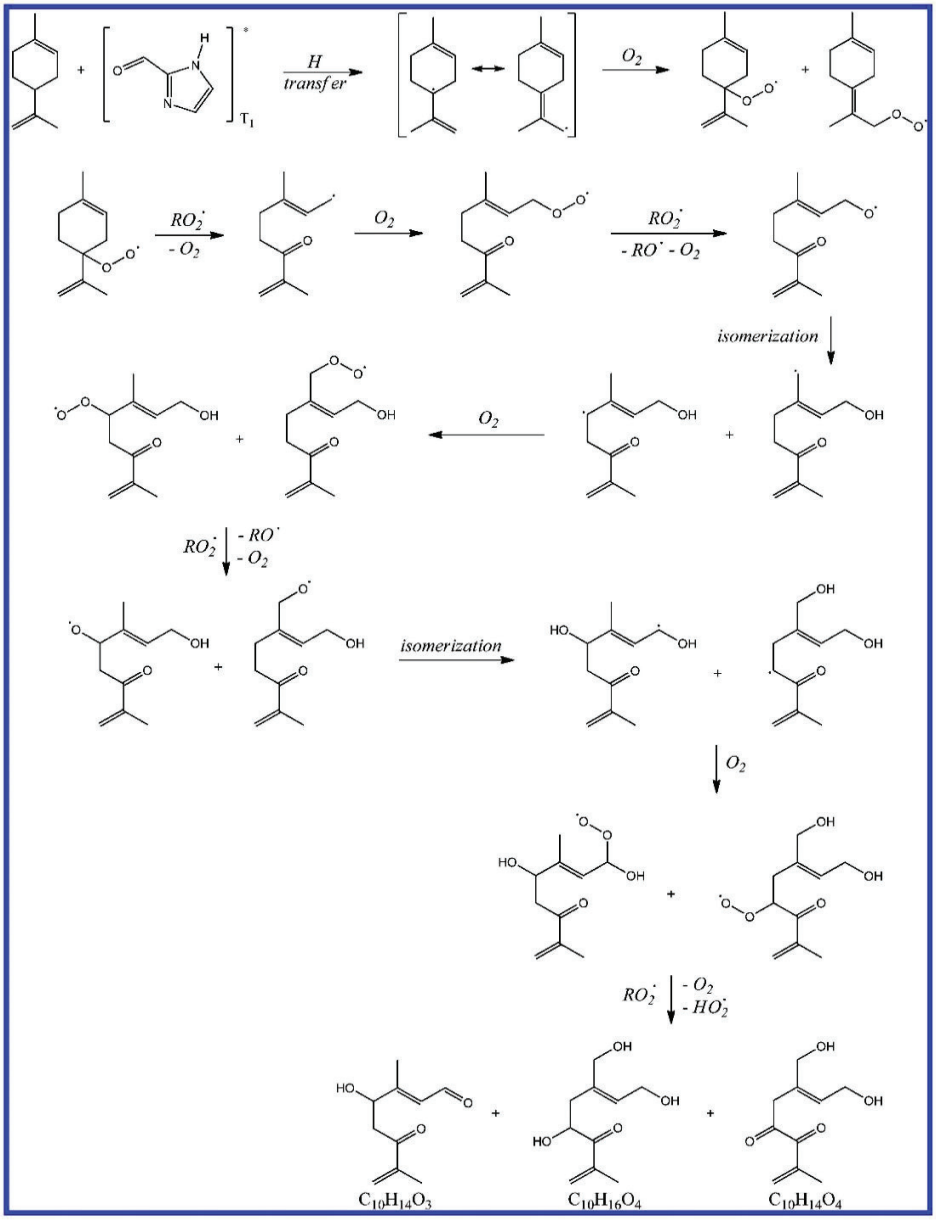

Figure 7. Limonene photosensitized oxidation mechanism initiated by hydrogen abstraction on limonene molecule through reaction with IC triplet state and based on the peroxy radical chemistry. Example for the formation of three compounds keeping the C_{10} limonene skeleton by two steps of isomerization.

structure) are emitted in large amounts by biogenic and anthropogenic sources.[36−38] Their direct uptake into the particulate phase without the need of previous gas phase oxidation and partitioning steps and the subsequent fast formation of highly oxygenated products, could lead to significant SOA formation even if other reactants are present in the particulate phase,[26] or if photosensitizers are present at trace quantities. Recent studies have shown that IC can indeed be formed within a time scale relevant for atmospheric processes (1 to 2 h), even if the reaction may not be complete and depends on involved reactant concentrations.[21,24,26] Furthermore, one may suppose that the recently evidenced near UV light-absorbing material formation via particulate phase chemistry of carbonyls with ammonium ions and amines,[17−20,22,39] potentially involves a variety of additional still unknown photosensitizers.

Beyond the reactive uptake of VOCs (or even SVOCs bearing hydrogen available for abstraction), in situ photosensitizer formation could also efficiently impact the chemistry of the particulate phase. Until now, the only source of radicals considered for the particulate phase was the transfer of oxidants from the gas phase (OH, O_3, NO_3, and halogens), photo-

Fenton chemistry, and nitrate photolysis.[40,41] The photo-induced processes studied in this work could represent a previously unaccounted for in situ particulate phase source of radicals. Furthermore, previous works reported experimental evidence potentially supporting such photosensitized processes.[21] In the SOA produced by glyoxal uptake in the presence of ammonium sulfate seeds, Galloway et al.[21] observed the formation of IC and, only in the presence of light, the coformation of highly oxidized organic species (e.g., glyoxylic, glycolic, formic acid). As no oxidant was added, no clear origin of these products, OH or some other radical mechanisms, has been evidenced. Formation of IC could thus be involved. In these experiments, as glyoxal was the only VOC to be added, the reaction of the IC triplet state would have to be with glyoxal. Moreover, this reaction is expected to be as efficient as with limonene because C−H bond dissociation energy on an aldehydic carbon is of the same order of magnitude as on an allylic carbon.[30] In that case, the in situ IC formation via glyoxal reactivity could interestingly be able to influence daytime fate of glyoxal within the particulate phase, enhancing its irreversible loss.

The results of this work suggest that, generally speaking, the presence of photosensitizers in ambient aerosol might influence (1) the daytime SOA growth via the reactive uptake of VOCs and (2) the O/C ratio and volatility of the organic fraction of the aerosol via the fast formation of highly oxidized products. As these two points are critical to assess SOA budget and properties, further research is now required to estimate the magnitude of these processes in real environments. In particular, it would be interesting to compare the rate of light-induced uptake of VOCs due to these processes and those of their gas phase oxidation processes. The comparison between these different pathways in the atmosphere could also be based on the identification of different tracers. The identification of other potential photosensitizers is also necessary.

■ AUTHOR INFORMATION

Corresponding Author

*Phone: (33) (0)4 37 42 36 81; fax: (33) (0)4 72 44 84 38; e-mail: christian.george@ircelyon.univ-lyon1.fr.

Notes

The authors declare no competing financial interest.

■ ACKNOWLEDGMENTS

The research leading to these results has received funding from the European Research Council under the European Union's Seventh Framework Programme (FP/2007-2013)/ERC Grant Agreement 290852-AIRSEA.

■ REFERENCES

(1) Jimenez, J. L.; Canagaratna, M. R.; Donahue, N. M.; Prevot, A. S. H.; Zhang, Q.; Kroll, J. H.; DeCarlo, P. F.; Allan, J. D.; Coe, H.; Ng, N. L.; Aiken, A. C.; Docherty, K. S.; Ulbrich, I. M.; Grieshop, A. P.; Robinson, A. L.; Duplissy, J.; Smith, J. D.; Wilson, K. R.; Lanz, V. A.; Hueglin, C.; Sun, Y. L.; Tian, J.; Laaksonen, A.; Raatikainen, T.; Rautiainen, J.; Vaattovaara, P.; Ehn, M.; Kulmala, M.; Tomlinson, J. M.; Collins, D. R.; Cubison, M. J. E.; Dunlea, J.; Huffman, J. A.; Onasch, T. B.; Alfarra, M. R.; Williams, P. I.; Bower, K.; Kondo, Y.; Schneider, J.; Drewnick, F.; Borrmann, S.; Weimer, S.; Demerjian, K.; Salcedo, D.; Cottrell, L.; Griffin, R.; Takami, A.; Miyoshi, T.; Hatakeyama, S.; Shimono, A.; Sun, J. Y.; Zhang, Y. M.; Dzepina, K.; Kimmel, J. R.; Sueper, D.; Jayne, J. T.; Herndon, S. C.; Trimborn, A. M.; Williams, L. R.; Wood, E. C.; Middlebrook, A. M.; Kolb, C. E.; Baltensperger, U.; Worsnop, D. R. Evolution of organic aerosols in the atmosphere. *Science* **2009**, *326*, 1525−1529.

(2) Hallquist, M.; Wenger, J. C.; Baltensperger, U.; Rudich, Y.; Simpson, D.; Claeys, M.; Dommen, J.; Donahue, N. M.; George, C.; Goldstein, A. H.; Hamilton, J. F.; Herrmann, H.; Hoffmann, T.; Iinuma, Y.; Jang, M.; Jenkin, M. E.; Jimenez, J. L.; Kiendler-Scharr, A.; Maenhaut, W.; McFiggans, G.; Mentel, T. F.; Monod, A.; Prevot, A. S. H.; Seinfeld, J. H.; Surratt, J. D.; Szmigielski, R.; Wildt, J. The formation, properties and impact of secondary organic aerosol: Current and emerging issues. *Atmos. Chem. Phys.* **2009**, *9*, 5155−5236.

(3) Hodzic, A.; Jimenez, J. L.; Madronich, S.; Aiken, A. C.; Bessagnet, B.; Curci, G.; Fast, J.; Lamarque, J. F.; Onasch, T. B.; Roux, G.; Schauer, J. J.; Stone, E. A.; Ulbrich, I. M. Modeling organic aerosols during MILAGRO: Importance of biogenic secondary organic aerosols. *Atmos. Chem. Phys.* **2009**, *9*, 6949−6981.

(4) Shrivastava, M.; Lipsky, E. M.; Stanier, C. O.; Robinson, A. L. Modeling semivolatile organic aerosol mass emissions from combustion systems. *Environ. Sci. Technol.* **2006**, *40*, 2671−2677.

(5) Robinson, A. L.; Donahue, N. M.; Shrivastava, M. K.; Weitkamp, E. A.; Sage, A. M.; Grieshop, A. P.; Lane, T. E.; Pierce, J. R.; Pandis, S. N. Rethinking organic aerosols: Semivolatile emissions and photochemical aging. *Science* **2007**, *315*, 1259−1262.

(6) Dzepina, K.; Volkamer, R. M.; Madronich, S.; Tulet, P.; Ulbrich, I. M.; Zhang, Q.; Cappa, C. D.; Ziemann, P. J.; Jimenez, J. L. Evaluation of recently-proposed secondary organic aerosol models for a case study in Mexico City. *Atmos. Chem. Phys.* **2009**, *9*, 5681−5709.

(7) Shrivastava, M.; Fast, J.; Easter, R.; Gustafson, W. I., Jr.; Zaveri, R. A.; Jimenez, J. L.; Saide, P.; Hodzic, A. Modeling organic aerosols in a megacity: Comparison of simple and complex representations of the volatility basis set approach. *Atmos. Chem. Phys.* **2011**, *11*, 6639−6662.

(8) Fu, T. M.; Jacob, D. J.; Wittrock, F.; Burrows, J. P.; Vrekoussis, M.; Henze, D. K. Global budgets of atmospheric glyoxal and methylglyoxal, and implications for formation of secondary organic aerosols. *J. Geophys. Res.—Atmos.* **2008**, *113*, D15303.

(9) Volkamer, R.; Jimenez, J. L.; San Martini, F.; Dzepina, K.; Zhang, Q.; Salcedo, D.; Molina, L. T.; Worsnop, D. R.; Molina, M. J. Secondary organic aerosol formation from anthropogenic air pollution: Rapid and higher than expected. *Geophys. Res. Lett.* **2006**, *33*, L17811.

(10) Volkamer, R.; San Martini, F.; Molina, L. T.; Salcedo, D.; Jimenez, J. L.; Molina, M. J. A missing sink for gas-phase glyoxal in Mexico City: Formation of secondary organic aerosol. *Geophys. Res. Lett.* **2007**, *34*, L19807.

(11) Volkamer, R.; Ziemann, P. J.; Molina, M. J. Secondary organic aerosol formation from acetylene (C_2H_2): Seed effect on SOA yields due to organic photochemistry in the aerosol aqueous phase. *Atmos. Chem. Phys.* **2009**, *9*, 1907−1928.

(12) Waxman, E. M.; Dzepina, K.; Ervens, B.; Lee-Taylor, J.; Aumont, B.; Jimenez, J. L.; Madronich, S.; Volkamer, R. Secondary organic aerosol formation from semi- and intermediate-volatility organic compounds and glyoxal: Relevance of O/C as a tracer for aqueous multiphase chemistry. *Geophys. Res. Lett.* **2013**, *40*, 978−982.

(13) Lim, Y. B.; Tan, Y.; Perri, M. J.; Seitzinger, S. P.; Turpin, B. J. Aqueous chemistry and its role in secondary organic aerosol (SOA) formation. *Atmos. Chem. Phys.* **2010**, *10*, 10521−10539.

(14) Ervens, B.; Volkamer, R. Glyoxal processing by aerosol multiphase chemistry: Towards a kinetic modeling framework of secondary organic aerosol formation in aqueous particles. *Atmos. Chem. Phys.* **2010**, *10*, 8219−8244.

(15) Loeffler, K. W.; Koehler, C. A.; Paul, N. M.; De Haan, D. O. Oligomer formation in evaporating aqueous glyoxal and methyl glyoxal solutions. *Environ. Sci. Technol.* **2006**, *40*, 6318−6323.

(16) Hastings, W. P.; Koehler, C. A.; Bailey, E. L.; De Haan, D. O. Secondary organic aerosol formation by glyoxal hydration and oligomer formation: Humidity effects and equilibrium shifts during analysis. *Environ. Sci. Technol.* **2005**, *39*, 8728−8735.

(17) Nozière, B.; Dziedzic, P.; Córdova, A. Products and kinetics of the liquid-phase reaction of glyoxal catalyzed by ammonium ions (NH_4^+). *J. Phys. Chem. A* **2009**, *113*, 231−237.

(18) Kampf, C. J.; Jakob, R.; Hoffmann, T. Identification and characterization of aging products in the glyoxal/ammonium sulfate system - implications for light-absorbing material in atmospheric aerosols. *Atmos. Chem. Phys.* **2012**, *12*, 6323−6333.
(19) Shapiro, E. L.; Szprengiel, J.; Sareen, N.; Jen, C. N.; Giordano, M. R.; McNeill, V. F. Light-absorbing secondary organic material formed by glyoxal in aqueous aerosol mimics. *Atmos. Chem. Phys.* **2009**, *9*, 2289−2300.
(20) Bones, D. L.; Henricksen, D. K.; Mang, S. A.; Gonsior, M.; Bateman, A. P.; Nguyen, T. B.; Cooper, W. J.; Nizkorodov, S. A. Appearance of strong absorbers and fluorophores in limonene-O_3 secondary organic aerosol due to NH_4^+-mediated chemical aging over long time scales. *J. Geophys. Res.—Atmos.* **2010**, *115*, D05203.
(21) Galloway, M. M.; Chhabra, P. S.; Chan, A. W. H.; Surratt, J. D.; Flagan, R. C.; Seinfeld, J. H.; Keutsch, F. N. Glyoxal uptake on ammonium sulphate seed aerosol: Reaction products and reversibility of uptake under dark and irradiated conditions. *Atmos. Chem. Phys.* **2009**, *9*, 3331−3345.
(22) De Haan, D. O.; Hawkins, L. N.; Kononenko, J. A.; Turley, J. J.; Corrigan, A. L.; Tolbert, M. A.; Jimenez, J. L. Formation of nitrogen-containing oligomers by methylglyoxal and amines in simulated evaporating cloud droplets. *Environ. Sci. Technol.* **2011**, *45*, 984−991.
(23) Trainic, M.; Riziq, A. A.; Lavi, A.; Flores, J. M.; Rudich, Y. The optical, physical and chemical properties of the products of glyoxal uptake on ammonium sulfate seed aerosols. *Atmos. Chem. Phys.* **2011**, *11*, 9697−9707.
(24) Yu, G.; Bayer, A. R.; Galloway, M. M.; Korshavn, K. J.; Fry, C. G.; Keutsch, F. N. Glyoxal in aqueous ammonium sulfate solutions: Products, kinetics and hydration effects. *Environ. Sci. Technol.* **2011**, *45*, 6336−6342.
(25) Monge, M. E.; Rosenørn, T.; Favez, O.; Müller, M.; Adler, G.; Abo Riziq, A.; Rudich, Y.; Herrmann, H.; George, C.; D'Anna, B. Alternative pathway for atmospheric particles growth. *Proc. Natl. Acad. Sci. U.S.A.* **2012**, *109*, 6840−6844.
(26) Aregahegn, K. Z.; Noziere, B.; George, C. Organic aerosol formation photo-enhanced by the formation of secondary photosensitizers in aerosols. *Faraday Discuss.* **2013**, *165*, 123−134.
(27) Canonica, S.; Jans, U.; Stemmler, K.; Hoigne, J. Transformation kinetics of phenols in water: Photosensitization by dissolved natural organic material and aromatic ketones. *Environ. Sci. Technol.* **1995**, *29*, 1822−1831.
(28) Jammoul, A.; Dumas, S.; D'Anna, B.; George, C. Photoinduced oxidation of sea salt halides by aromatic ketones: A source of halogenated radicals. *Atmos. Chem. Phys.* **2009**, *9*, 4229−4237.
(29) Tinel, L.; Dumas, S.; George, C. A time resolved study of the multiphase chemistry of excited carbonyls: Imidazole-2-carboxaldehyde and halides. *C. R. Chim.* **2013**.
(30) Blanksby, S. J.; Ellison, G. B. Bond dissociation energies of organic molecules. *Acc. Chem. Res.* **2003**, *36*, 255−263.
(31) Leungsakul, S.; Jeffries, H. E.; Kamens, R. M. A kinetic mechanism for predicting secondary aerosol formation from the reactions of D-limonene in the presence of oxides of nitrogen and natural sunlight. *Atmos. Environ.* **2005**, *39*, 7063−7082.
(32) Jaoui, M.; Corse, E.; Kleindienst, T. E.; Offenberg, J. H.; Lewandowski, M.; Edney, E. O. Analysis of secondary organic aerosol compounds from the photooxidation of D-limonene in the oresence of NO_x and their detection in ambient $PM_{2.5}$. *Environ. Sci. Technol.* **2006**, *40*, 3819−3828.
(33) Chacon-Madrid, H. J.; Donahue, N. M. Fragmentation vs. functionalization: Chemical aging and organic aerosol formation. *Atmos. Chem. Phys.* **2011**, *11*, 10553−10563.
(34) von Sonntag, C.; Schuchmann, H.-P. The elucidation of peroxyl radical reactions in aqueous solution with the help of radiation-chemical methods. *Angew. Chem., Int. Ed.* **1991**, *30*, 1229−1253.
(35) Atkinson, R. Gas-phase tropospheric chemistry of volatile organic compounds 0.1. Alkanes and alkenes. *J. Phys. Chem. Ref. Data* **1997**, *26*, 215−290.
(36) Tsigaridis, K.; Kanakidou, M. Global modelling of secondary organic aerosol in the troposphere: A sensitivity analysis. *Atmos. Chem. Phys.* **2003**, *3*, 1849−1869.
(37) Seinfeld, J. H.; Pankow, J. F. Organic atmospheric particulate material. *Annu. Rev. Phys. Chem.* **2003**, *54*, 121−140.
(38) Guenther, A.; Karl, T.; Harley, P.; Wiedinmyer, C.; Palmer, P. I.; Geron, C. Estimates of global terrestrial isoprene emissions using MEGAN (Model of Emissions of Gases and Aerosols from Nature). *Atmos. Chem. Phys.* **2006**, *6*, 3181−3210.
(39) Updyke, K. M.; Nguyen, T. B.; Nizkorodov, S. A. Formation of brown carbon via reactions of ammonia with secondary organic aerosols from biogenic and anthropogenic precursors. *Atmos. Environ.* **2012**, *63*, 22−31.
(40) Chevallier, E.; Jolibois, R. D.; Meunier, N.; Carlier, P.; Monod, A. "Fenton-like" reactions of methylhydroperoxide and ethylhydroperoxide with Fe^{2+} in liquid aerosols under tropospheric conditions. *Atmos. Environ.* **2004**, *38* (4), 921−933.
(41) Nguyen, T. B.; Coggon, M. M.; Flagan, R. C.; Seinfeld, J. H. Reactive uptake and photo-fenton oxidation of glycolaldehyde in aerosol liquid water. *Environ. Sci. Technol.* **2013**, *47* (9), 4307−4316.

8 General conclusions and perspectives

This study was devoted to the investigation of the photosensitized reactions that contribute to SOA formation and aging in a simulated aerosol flow reactor.

Despite its contribution for the formation of SOA and light absorbing compound(s), the multiphase chemistry of glyoxal was never studied before for the photosensitizing properties it may convey to tropospheric aerosols. Therefore, the photosensitized SOA growth as well as the identification of photosensitizer arising from condensed phase chemistry of glyoxal are reported here for the first time. Although some studies showed that glyoxal leads to an increase in SOA mass in the presence of light (Volkamer et al., 2009), the reaction product that is responsible for such SOA growth was not identified beforehand.

It is shown here that imidazole-2-carboxaldehyde drives photosensitized SOA mass and particle size increase in the presence of reactive gaseous volatile organic compounds. This study was performed with an aerosol flow tube and in the presence of appropriate particulate photosensitizer, gaseous VOC and light. The aerosol flow tube allowed to employ experimental conditions that were close to atmospheric ones. The influence of experimental parameters such as light, VOC type and concentration and relative humidity were investigated. It was observed that organic particles were growing with light in the presence of VOC and photosensitizer (imidazole-2-caroxaldehyde), with no new particle formation and without traditional gas phase oxidants (OH, NO_x and O_3). However, this work evidenced that imidazole-2-carboxaldehyde photosensitized SOA growth requires molecular oxygen in the system.

The SOA growth obtained in this work can be compared with those observed in the atmosphere, such as the one observed in the MCMA-2003 campaign in Mexico City, which was largely attributed

to glyoxal reactions in the aerosols (Volkamer et al., 2007). On 9 April 2003 a steady SOA growth corresponding of 3.3 μg m^{-3} h^{-1} (Volkamer et al., 2006, Volkamer et al., 2007) was observed over 6 h of sunlight, and varying between ~2 and 5.2 μg m^{-3} h^{-1}. In our experiments, a SOA mass growth of 3.2 μg m^{-3} hr^{-1} was obtained when exposing seed particles to 500 ppbv of limonene for 40 min. As the total concentration of VOCs expected to contribute to these processes (tertiary alkenes, branched aromatic.) in Mexico City might not exceed 100 ppbv (Fortner et al., 2009, Velasco et al., 2007) the new processes might account for 5 to 10% of the SOA growth observed at this location. This estimation indicates that these new processes might make a significant contribution to SOA mass in the atmosphere. Regarding the SOA size change, this study found that ca. 20 nm SOA growth was observed in the presence of 500 ppbv of limonene within 40 min of irradiation time. Such observation convey to aged aerosol some autophotocatalysed properties that could be a significant process in the troposphere. But further investigation is now needed, in particular of the SOA mass produced as a function of VOC concentrations, in order to refine this estimate.

From the grown particle composition analysis, highly oxygenated VOC products and some nitrogen containing compounds were found. The imidazole-2-carboxaldehyde based photochemistry, therefore, evidenced that molecular oxygen is necessary for SOA growth; a mechanism explaining such phenomenon was proposed and is initiated by direct abstraction of hydrogen atom from the added VOC by the excited triplet state of imidazole-2-carboxaldehyde leading to the formation of allylic radical (in the case of limonene). The peroxyl radical due to the addition of molecular oxygen leads to a large oxygenated products that leads to increase in mass and size of SOA particles.

The photochemistry of imidazole-2-carboxaldehyde was further characterized by using Laser Flash Photolysis (LFP) technique. The triplet-triplet absorption maximum falls on 330 nm with the first order decay rate constant of (7.73 ± 0.04) x 10^5 s^{-1}. The corresponding lifetime of IC was found

to be 1.29 μs in which the value agreed with recently published value (Tinel et al., 2014). Furthermore, the quenching rate of excited triplet state of imidazole-2-carboxaldehyde by limonene was (1.8 ± 0.06) x 10^7 s^{-1}, decreased the decay rate by four.

The interaction between excited triplet imidazole-2-carboxaldehyde and VOCs in the flow tube can produces peroxyl radicals, hydroperoxyl and alkyl peroxy radical. Gaseous hydroperoxyl radicals (HO_2) are produced during photocatalytic process in the presence of oxygen in the system. The HO_2 flux produced during SOA growth initiated by imidazole-2-carboxaldehyde is estimated at around 2.78 x 10^{12} molecule cm^{-2} s^{-1} under irradiation between 300 and 420 nm at 500 ppbv of gaseous limonene and <15% of RH. The HO_2 production was evidenced by the addition of nitric oxide (NO) that showed a decrease in NO concentration and resulted a production of NO_2.

Altogether, this study clearly demonstrates that in-situ generated products called imidazole-2-carboxaldehyde from tropospheric dicarbonyls (i.e. glyoxal) induced photosensitizing properties that induces fast and significant SOA growth. The mechanism involves the use of light to initiate the formation of excited triplet state of imidazole-2-carboxaldehyde that will interact with VOC through hydrogen abstraction. In the presence of molecular oxygen in the system, the photosensitizer regenerated back to its ground state by forming hydroperoxyl radical. In addition to this, the radical formed from hydrogen abstraction undergo oxygenation to produce peroxyl radical, which will undergo continuous oxygenation to a free radical VOC.

1H-imidazole-2-carboxaldehyde is the one the reaction product of glyoxal and found to be an efficient photosensitizer. On the basis of glyoxal condensed phase chemistry evidenced in this work that photosensitized SOA growth in the atmosphere is thus expected to be autophotocatalytic. The presence of photosensitizer in the ambient aerosol might generally influence the daytime SOA growth and uptake of VOCs and volatility of organic fraction and radical formations. However, further

investigation will still be needed to complete the story of imidazole-2-carboxaldehyde based photosensitized SOA growth and aging.

- Based on the ubiquitousness of both glyoxal and ammonium sulfate in the atmosphere, imidazole-2-carboxaldehyde might be found in the real atmosphere but the production rate and atmospheric concentration of imidazole-2-carboxaldehyde need to be well quantified.
- Apart from the traditional gas phase oxidants initiated SOA formation and aging, photosensitized SOA growth can also be possible in the real atmospheric conditions. It is now proofed that photosensitized processes in the presences of hydrogen donor produce hydroperoxyl radicals. The HO_2 flux from imidazole-2-carboxaldehyde sensitized SOA growth in the presence of 500 ppbv of limonene in our system was estimated in indirect way. Direct HO_2 production measurement would be interesting to estimate photosensitized production of HO_2 in the real atmosphere.
- Imidazole-2-carboxaldehyde can be considered as a triplet photosensitizer, nevertheless, further investigation of photochemical and photophysical properties are needed for its formation efficiency in the atmosphere as well as laboratory studies.
- Estimating the magnitude of the reactive uptake of VOCs onto the aerosol surface during photosensitized SOA growth, which in turns the determination of the rate of light induced reactive uptake of VOC, would be an interesting area of research in this regards.
- Apart from the conversion of NO/NO_2 and contribution to SOA mass increases, the mechanism of further SOA mass increase due to the addition of NO was not precisely defined. Indeed, products like OH radical and O_3 are formed which can strongly contribute for SOA growth. However, mechanistic investigations are still required.

References

AFSHARI, E. & SCHMIDT, R. 1991. Isotope-dependent quenching of singlet molecular oxygen ($^1\Delta g$) by ground-state oxygen in several perhalogenated solvents. *Chem. Phys. Lett.,* 184**,** 128-132.

AGUER, J. P. & RICHARD, C. 1993. Use of furoin as probe molecule for the involvement of singlet oxygen in aqueous phase photoinduced transformations. *Toxicol. Environ. Chem.,* 39**,** 217-227.

AGUER, J. P. & RICHARD, C. 1996. Reactive species produced on irradiation at 365 nm of aqueous solutions of humic acids. *J. Photochem. Photobiol. ,* 93**,** 193-198.

ALFONSO, L. & RAGA, G. B. 2002. Estimating the impact of natural and anthropogenic emissions on cloud chemistry: Part I. Sulfur cycle. *Atmos. Res.,* 62**,** 33-55.

AMMAR, R., MONGE, M. E., GEORGE, C. & D'ANNA, B. 2010. Photoenhanced NO2 Loss on Simulated Urban Grime. *ChemPhysChem,* 11**,** 3956-3961.

ANDREAE, M. O. & ROSENFELD, D. 2008. Aerosol–cloud–precipitation interactions. Part 1. The nature and sources of cloud-active aerosols. *Earth-Sci. Rev.,* 89**,** 13-41.

AREGAHEGN, K. Z., NOZIERE, B. & GEORGE, C. 2013. Organic aerosol formation photo-enhanced by the formation of secondary photosensitizers in aerosols. *Faraday Discuss.,* 165**,** 123-134.

ARNOLD, I. & COMES, F. J. 1979. Temperature dependence of the reactions O(3P) + O3 → 2O2 and O(3P) + O2 + M → O3 + M. *Chem. Phys.,* 42**,** 231-239.

ASCHMANN, S. M., CHEW, A. A., AREY, J. & ATKINSON, R. 1997b. Products of the Gas-Phase Reaction of OH Radicals with Cyclohexane: Reactions of the Cyclohexoxy Radical. *J. Phys. Chem. A,* 101**,** 8042-8048.

ATKINSON, R. 1990. Gas-phase tropospheric chemistry of organic compounds: A review. *Atmos. Environ. A: General Topics,* 24**,** 1-41.

ATKINSON, R. 2000. Atmospheric chemistry of VOCs and NOx. *Atmos. Environ.,* 34**,** 2063-2101.

ATKINSON, R. & AREY, J. 1998. Atmospheric Chemistry of Biogenic Organic Compounds. *Acc. Chem. Res.,* 31**,** 574-583.

ATKINSON, R. & AREY, J. 2003a. Atmospheric Degradation of Volatile Organic Compounds. *Chem. Rev.,* 103**,** 4605-4638.

ATKINSON, R. & AREY, J. 2003b. Gas-phase tropospheric chemistry of biogenic volatile organic compounds: a review. *Atmos. Environ.,* 37, Supplement 2**,** 197-219.

ATKINSON, R., AREY, J. & TUAZON, E. C. 2003. Atmospheric Chemistry of Volatile Organic Compounds and their Atmospheric Reaction Products. *Report*.

ATKINSON, R. & ASCHMANN, S. 1993. Atmospheric chemistry of the monoterpene reaction products nopinone, camphenilone, and 4-acetyl-1-methylcyclohexene. *J. Atmos. Chem.,* 16**,** 337-348.

ATKINSON, R., BAULCH, D. L., COX, R. A., CROWLEY, J. N., HAMPSON, R. F., HYNES, R. G., JENKIN, M. E., ROSSI, M. J. & TROE, J. 2004. Evaluated kinetic and photochemical data for atmospheric chemistry: Volume I - gas phase reactions of Ox, HOx, NOx and SOx species. *Atmos. Chem. Phys.,* 4**,** 1461-1738.

ATKINSON, R., BAULCH, D. L., COX, R. A., CROWLEY, J. N., HAMPSON, R. F., HYNES, R. G., JENKIN, M. E., ROSSI, M. J., TROE, J. & SUBCOMMITTEE, I. 2006. Evaluated kinetic and photochemical data for atmospheric chemistry: Volume II – gas phase reactions of organic species. *Atmos. Chem. Phys.,* 6**,** 3625-4055.

ATKINSON, R., BAULCH, D. L., COX, R. A., HAMPSON, R. F., KERR, J. A., ROSSI, M. J. & TROE, J. 1999. Evaluated Kinetic and Photochemical Data for Atmospheric Chemistry, Organic Species: Supplement VII. *J. Phys. Chem. Ref. Data,* 28**,** 191-393.

BARDWELL, M. W., BACAK, A., TERESA RAVENTOS, M., PERCIVAL, C. J., SANCHEZ-REYNA, G. & SHALLCROSS, D. E. 2003. Kinetics of the HO2 + NO reaction: A temperature and pressure dependence study using chemical ionisation mass spectrometry. *Phys. Chem. Chem. Phys.,* 5**,** 2381-2385.

BAULCH, D. L., DRYSDALE, D. D. & HORNE, D. G. 1973. Evaluated Kinetic Data for High Temperature Reactions, Volume 2, Homogeneous Gas Phase Reactions of the H2-N2-O2 System.

BAXTER, R. M. & CAREY, J. H. 1983. Evidence for photochemical generation of superoxide ion in humic waters. *Nature,* 306**,** 575-576.

BENNADJI, H., GLAUDE, P. A., CONIGLIO, L. & BILLAUD, F. 2011. Experimental and kinetic modeling study of ethyl butanoate oxidation in a laminar tubular plug flow reactor. *Fuel,* 90**,** 3237-3253.

BERNARD, F., FEDIOUN, I., PEYROUX, F., QUILGARS, A., DAËLE, V. & MELLOUKI, A. 2012. Thresholds of secondary organic aerosol formation by ozonolysis of monoterpenes measured in a laminar flow aerosol reactor. *J. Aerosol Sci.,* 43**,** 14-30.

BETTERTON, E. A. & HOFFMANN, M. R. 1988. Henry's law constants of some environmentally important aldehydes. *Environ. Sci. Technol.,* 22**,** 1415-1418.

BÖGE, O., MIAO, Y., PLEWKA, A. & HERRMANN, H. 2006. Formation of secondary organic particle phase compounds from isoprene gas-phase oxidation products: An aerosol chamber and field study. *Atmos. Environ.,* 40**,** 2501-2509.

BOWLER, C. & BRIMBLECOMBE, P. 1992. Archives and air pollution history. *J. Soc. Archivists,* 13**,** 136-142.

BURDON, J. 2001. Are the raditional concepts of the structures of humic substances realistic? *Soil Science,* 166**,** 752-769.

BURKHOLDER, J. B., BAYNARD, T., RAVISHANKARA, A. R. & LOVEJOY, E. R. 2007. Particle nucleation following the O3 and OH initiated oxidation of α-pinene and β-pinene between 278 and 320 K. *J. Geophys. Res. - Atmos,* 112**,** D10216.

BUXTON, G. V., MALONE, T. N. & ARTHUR SALMON, G. 1997. Oxidation of glyoxal initiated by OH in oxygenated aqueous solution. *J. Chem. Soc., Faraday Trans.,* 93**,** 2889-2891.

CANONICA, S., HELLRUNG, B., MÜLLER, P. & WIRZ, J. 2006. Aqueous Oxidation of Phenylurea Herbicides by Triplet Aromatic Ketones. *Environ. Sci. Technol.,* 40**,** 6636-6641.

CANONICA, S., HELLRUNG, B. & WIRZ, J. 2000. Oxidation of Phenols by Triplet Aromatic Ketones in Aqueous Solution. *J. Phys. Chem.,* 104**,** 1226-1232.

CANONICA, S., JANS, U., STEMMLER, K. & HOIGNE, J. 1995. Transformation Kinetics of Phenols in Water: Photosensitization by Dissolved Natural Organic Material and Aromatic Ketones. *Environ. Sci. Technol.,* 29**,** 1822-1831.

CARLSSON, D. J., SUPRUNCHUK, T. & WILES, D. M. 1974. The Quenching of Singlet Oxygen (1Δg) by Transition Metal Chelates. *Can. J. Chem.,* 52**,** 3728-3737.

CARLTON, A. G., TURPIN, B. J., ALTIERI, K. E., SEITZINGER, S., REFF, A., LIM, H.-J. & ERVENS, B. 2007. Atmospheric oxalic acid and SOA production from glyoxal: Results of aqueous photooxidation experiments. *Atmos. Environ.,* 41**,** 7588 - 7602

CARLTON, A. G., WIEDINMYER, C. & KROLL, J. H. 2009. A review of Secondary Organic Aerosol (SOA) formation from isoprene. *Atmos. Chem. Phys.,* 9**,** 4987-5005.

CHEBBI, A. & CARLIER, P. 1996. Carboxylic acids in the troposphere, occurrence, sources, and sinks: A review. *Atmos. Environ.,* 30**,** 4233-4249.

CLAEYS, M., WANG, W., ION, A. C., KOURTCHEV, I., GELENCSÃ©R, A. S. & MAENHAUT, W. 2004. Formation of secondary organic aerosols from isoprene and its gas-phase oxidation products through reaction with hydrogen peroxide. *Atmos. Environ.,* 38**,** 4093-4098.

CLENNAN, E. L. & PACE, A. 2005. Advances in singlet oxygen chemistry. *Tetrahedron,* 61**,** 6665-6691.

CRUTZEN, P. J. 1979. The Role of NO and NO2 in the Chemistry of the Troposphere and Stratosphere. *Annu. Rev. Earth and Planetary Sci.,* 7**,** 443-472.

DAS, P. K., ENCINAS, M. V. & SCAIANO, J. C. 1981. Laser flash photolysis study of the reactions of carbonyl triplets with phenols and photochemistry of p-hydroxypropiophenone. *J. Am. Chem. Soc.,* 103**,** 4154-4162.

DEBUS, H. 1858. Ueber die Einwirkung des Ammoniaks auf Glyoxal. *Justus Liebigs Annalen der Chemie,* 107**,** 199-208.

DILLON, T. J., BLITZ, M. A. & HEARD, D. E. 2006. Determination of the Rate Coefficients for the Reactions IO + NO_2 + M (Air) → $IONO_2$ + M and $O(^3P)$ + NO_2 → O_2 + NO Using Laser-Induced Fluorescence Spectroscopy. *J. Phys. Chem. A,* 110**,** 6995-7002.

EDNEY, E. O., KLEINDIENST, T. E., JAOUI, M., LEWANDOWSKI, M., OFFENBERG, J. H., WANG, W. & CLAEYS, M. 2005. Formation of 2-methyl tetrols and 2-methylglyceric acid in secondary organic aerosol from laboratory irradiated isoprene/NOX/SO2/air mixtures and their detection in ambient PM2.5 samples collected in the eastern United States. *Atmos. Environ.,* 39**,** 5281-5289.

EHN, M., THORNTON, J. A., KLEIST, E., SIPILA, M., JUNNINEN, H., PULLINEN, I., SPRINGER, M., RUBACH, F., TILLMANN, R., LEE, B., LOPEZ-HILFIKER, F., ANDRES, S., ACIR, I.-H., RISSANEN, M., JOKINEN, T., SCHOBESBERGER, S., KANGASLUOMA, J., KONTKANEN, J., NIEMINEN, T., KURTEN, T., NIELSEN, L. B., JORGENSEN, S., KJAERGAARD, H. G., CANAGARATNA, M., MASO, M. D., BERNDT, T., PETAJA, T., WAHNER, A., KERMINEN, V.-M., KULMALA, M., WORSNOP, D. R., WILDT, J. & MENTEL, T. F. 2014. A large source of low-volatility secondary organic aerosol. *Nature,* 506**,** 476-479.

ERVENS, B. & VOLKAMER, R. 2010. Glyoxal processing by aerosol multiphase chemistry: towards a kinetic modeling framework of secondary organic aerosol formation in aqueous particles. *Atmos. Chem. Phys.,* 10**,** 8219 - 8244.

FINLAYSON-PITTS, B. J. & PITTS, J. N. 1997. Tropospheric Air Pollution: Ozone, Airborne Toxics, Polycyclic Aromatic Hydrocarbons, and Particles. *Science,* 276**,** 1045-1051.

FINLAYSON-PITTS, B. J. & PITTS, J. N. 2000. *Chemistry of the Upper and Lower Atmosphere: Theory, Experiments, and Applications*, Academic Press.

FOOTE, C. S. 1968. Photosensitized oxygenations and the role of singlet oxygen. *Acc. Chem. Res.,* 1**,** 104-110.

FORMOSINHO, S. J. 1976. Photochemical hydrogen abstractions as radiationless transitions. Part 1.-Ketones, aldehydes and acids. *J. Chem. Soc., Faraday Trans.,* 72**,** 1313-1331.

FORTNER, E. C., ZHENG, J., ZHANG, R., BERK KNIGHTON, W., VOLKAMER, R. M., SHEEHY, P., MOLINA, L. & ANDRÉ, M. 2009. Measurements of Volatile Organic Compounds Using Proton Transfer Reaction â€“ Mass Spectrometry during the MILAGRO 2006 Campaign. *Atmos. Chem. Phys.,* 9**,** 467 - 481.

FRAMPTON, M., PRYOR, W., CUETO, R., COX, C., MORROW, P. & UTELL, M. 1999. Ozone Exposure Increases Aldehydes in Epithelial Lining Fluid in Human Lung. *American Journal of Respiratory and Critical Care Medicine,* 159**,** 1134-1137.

FU, T., JACOB, D. J., WITTROCK, F., BURROWS, J. P., VREKOUSSIS, M. & HENZE, D. K. 2008. Global budgets of atmospheric glyoxal and methylglyoxal, and implications for formation of secondary organic aerosols. *J. Geophys. Res.,* 113**,** D15303.

FUCHS, N. A. 1963. On the stationary charge distribution on aerosol particles in a bipolar ionic atmosphere. *Geofisica pura e applicata,* 56**,** 185-193.

GALLOWAY, M. M., CHHABRA, P. S., CHAN, A. W. H., SURRATT, J. D., FLAGAN, R. C., SEINFELD, J. H. & KEUTSCH, F. N. 2009. Glyoxal uptake on ammonium sulphate seed aerosol: reaction products and reversibility of uptake under dark and irradiated conditions. *Atmos. Chem. Phys.,* 9**,** 3331-3345.

GARDNER, E. P., SPERRY, P. D. & CALVERT, J. G. 1987. Primary quantum yields of NO2 photodissociation. *J. Geophy. Res.,* 92**,** 6642-6652.

GEORGE, C., STREKOWSKI, R. S., KLEFFMANN, J., STEMMLER, K. & AMMANN, M. 2005. Photoenhanced uptake of gaseous NO2 on solid organic compounds: a photochemical source of HONO? *Faraday Discussions,* 130**,** 195-210.

GREENBLATT, G. D. & WIESENFELD, J. R. 1983. Time-resolved resonance fluorescence studies of O(1D2) yields in the photodissociation of O3 at 248 and 308 nm. *J. Chem. Phys.,* 78**,** 4924-4928.

GREER, A. 2006. Christopher Foote's Discovery of the Role of Singlet Oxygen [1O2 (1Î"g)] in Photosensitized Oxidation Reactions. *Acc. Chem. Res.,* 39**,** 797-804.

GRIFFIN, R. J., COCKER, D. R., III, FLAGAN, R. C. & SEINFELD, J. H. 1999. Organic aerosol formation from the oxidation of biogenic hydrocarbons. *J. Geophys. Res.,* 104**,** 3555-3567.

GRILLER, D., HOWARD, J. A., MARRIOTT, P. R. & SCAIANO, J. C. 1981. Absolute rate constants for the reactions of tert-butoxyl, tert-butylperoxyl, and benzophenone triplet with amines: the importance of a stereoelectronic effect. *J. Am. Chem. Soc.,* 103**,** 619-623.

GROSJEAN, D., GROSJEAN, E. & GERTLER, A. W. 2000. On-Road Emissions of Carbonyls from Light-Duty and Heavy-Duty Vehicles. *Environ. Sci. Technol.,* 35**,** 45-53.

GROSJEAN, D., VAN CAUWENBERGHE, K., SCHMID, J. P., KELLEY, P. E. & PITTS, J. N. 1978. Identification of C3-C10 aliphatic dicarboxylic acids in airborne particulate matter. *Environ. Sci. Technol.,* 12**,** 313-317.

GUENTHER, A., GERON, C., PIERCE, T., LAMB, B., HARLEY, P. & FALL, R. 2000. Natural emissions of non-methane volatile organic compounds, carbon monoxide, and oxides of nitrogen from North America. *Atmos. Environ.,* 34**,** 2205-2230.

GUENTHER, A., KARL, T., HARLEY, P., WIEDINMYER, C., PALMER, P. I. & GERON, C. 2006. Estimates of global terrestrial isoprene emissions using MEGAN (Model of Emissions of Gases and Aerosols from Nature). *Atmos. Chem. Phys.,* 6**,** 3181-3210.

HAAG, W. R. & MILL, T. 1987. Rate constants for interaction of $^1O_2(^1\Delta_g)$ with azide ion in water. *Photochem. Photobiol.,* 45**,** 317-321.

HALLQUIST, M., WENGER, J. C., BALTENSPERGER, U., RUDICH, Y., SIMPSON, D., CLAEYS, M., DOMMEN, J., DONAHUE, N. M., GEORGE, C., GOLDSTEIN, A. H., HAMILTON, J. F., HERRMANN, H., HOFFMANN, T., IINUMA, Y., JANG, M., JENKIN, M. E., JIMENEZ, J. L., KIENDLER-SCHARR, A., MAENHAUT, W., MCFIGGANS, G., MENTEL, T. F., MONOD, A., PRÉVÔT, A. S. H., SEINFELD, J. H., SURRATT, J. D., SZMIGIELSKI, R. & WILDT, J. 2009. The formation, properties and impact of secondary organic aerosol: current and emerging issues. *Atmos. Chem. Phys.,* 9**,** 5155-5236.

HAO, L.-Q., WANG, Z.-Y., HUANG, M.-Q., FANG, L. & ZHANG, W.-J. 2007. Effects of seed aerosols on the growth of secondary organic aerosols from the photooxidation of toluene. *J. Environ. Sci.,* 19**,** 704-708.

HAYS, M. D., GERON, C. D., LINNA, K. J., SMITH, N. D. & SCHAUER, J. J. 2002. Speciation of Gas-Phase and Fine Particle Emissions from Burning of Foliar Fuels. *Environ. Sci. Technol.,* 36**,** 2281-2295.

HEARD, D. E. & PILLING, M. J. 2003. Measurement of OH and HO2 in the Troposphere. *Chem. Rev.,* 103**,** 5163-5198.

HENZE, D. K. & SEINFELD, J. H. 2006. Global secondary organic aerosol from isoprene oxidation. *Geophys. Res. Lett.,* 33**,** L09812.

HENZE, D. K., SEINFELD, J. H., NG, N. L., KROLL, J. H., FU, T.-M., JACOB, D. J. & HEALD, C. L. 2008. Global modeling of secondary organic aerosol formation from aromatic hydrocarbons: high- vs. low-yield pathways. *Atmos. Chem. Phys.,* 8.

HERNDON, S. C., VILLALTA, P. W., NELSON, D. D., JAYNE, J. T. & ZAHNISER, M. S. 2000. Rate Constant Measurements for the Reaction of HO2 with O3 from 200 to 300 K Using a Turbulent Flow Reactor†. *J. Phys. Chem. A,* 105**,** 1583-1591.

HOFFMANN, T., ODUM, J., BOWMAN, F., COLLINS, D., KLOCKOW, D., FLAGAN, R. & SEINFELD, J. 1997. Formation of Organic Aerosols from the Oxidation of Biogenic Hydrocarbons. *J. Atmos. Chem.,* 26**,** 189-222.

HOFZUMAHAUS, A., KRAUS, A. & MÜLLER, M. 1999. Solar actinic flux spectroradiometry: a technique for measuring photolysis frequencies in the atmosphere. *App. Opt.,* 38**,** 4443-4460.

HOFZUMAHAUS, A., ROHRER, F., LU, K., BOHN, B., BRAUERS, T., CHANG, C.-C., FUCHS, H., HOLLAND, F., KITA, K., KONDO, Y., LI, X., LOU, S., SHAO, M., ZENG, L., WAHNER, A. & ZHANG, Y. 2009. Amplified Trace Gas Removal in the Troposphere. *Science,* 324**,** 1702-1704.

HURLEY, M. D., SOKOLOV, O., WALLINGTON, T. J., TAKEKAWA, H., KARASAWA, M., KLOTZ, B., BARNES, I. & BECKER, K. H. 2001. Organic Aerosol Formation during the Atmospheric Degradation of Toluene. *Environ. Sci. Technol.,* 35**,** 1358-1366.

IPCC 1995. Second assesment on Climate change. *IPCC report*.

IPCC 2013. Climate Change 2013: The physical Science Basis. *IPCC report*.

IZUMI, K. & FUKUYAMA, T. 1990. Photochemical aerosol formation from aromatic hydrocarbons in the presence of NOx. *Atmos. Environ. A: General Topics,* 24**,** 1433-1441.

JACOBSON, M. C., HANSSON, H. C., NOONE, K. J. & CHARLSON, R. J. 2000. Organic atmospheric aerosols: Review and state of the science. *Rev. Geophys.,* 38**,** 267-294.

JAMMOUL, A., GLIGOROVSKI, S., GEORGE, C. & D'ANNA, B. 2008. Photosensitized Heterogeneous Chemistry of Ozone on Organic Films. *J. Phys. Chem. A,* 112**,** 1268-1276.

JANG, M., CZOSCHKE, N. M., LEE, S. & KAMENS, R. M. 2002. Heterogeneous Atmospheric Aerosol Production by Acid-Catalyzed Particle-Phase Reactions. *Science,* 298**,** 814-817.

JANG, M. & KAMENS, R. M. 2001. Atmospheric Secondary Aerosol Formation by Heterogeneous Reactions of Aldehydes in the Presence of a Sulfuric Acid Aerosol Catalyst. *Environ. Sci. Technol.,* 35**,** 4758-4766.

JENKIN, M. E. & CLEMITSHAW, K. C. 2000. Ozone and other secondary photochemical pollutants: chemical processes governing their formation in the planetary boundary layer. *Atmos. Environ.,* 34**,** 2499-2527.

KAMPF, C. J., JAKOB, R. & HOFFMANN, T. 2012. Identification and characterization of aging products in the glyoxal/ammonium sulfate system - implications for light-absorbing material in atmospheric aerosols. *Atmos. Chem. Phys.,* 12**,** 6323-6333.

KANAKIDOU, M., SEINFELD, J. H., PANDIS, S. N., BARNES, I., DENTENER, F. J., FACCHINI, M. C., VAN DINGENEN, R., ERVENS, B., NENES, A., NIELSEN, C. J., SWIETLICKI, E., PUTAUD, J. P., BALKANSKI, Y., FUZZI, S., HORTH, J., MOORTGAT, G. K., WINTERHALTER, R., MYHRE, C. E. L., TSIGARIDIS, K., VIGNATI, E., STEPHANOU, E. G. & WILSON, J. 2005. Organic aerosol and global climate modelling: a review. *Atmos. Chem. Phys.,* 5**,** 1053-1123.

KERMINEN, V.-M., OJANEN, C., PAKKANEN, T., HILLAMO, R., AURELA, M. & MERILÃ¤INEN, J. 2000. LOW-MOLECULAR-WEIGHT DICARBOXYLIC ACIDS IN AN URBAN AND RURAL ATMOSPHERE. *J. Aerosol Sci.,* 31**,** 349-362.

KEYWOOD, M. D., KROLL, J. H., VARUTBANGKUL, V., BAHREINI, R., FLAGAN, R. C. & SEINFELD, J. H. 2004. Secondary Organic Aerosol Formation from Cyclohexene Ozonolysis: Effect of OH Scavenger and the Role of Radical Chemistry. *Environ. Sci. Technol.,* 38**,** 3343-3350.

KHAN, A. U. 1976. Singlet molecular oxygen. A new kind of oxygen. *J. Phys. Chem.,* 80**,** 2219-2228.

KOKKOLA, H., YLI-PIRILÄ, P., VESTERINEN, M., KORHONEN, H., KESKINEN, H., ROMAKKANIEMI, S., HAO, L., KORTELAINEN, A., JOUTSENSAARI, J., WORSNOP, D. R., VIRTANEN, A. & LEHTINEN, K. E. J. 2014. The role of low volatile organics on secondary organic aerosol formation. *Atmos. Chem. Phys.,* 14**,** 1689-1700.

KROLL, J. H., HANISCO, T. F., DONAHUE, N. M., DEMERJIAN, K. L. & ANDERSON, J. G. 2001. Accurate, direct measurements of oh yields from gas-phase ozone-alkene reactions using an in situ LIF Instrument. *Geophys. Res. Lett.,* 28**,** 3863-3866.

KROLL, J. H., NG, N. L., MURPHY, S. M., VARUTBANGKUL, V., FLAGAN, R. C. & SEINFELD, J. H. 2005. Chamber studies of secondary organic aerosol growth by reactive uptake of simple carbonyl compounds. *J. Geophys. Res. -Atmos,* 110**,** D23207.

LATHIOOR, E. C. & LEIGH, W. J. 2001. Geometric and solvent effects on intramolecular phenolic hydrogen abstraction by carbonyl n,π* and π,π* triplets. *Can. J. Chem.,* 79**,** 1851-1863.

LATHIOOR, E. C., LEIGH, W. J. & ST. PIERRE, M. J. 1999. Geometrical Effects on Intramolecular Quenching of Aromatic Ketone (π,π*) Triplets by Remote Phenolic Hydrogen Abstraction. *J. Am. Chem. Soc.,* 121**,** 11984-11992.

LAVVAS, P., YELLE, R. V., KOSKINEN, T., BAZIN, A., VUITTON, V., VIGREN, E., GALAND, M., WELLBROCK, A., COATES, A. J., WAHLUND, J.-E., CRARY, F. J. & SNOWDEN, D. 2013. Aerosol growth in Titan's ionosphere. *Proc. Natl. Acad. Sci. ,* 110**,** 2729-2734.

LEIGH, W. J., LATHIOOR, E. C. & ST. PIERRE, M. J. 1996. Photoinduced Hydrogen Abstraction from Phenols by Aromatic Ketones. A New Mechanism for Hydrogen Abstraction by Carbonyl n,π* and π,π* Triplets. *J. Am. Chem. Soc.,* 118**,** 12339-12348.

LEUNGSAKUL, S., JAOUI, M. & KAMENS, R. M. 2005. Kinetic Mechanism for Predicting Secondary Organic Aerosol Formation from the Reaction of d-Limonene with Ozone. *Environ. Sci. Technol.,* 39**,** 9583-9594.

LEY, C., CHRISTMANN, J., IBRAHIM, A., STEFANO, L. H. D. & ALLONAS, X. 2014. Tailoring of organic dyes with oxidoreductive compounds to obtain photocyclic radical generator systems exhibiting photocatalytic behavior. *Beilstein J. Org. Chem.,* 10**,** 936-947.

LIBRANDO, V. & TRINGALI, G. 2005. Atmospheric fate of OH initiated oxidation of terpenes. Reaction mechanism of α-pinene degradation and secondary organic aerosol formation. *J. Environ. Manag.,* 75**,** 275-282.

LIGGIO, J., LI, S.-M. & MCLAREN, R. 2005a. Heterogeneous Reactions of Glyoxal on Particulate Matter: Identification of Acetals and Sulfate Esters. *Environ. Sci. Technol.,* 39**,** 1532-1541.

LIGGIO, J., LI, S.-M. & MCLAREN, R. 2005b. Reactive uptake of glyoxal by particulate matter. *J. Geophys. Res.,* 110**,** D10304.

LIGHTSTONE, J. M., ONASCH, T. B., IMRE, D. & OATIS, S. 2000. Deliquescence, Efflorescence, and Water Activity in Ammonium Nitrate and Mixed Ammonium Nitrate/Succinic Acid Microparticles. *J. Phys. Chem. A,* 104**,** 9337-9346.

LIM, Y. B., TAN, Y., PERRI, M. J., SEITZINGER, S. P. & TURPIN, B. J. 2010. Aqueous chemistry and its role in secondary organic aerosol (SOA) formation. *Atmos. Chem. Phys.,* 10**,** 10521-10539.

LIMBECK, A. & PUXBAUM, H. 1999. Organic acids in continental background aerosols. *Atmos. Environ.,* 33**,** 1847-1852.

MAGNERON, I., MELLOUKI, A., LE BRAS, G., MOORTGAT, G. K., HOROWITZ, A. & WIRTZ, K. 2005. Photolysis and OH-Initiated Oxidation of Glycolaldehyde under Atmospheric Conditions. *J. Phys. Chem. A,* 109**,** 4552-4561.

MAKSYMIUK, C. S., GAYAHTRI, C., GIL, R. R. & DONAHUE, N. M. 2009. Secondary organic aerosol formation from multiphase oxidation of limonene by ozone: mechanistic constraints via two-dimensional heteronuclear NMR spectroscopy. *Phys. Chem. Chem. Phys.,* 11**,** 7810-7818.

MARTÍNEZ, E., CABAÑAS, B., ARANDA, A., MARTÍN, P. & SALGADO, S. 1999. Absolute Rate Coefficients for the Gas-Phase Reactions of NO3 Radical with a Series of Monoterpenes at T = 298 to 433 K. *J. Atmos. Chem.,* 33**,** 265-282.

MENSAH, A. A., HOLZINGER, R., OTJES, R. & TRIMBORN, A. 2012. Aerosol chemical composition at Cabauw, The Netherlands as observed in two intensive periods in May 2008 and March 2009. *Atmos. Chem. Phys.,* 12.

MIYOSHI, A., HATAKEYAMA, S. & WASHIDA, N. 1994. OH radical- initiated photooxidation of isoprene: An estimate of global CO production. *J. Geophys. Res. - Atmos,* 99**,** 18779-18787.

MONGE, M. E., ROSENØRN, T., FAVEZ, O., MÜLLER, M., ADLER, G., ABO RIZIQ, A., RUDICH, Y., HERRMANN, H., GEORGE, C. & D'ANNA, B. 2012. Alternative pathway for atmospheric particles growth. *Proc. Natl. Acad. Sci. ,* 109**,** 6840-6844.

MONROE, B. M. & MROWCA, J. J. 1979. Quenching of singlet oxygen by nickel complexes. *J. Phys. Chem.,* 83**,** 591-595.

MOONEN, P. C., CAPE, J. N., STORETON-WEST, R. L. & MCCOLM, R. 1998. Measurement of the NO + O3 Reaction Rate at Atmospheric Pressure Using Realistic Mixing Ratios. *J. Atmos. Chem.,* 29**,** 299-314.

MUNGER, J. W., JACOB, D. J., DAUBE, B. C., HOROWITZ, L. W., KEENE, W. C. & HEIKES, B. G. 1995. Formaldehyde, glyoxal, and methylglyoxal in air and cloudwater at a rural mountain site in central Virginia. *J. Geophys. Res. - Atmos,* 100**,** 9325-9333.

MYRIOKEFALITAKIS, S., VREKOUSSIS, M., TSIGARIDIS, K., WITTROCK, F., RICHTER, A., BRÜHL, C., VOLKAMER, R., BURROWS, J. P. & KANAKIDOU, M. 2008. The influence of natural and anthropogenic secondary sources on the glyoxal global distribution. *Atmos. Chem. Phys.,* 8**,** 4965 - 4981.

NATIONAL RESEARCH COUNCIL 1991. *Rethinking the Ozone Problem in Urban and Regional Air Pollution*, The National Academies Press.

NET, S., NIETO-GLIGOROVSKI, L., GLIGOROVSKI, S., TEMIME-ROUSELL, B., BARBATI, S., LAZAROU, Y. G. & WORTHAM, H. 2009. Heterogeneous light-induced ozone processing on the organic coatings in the atmosphere. *Atmos. Environ.,* 43**,** 1683-1692.

NIETO-GLIGOROVSKI, L., NET, S., GLIGOROVSKI, S., ZETZSCH, C., JAMMOUL, A., D'ANNA, B. & GEORGE, C. 2008. Interactions of ozone with organic surface films in the presence of simulated sunlight: impact on wettability of aerosols. *Phys. Chem. Chem. Phys.,* 10**,** 2964-2971.

NOBLE, C. A. & PRATHER, K. A. 1998. Single Particle Characterization of Albuterol Metered Dose Inhaler Aerosol in Near Real-Time. *Aerosol Sci. Technol.,* 29**,** 294-306.

NOZIÈRE, B., DZIEDZIC, P. & CORDOVA, A. 2009. Products and Kinetics of the Liquid-Phase Reaction of Glyoxal Catalyzed by Ammonium Ions (NH4+). *J. Phys. Chem.,* 113**,** 231-237.

ODUM, J. R., HOFFMANN, T., BOWMAN, F., COLLINS, D., FLAGAN, R. C. & SEINFELD, J. H. 1996. Gas/Particle Partitioning and Secondary Organic Aerosol Yields. *Environ. Sci. Technol.,* 30**,** 2580-2585.

OGILBY, P. R. 2010. Singlet oxygen: there is indeed something new under the sun. *Chem. Soc. Rev.,* 39**,** 3181-3209.

OH, S. & ANDINO, J. M. 2000. Effects of ammonium sulfate aerosols on the gas-phase reactions of the hydroxyl radical with organic compounds. *Atmos. Environ.,* 34**,** 2901-2908.

ORTEGA, A. M., DAY, D. A., CUBISON, M. J., BRUNE, W. H., BON, D., DE GOUW, J. A. & JIMENEZ, J. L. 2013. Secondary organic aerosol formation and primary organic aerosol oxidation from biomass-burning smoke in a flow reactor during FLAME-3. *Atmos. Chem. Phys.,* 13**,** 11551-11571.

PANDIS, S. N., HARLEY, R. A., CASS, G. R. & SEINFELD, J. H. 1992. Secondary organic aerosol formation and transport. *Atmos. Environ. A: General Topics,* 26**,** 2269-2282.

PANDIS, S. N., PAULSON, S. E., SEINFELD, J. H. & FLAGAN, R. C. 1991. Aerosol formation in the photooxidation of isoprene and β-pinene. *Atmos. Environ. A: General Topics,* 25**,** 997-1008.

PEETERS, J., BOULLART, W., PULTAU, V., VANDENBERK, S. & VEREECKEN, L. 2007. Structure−Activity Relationship for the Addition of OH to (Poly)alkenes: Site-Specific and Total Rate Constants. *J. Phys. Chem. A,* 111**,** 1618-1631.

PERRAUD, V., BRUNS, E. A., EZELL, M. J., JOHNSON, S. N., YU, Y., ALEXANDER, M. L., ZELENYUK, A., IMRE, D., CHANG, W. L., DABDUB, D., PANKOW, J. F. & FINLAYSON-PITTS, B. J. 2012. Nonequilibrium atmospheric secondary organic aerosol formation and growth. *Proc. Natl. Acad. Sci. ,* 109**,** 2836-2841.

PIÖTZ, J. & MAIER, M. 1987. Temperature dependence of the relaxation rate constants of the a $^{1}\Delta g$ and b $^{1}\Sigma^{+}g$ states of oxygen isotopes. *Chem. Phys. Lett.,* 138**,** 419-424.

POPE, C. A., BURNETT, R. T., THUN, M. J., CALLE, E. E., KREWSKI, D., ITO, K. & THURSTON, G. D. 2002. Lung Cancer, Cardiopulmonary Mortality, and Long-term Exposure to Fine Particulate Air Pollution. *Am. Med. Ass.,* 287**,** 1132-1141.

PÖSCHL, U. 2005. Atmospheric Aerosols: Composition, Transformation, Climate and Health Effects. *Angew.Chem. Int. Ed.,* 44**,** 7520-7540.

POSPĬŠIL, J., NEŠPŮREK, S. & PILAŘ, J. 2008. Impact of photosensitized oxidation and singlet oxygen on degradation ofÂ stabilized polymers. *Polym. Degrad. Stabil.,* 93**,** 1681-1688.

PRATHER, M., EHHALT, D., DENTENER, F., DERWENT, R., DLUGOKENCKY, E., ISAKSEN, E. H. I., KATIMA, J., V.KIRCHHOFF, MATSON, P., MIDGLEY, P. & WANG, M. 2001. Climate Change 2001: The Scientific Basis. *IPCC report*.

PROGRAM, U. S. C. C. S. 2009. Atmospheric Aerosol Properties and Climate Impacts.

RAGONE, F., SAAVEDRA, H. H. M., GARA, P. M. D., RUIZ, G. T. & WOLCAN, E. 2013. Photosensitized Generation of Singlet Oxygen from Re(I) Complexes: A Photophysical Study Using LIOAS and Luminescence Techniques. *J. Phys. Chem. A,* 117**,** 4428-4435.

RAVISHANKARA, A. R., WINE, P. H. & NICOVICH, J. M. 1983. Pulsed laser photolysis study of the reaction between O(3P) and HO2. *J. Chem. Phys.,* 78**,** 6629-6639.

REHM, D. & WELLER, A. 1970. Kinetics of Fluorescence Quenching by Electron and H-Atom Transfer. *Isr. J. Chem.,* 8**,** 259-271.

RÖHRL, A. & LAMMEL, G. 2002. Determination of malic acid and other C4 dicarboxylic acids in atmospheric aerosol samples. *Chemosphere,* 46**,** 1195-1199.

ROOD, M. J., SHAW, M. A., LARSON, T. V. & COVERT, D. S. 1989. Ubiquitous nature of ambient metastable aerosol. *Nature,* 337**,** 537-539.

ROSENFELD, D. & WOODLEY, W. L. 2000. Deep convective clouds with sustained supercooled liquid water down to -37.5[thinsp][deg]C. *Nature,* 405**,** 440-442.

ROSSIGNOL, S., AREGAHEGN, K. Z., TINEL, L., FINE, L., NOZIÈRE, B. & GEORGE, C. 2014. Glyoxal Induced Atmospheric Photosensitized Chemistry Leading to Organic Aerosol Growth. *Environ. Sci. Technol.,* 48**,** 3218-3227.

RUDICH, Y., DONAHUE, N. M. & MENTEL, T. F. 2007. Aging of Organic Aerosol: Bridging the Gap Between Laboratory and Field Studies. *Annu. Rev. Phys. Chem.,* 58**,** 321-352.

SANDER, S. P., FRIEDL, R. R., GOLDEN, D. M., M.J. KURYLO, R. E. H., V.L. ORKIN, G. K. M., RAVISHANKARA, A. R., KOLB, C. E., MOLINA, M. J. & FINLAYSON-PITTS, B. J. 2002. Chemical Kinetics and Photochemical Data for Use in Atmospheric Studies. Evaluation Number 14 *JPL Publication 02-25, Jet Propulsion Laboratory*.

SATO, K., NAKAO, S., CLARK, C. H., QI, L. & COCKER III, D. R. 2011. Secondary organic aerosol formation from the photooxidation of isoprene, 1,3-butadiene, and 2,3-dimethyl-1,3-butadiene under high NOx conditions. *Atmos. Chem. Phys.,* 11**,** 7301-7317.

SAUNDERS, S. M., JENKIN, M. E., DERWENT, R. G. & PILLING, M. J. 2003. Protocol for the development of the Master Chemical Mechanism, MCM v3 (Part A): tropospheric degradation of non-aromatic volatile organic compounds. *Atmos. Chem. Phys.,* 3**,** 161 - 180.

SAXENA, P. & HILDEMANN, L. 1996. Water-soluble organics in atmospheric particles: A critical review of the literature and application of thermodynamics to identify candidate compounds. *J. Atmos. Chem.,* 24**,** 57-109.

SCHWEITZER, F., MAGI, L., MIRABEL, P. & GEORGE, C. 1998. Uptake Rate Measurements of Methanesulfonic Acid and Glyoxal by Aqueous Droplets. *J. Phys. Chem. A,* 102**,** 593-600.

SEINFELD, J. H. & PANDIS, S. N. 2006. Atmospheric Chemistry and Physics, From Air Pollution to Climate Change. *Book,* second edition**,** 1248.

SEINFELD, J. H. & PANKOW, J. F. 2003. Organic atmospheric particulate material. *Annu. Rev. Earth and Planetary Sci.,* 54**,** 121-140.

SHAPIRO, E. L., SZPRENGIEL, J., SAREEN, N., JEN, C. N., GIORDANO, M. R. & MCNEILL, V. F. 2009. Light-absorbing secondary organic material formed by glyoxal in aqueous aerosol mimics. *Atmos. Chem. Phys.,* 9**,** 2289-2300.

SMITH, D. F., KLEINDIENST, T. E. & MCIVER, C. D. 1999. Primary Product Distributions from the Reaction of OH with m-, p-Xylene, 1,2,4- and 1,3,5-Trimethylbenzene. *J. Atmos. Chem.,* 34**,** 339-364.

SMITH, D. F., MCIVER, C. D. & KLEINDIENST, T. E. 1998. Primary Product Distribution from the Reaction of Hydroxyl Radicals with Toluene at ppb NOX Mixing Ratios. *J. Atmos. Chem.,* 30**,** 209-228.

SPAULDING, R. S., SCHADE, G. W., GOLDSTEIN, A. H. & CHARLES, M. J. 2003. Characterization of secondary atmospheric photooxidation products: Evidence for biogenic and anthropogenic sources. *J. Geophys. Res. - Atmos,* 108**,** 4247.

STEMMLER, K., AMMANN, M., DONDERS, C., KLEFFMANN, J. & GEORGE, C. 2006. Photosensitized reduction of nitrogen dioxide on humic acid as a source of nitrous acid. *Nature,* 440**,** 195-198.

TAKAGI, H., WASHIDA, N., BANDOW, H., AKIMOTO, H. & OKUDA, M. 1981. Photooxidation of C5-C7 cycloalkanes in the nitric oxide-water-air system. *J. Phys. Chem.,* 85**,** 2701-2705.

TINEL, L., DUMAS, S. & GEORGE, C. 2014. A time-resolved study of the multiphase chemistry of excited carbonyls: Imidazole-2-carboxaldehyde and halides. *Comptes Rendus Chimie,* 17**,** 801-807.

TRAINIC, M., ABO RIZIQ, A., LAVI, A. & RUDICH, Y. 2012. Role of Interfacial Water in the Heterogeneous Uptake of Glyoxal by Mixed Glycine and Ammonium Sulfate Aerosols. *J. Phys. Chem.,* 116**,** 5948 - 5957.

TRAINIC, M., RIZIQ, A. A., LAVI, A., FLORES, J. M. & RUDICH, Y. 2011. The optical, physical and chemical properties of the products of glyoxal uptake on ammonium sulfate seed aerosols. *Atmos. Chem. Phys. ,* 11**,** 9697 - 9707.

TROE, J. 2000. Are primary quantum yields of NO2 photolysis at $\lambda \leq 398$ nm smaller than unity? . *Z. Physik. Chem.,* 214**,** 573-581.

TWOMEY, S. 1977. The Influence of Pollution on the Shortwave Albedo of Clouds. *J. Atmos. Sci.,* 34**,** 1149-1152.

VAN ZELM, R., HUIJBREGTS, M. A. J., DEN HOLLANDER, H. A., VAN JAARSVELD, H. A., SAUTER, F. J., STRUIJS, J., VAN WIJNEN, H. J. & VAN DE MEENT, D. 2008. European characterization factors for human health damage of PM10 and ozone in life cycle impact assessment. *Atmos. Environ.,* 42**,** 441-453.

VELASCO, E., LAMB, B., WESTBERG, H., ALLWINE, E., SOSA, G., ARRIAGA-COLINA, J. L., JOBSON, B. T., ALEXANDER, M. L., PRAZELLER, P., KNIGHTON, W. B., ROGERS, T. M., GRUTTER, M., HERNDON, S. C., KOLB, C. E., ZAVALA, M., DE FOY, B., VOLKAMER, R., MOLINA, L. T. & MOLINA, M. J. 2007. Distribution, magnitudes, reactivities, ratios and diurnal patterns of volatile organic compounds in the Valley of Mexico during the MCMA 2002 & 2003 field campaigns. *Atmos. Chem. Phys.,* 7**,** 329 - 353.

VERHEES, P. W. C. & ADEMA, E. H. 1985. The NO2-O3 system at sub-ppm concentrations: Influence of temperature and relative humidity. *J. Atmos. Chem.,* 2**,** 387-403.

VIONE, D., MAURINO, V., MINERO, C., PELIZZETTI, E., HARRISON, M. A. J., OLARIU, R.-I. & ARSENE, C. 2006. Photochemical reactions in the tropospheric aqueous phase and on particulate matter. *Chem. Soc. Rev.,* 35**,** 441-453.

VOLKAMER, R., JIMENEZ, J. L., SAN MARTINI, F., DZEPINA, K., ZHANG, Q., SALCEDO, D., MOLINA, L. T., WORSNOP, D. R. & MOLINA, M. J. 2006. Secondary organic aerosol formation from anthropogenic air pollution: Rapid and higher than expected. *Geophys. Res. Lett.,* 33**,** L17811.

VOLKAMER, R., MOLINA, L. T., MOLINA, M. J., SHIRLEY, T. & BRUNE, W. H. 2005. DOAS measurement of glyoxal as an indicator for fast VOC chemistry in urban air. *Geophys. Res. Lett.,* 32**,** L08806.

VOLKAMER, R., PLATT, U. & WIRTZ, K. 2001. Primary and Secondary Glyoxal Formation from Aromatics: Experimental Evidence for the Bicycloalkyl–Radical Pathway from Benzene, Toluene, and p-Xylene. *J. Phys. Chem. A,* 105**,** 7865-7874.

VOLKAMER, R., SAN MARTINI, F., MOLINA, L. T., SALCEDO, D., JIMENEZ, J. L. & MOLINA, M. J. 2007. A missing sink for gas-phase glyoxal in Mexico City: Formation of secondary organic aerosol. *Geophys. Res. Lett.,* 34**,** L19807.

VOLKAMER, R., ZIEMANN, P. J. & MOLINA, M. J. 2009. Secondary Organic Aerosol Formation from Acetylene (C2H2): seed effect on SOA yields due to organic photochemistry in the aerosol aqueous phase. *Atmos. Chem. Phys.,* 9**,** 1907-1928.

WALLING, C. & GIBIAN, M. J. 1965. Hydrogen Abstraction Reactions by the Triplet States of Ketones1. *J. Am. Chem. Soc.,* 87**,** 3361-3364.

WALLINGTON, T. J., DAGAUT, P. & KURYLO, M. J. 1992. UV absorption cross sections and reaction kinetics and mechanisms for peroxy radicals in the gas phase. *Chem. Rev.,* 92**,** 667-710.

WARNECK, P. 2003. In-cloud chemistry opens pathway to the formation of oxalic acid in the marine atmosphere. *Atmos. Environ.,* 37**,** 2423-2427.

WHITEY, K. T. 2007. The physical characteristics of sulfur aerosols. *Atmospheric Environment,* 41, Supplement**,** 25-49.

WIEDENSOHLER, A. 1988. An approximation of the bipolar charge distribution for particles in the submicron size range. *J. Aerosol Sci.,* 19**,** 387-389.

WILD, E., KLINGSHIRN, H. & MAIER, M. 1984. Relaxation of the $^{1}\Delta g$ state in pure liquid oxygen and in liquid mixtures of $^{16}O_2$ and $^{18}O_2$. *J. Photochem.,* 25**,** 131-143.

WUEBBLES, D. J., GRANT, K. E., CONNELL, P. S. & PENNER, J. E. 1989. The Role of Atmospheric Chemistry in Climate Change. *JAPCA,* 39**,** 22-28.

WWW.UV-VIS-SPECTRAL-ATLAS-MAINZ.ORG.

YOU, K., YIN, D., MAO, L., LIU, P. & LUO, H. A. 2011. Selective photosensitized oxidation and its catalytic regulation of monoterpene with molecular oxygen in different reaction media. *J. Photochem. Photobiol.,* 217**,** 321-325.

YU, G., BAYER, A. R., GALLOWAY, M. M., KORSHAVN, K. J., FRY, C. G. & KEUTSCH, F. N. 2011. Glyoxal in Aqueous Ammonium Sulfate Solutions: Products, Kinetics and Hydration Effects. *Environ. Sci. Technol.,* 45**,** 6336 - 6342.

ZHANG, I., Q., STANIER, O., C., CANAGARATNA, R., M., JAYNE, T., J., WORSNOP, R., D., PANDIS, N., S., JIMENEZ & L., J. 2004. Insights into the chemistry of new particle formation and growth events in Pittsburgh based on aerosol mass spectrometry. *Environ. Sci. Technol.,* 38**,** 4797 - 4809.

ZHANG, H., RATTANAVARAHA, W., ZHOU, Y., BAPAT, J., ROSEN, E. P., SEXTON, K. G. & KAMENS, R. M. 2011. A new gas-phase condensed mechanism of isoprene-NOx photooxidation. *Atmos. Environ.,* 45**,** 4507-4521.

ZHANG, J., HUFF HARTZ, K. E., PANDIS, S. N. & DONAHUE, N. M. 2006. Secondary Organic Aerosol Formation from Limonene Ozonolysis: Homogeneous and Heterogeneous Influences as a Function of NOx. *J. Phys. Chem. A,* 110**,** 11053-11063.

ZHAO, J., WU, W., SUN, J. & GUO, S. 2013. Triplet photosensitizers: from molecular design to applications. *Chem. Soc. Rev.,* 42**,** 5323-5351.

ZOGORSKI, J. S., CARTER, J. M., IVAHNENKO, T., LAPHAM, W. W., MORAN, M. J., ROWE, B. L., SQUILLACE, P. J. & TOCCALINO, P. L. 2006. The Quality of Our Nation's Waters: Volatile Organic Compounds in the Nation's Ground Water and Drinking-Water Supply Wells. *Circular 1292. Reston, VA: U.S. Geological Survey*.